

# 1 FLUXNET-CH4: A global, multi-ecosystem dataset and analysis 2 of methane seasonality from freshwater wetlands

3

4 Kyle B. Delwiche<sup>1</sup>, Sara Helen Knox<sup>2</sup>, Avni Malhotra<sup>1</sup>, Etienne Fluet-Chouinard<sup>1</sup>, Gavin  
5 McNicol<sup>1</sup>, Sarah Feron<sup>1,3</sup>, Zutao Ouyang<sup>1</sup>, Dario Papale<sup>4,5</sup>, Carlo Trotta<sup>5</sup>, Eleonora Canfora<sup>5</sup>,  
6 You-Wei Cheah<sup>6</sup>, Danielle Christianson<sup>6</sup>, Ma. Carmelita R. Alberto<sup>7</sup>, Pavel Alekseychik<sup>8</sup>, Mika  
7 Aurela<sup>9</sup>, Dennis Baldocchi<sup>1</sup>, Sheel Bansal<sup>11</sup>, David P. Billesbach<sup>12</sup>, Gil Bohrer<sup>13</sup>, Rosvel  
8 Bracho<sup>14</sup>, Nina Buchmann<sup>15</sup>, David I. Campbell<sup>16</sup>, Gerardo Celis<sup>17</sup>, Jiquan Chen<sup>18</sup>, Weinan  
9 Chen<sup>19</sup>, Housen Chu<sup>2</sup>, Higo J Dalmagro<sup>21</sup>, Sigrid Dengel<sup>6</sup>, Ankur R Desai<sup>22</sup>, Matteo Detto<sup>23</sup>, Han  
10 Dolman<sup>24</sup>, Elke Eichelmann<sup>25</sup>, Eugenie Euskirchen<sup>26</sup>, Daniela Famulari<sup>27</sup>, Kathrin Fuchs<sup>28</sup>,  
11 Mathias Goeckede<sup>29</sup>, Sébastien Gogo<sup>3</sup>, Mangaliso J. Gondwe<sup>31</sup>, Jordan P Goodrich<sup>16</sup>, Pia  
12 Gottschalk<sup>32</sup>, Scott L. Graham<sup>33</sup>, Martin Heimann<sup>29</sup>, Manuel Helbig<sup>34,35</sup>, Carole Helfter<sup>36</sup>, Kyle  
13 S. Hemes<sup>1,37</sup>, Takashi Hirano<sup>38</sup>, David Hollinger<sup>39</sup>, Lukas Hörtnagl<sup>15</sup>, Hiroki Iwata<sup>4</sup>, Adrien  
14 Jacotot<sup>3</sup>, Gerald Jurasinski<sup>41</sup>, Minseok Kang<sup>42</sup>, Kuno Kasak<sup>43</sup>, John King<sup>44</sup>, Janina Klatt<sup>45</sup>,  
15 Franziska Koebsch<sup>41</sup>, Ken W Krauss<sup>46</sup>, Derrick Y.F. Lai<sup>47</sup>, Annalea Lohila<sup>9,48</sup>, Ivan  
16 Mammarella<sup>48</sup>, Giovanni Manca<sup>49</sup>, Luca Belelli Marchesini<sup>5</sup>, Jaclyn Hatala Matthes<sup>51</sup>, Trofim  
17 Maximon<sup>52</sup>, Lutz Merbold<sup>53</sup>, Bhaskar Mitra<sup>54</sup>, Timothy H. Morin<sup>55</sup>, Eiko Nemitz<sup>36</sup>, Mats B.  
18 Nilsson<sup>56</sup>, Shuli Niu<sup>19</sup>, Walter C Oechel<sup>57</sup>, Patricia Y. Oikawa<sup>58</sup>, Keisuke Ono<sup>59</sup>, Matthias  
19 Peichl<sup>56</sup>, Olli Peltola<sup>9</sup>, Michele L. Reba<sup>6</sup>, Andrew D. Richardson<sup>61,62</sup>, William Riley<sup>6</sup>, Benjamin  
20 R. K. Runkle<sup>63</sup>, Youngryel Ryu<sup>64</sup>, Torsten Sachs<sup>32</sup>, Ayaka Sakabe<sup>65</sup>, Camilo Rey Sanchez<sup>1</sup>,  
21 Edward A Schuur<sup>66</sup>, Karina VR Schäfer<sup>67</sup>, Oliver Sonnentag<sup>68</sup>, Jed P. Sparks<sup>69</sup>, Ellen Stuart-  
22 Haëntjens<sup>7</sup>, Cove Sturtevant<sup>71</sup>, Ryan C. Sullivan<sup>72</sup>, Daphne J. Szutu<sup>1</sup>, Jonathan E Thom<sup>73</sup>,  
23 Margaret S. Torn<sup>6</sup>, Eeva-Stiina Tuittila<sup>74</sup>, Jessica Turner<sup>75</sup>, Masahito Ueyama<sup>76</sup>, Alex C.  
24 Valach<sup>1</sup>, Rodrigo Vargas<sup>77</sup>, Andrej Varlagin<sup>78</sup>, Alma Vazquez-Lule<sup>77</sup>, Joseph G. Verfaillie<sup>1</sup>,  
25 Timo Vesala<sup>48</sup>, George L Vourlitis<sup>79</sup>, Eric J. Ward<sup>46</sup>, Christian Wille<sup>32</sup>, Georg Wohlfahrt<sup>8</sup>, Guan  
26 Xhuan Wong<sup>81</sup>, Zhen Zhang<sup>82</sup>, Donatella Zona<sup>57, 83</sup>, Lisamarie Windham-Myers<sup>84</sup>, Benjamin  
27 Poulter<sup>85</sup>, Robert B. Jackson<sup>1, 37, 86</sup>

28

29

30

31 <sup>1</sup> Department of Earth System Science, Stanford University, Stanford, California

32 <sup>2</sup> Department of Geography, The University of British Columbia, Vancouver, British Columbia, Canada

33 <sup>3</sup> Department of Physics, University of Santiago de Chile, Santiago, Chile

34 <sup>4</sup> Dipartimento per la Innovazione nei Sistemi Biologici, Agroalimentari e Forestali, Università degli Studi della  
35 Tuscia, Largo dell'Università, Viterbo, Italy e Forestali, Università

36 <sup>5</sup> euroMediterranean Center on Climate Change CMCC, Lecce, Italy

37 <sup>6</sup> Earth and Environmental Sciences Area, Lawrence Berkeley National Lab, Berkeley, California

38 <sup>7</sup> International Rice Research Institute, Los Banos, Laguna, Philippines

39 <sup>8</sup> Natural Resources Institute Finland (LUKE), Helsinki, Finland

40 <sup>9</sup> Finnish Meteorological Institute, PO Box 501, 00101 Helsinki, Finland

41 <sup>10</sup> Department of Environmental Science, Policy and Management, University of California, Berkeley, CA, USA

42 <sup>11</sup> U.S. Geological Survey, Northern Prairie Wildlife Research Center, 8711 37th St Southeast, Jamestown, ND  
43 58401 USA

44 <sup>12</sup> University of Nebraska-Lincoln, Department of Biological Systems Engineering, Lincoln, NE 68583, USA

45 <sup>13</sup> Department of Civil, Environmental & Geodetic Engineering, Ohio State University

46 <sup>14</sup> School of Forest Resources and Conservation, University of Florida, Gainesville FL, 32611

47 <sup>15</sup> Department of Environmental Systems Science, Institute of Agricultural Sciences, ETH Zurich, 8092 Zurich,  
48 Switzerland  
49 <sup>16</sup> School of Science, University of Waikato, Hamilton, New Zealand  
50 <sup>17</sup> Agronomy Department, University of Florida, Gainesville FL, 32601  
51 <sup>18</sup> Department of Geography, Environment, and Spatial Sciences, Michigan State University, East Lansing, MI  
52 48823, USA  
53 <sup>19</sup> Institute of Geographic Sciences and Natural Resources Research, Chinese Academy of Sciences, Beijing 100101,  
54 PR China.  
55 <sup>20</sup> Climate and Ecosystem Sciences Division, Lawrence Berkeley National Lab, Berkeley, CA 94702, USA  
56 <sup>21</sup> Universidade de Cuiaba, Cuiaba, Mato Grosso, Brazil  
57 <sup>22</sup> Dept of Atmospheric and Oceanic Sciences, University of Wisconsin-Madison, Madison, WI 53706 USA  
58 <sup>23</sup> Department of Ecology and Evolutionary Biology, Princeton University, Princeton NJ, USA  
59 <sup>24</sup> Department of Earth Sciences, Vrije Universiteit, Amsterdam, Netherlands  
60 <sup>25</sup> School of Biology and Environmental Science, University College Dublin, Ireland  
61 <sup>26</sup> University of Alaska Fairbanks, Institute of Arctic Biology, Fairbanks, AK, USA  
62 <sup>27</sup> C NR - institute for Mediterranean Agricultural and Forest Systems, Piazzale Enrico Fermi, 1 Portici (Napoli)  
63 Italy  
64 <sup>28</sup> Institute of Meteorology and Climate Research - Atmospheric Environmental Research, Karlsruhe Institute of  
65 Technology (KIT Campus Alpin), 82467 Garmisch-Partenkirchen, Germany  
66 <sup>29</sup> Max Planck Institute for Biogeochemistry, Jena, Germany  
67 <sup>30</sup> ISTO, Université d'Orléans, CNRS, BRGM, UMR 7327, 45071, Orléans, France  
68 <sup>31</sup> Okavango Research Institute, University of Botswana, Maun, Botswana.  
69 <sup>32</sup> GFZ German Research Centre for Geosciences, Telegrafenberg, 14473 Potsdam, Germany  
70 <sup>33</sup> Manaaki Whenua - Landcare Research, Lincoln, NZ  
71 <sup>34</sup> Université de Montréal, Département de géographie, Université de Montréal, Montréal, QC H2V 0B3,  
72 Canada & Dalhousie University, Department of Physics and Atmospheric Science, Halifax, NS B2Y 1P3, Canada  
73 <sup>36</sup> UK Centre for Ecology and Hydrology, Edinburgh, UK  
74 <sup>37</sup> Woods Institute for the Environment, Stanford University, Stanford, California  
75 <sup>38</sup> Research Faculty of Agriculture, Hokkaido University, Sapporo, Japan  
76 <sup>39</sup> Northern Research Station, USDA Forest Service, Durham, NH 03824, USA  
77 <sup>40</sup> Department of Environmental Science, Faculty of Science, Shinshu University  
78 <sup>41</sup> University of Rostock, Rostock, Germany  
79 <sup>42</sup> National Center for Agro Meteorology, Seoul, South Korea  
80 <sup>43</sup> Department of Geography, University of Tartu, Vanemuise st 46, Tartu, 51410, Estonia  
81 <sup>44</sup> Department of Forestry and Environmental Resources, North Carolina State University, Raleigh, NC, USA  
82 <sup>45</sup> Vegetation Ecology, Institute of Ecology and Landscape, Department Landscape Architecture, Weihenstephan-  
83 Triesdorf University of Applied Sciences, Am Hofgarten 1, 85354 Freising, Germany  
84 <sup>46</sup> U.S. Geological Survey, Wetland and Aquatic Research Center, Lafayette LA  
85 <sup>47</sup> Department of Geography and Resource Management, The Chinese University of Hong Kong, Shatin, New  
86 Territories, Hong Kong SAR, China  
87 <sup>48</sup> Institute for Atmospheric and Earth System Research/Physics, Faculty of Science, University of Helsinki,  
88 Helsinki, Finland  
89 <sup>49</sup> European Commission, Joint Research Centre (JRC), Ispra, Italy.  
90 <sup>50</sup> Dept. of Sustainable Agro-Ecosystems and Bioresources, Research and Innovation Centre, Fondazione Edmund  
91 Mach, San Michele all'Adige, Italy  
92 <sup>51</sup> Department of Biological Sciences, Wellesley College, Wellesley, MA 02481, USA  
93 <sup>52</sup> Institute for Biological Problems of the Cryolithozone, RAS, Yakutsk, REp. Yakutia.  
94 <sup>53</sup> Mazingira Centre, International Livestock Research Institute (ILRI), Old Naivasha Road, PO Box 30709, 00100  
95 Nairobi, Kenya  
96 <sup>54</sup> Northern Arizona University, School of Informatics, Computing and Cyber Systems  
97 <sup>55</sup> Environmental Resources Engineering, SUNY College of Environmental Science and Forestry  
98 <sup>56</sup> Dept. of Forest Ecology and Management, Swedish University of Agricultural Sciences, 901 83 Umeå, Sweden  
99 <sup>57</sup> Dept. Biology, San Diego State University, San Diego, CA 92182, USA  
100 <sup>58</sup> Department of Earth and Environmental Sciences, Cal State East Bay, Hayward CA 94542 USA  
101 <sup>59</sup> National Agriculture and Food Research Organization, Tsukuba, Japan  
102 <sup>60</sup> USDA-ARS Delta Water Management Research Unit, Jonesboro, Arkansas 72401, United States

- 103 <sup>61</sup> School of Informatics, Computing & Cyber Systems, Northern Arizona University, Flagstaff, AZ 86011, USA  
104 <sup>62</sup> Center for Ecosystem Science and Society, Northern Arizona University, Flagstaff, AZ 86011, USA  
105 <sup>63</sup> Department of Biological & Agricultural Engineering, University of Arkansas, Fayetteville, Arkansas 72701,  
106 United States  
107 <sup>64</sup> Department of Landscape Architecture and Rural Systems Engineering, Seoul National University, South Korea  
108 <sup>65</sup> Hakubi center, Kyoto University, Kyoto, Japan  
109 <sup>66</sup> Department of Biological Sciences, Northern Arizona University, Flagstaff, AZ, USA  
110 <sup>67</sup> Dept of Earth and Environmental Science, Rutgers University Newark, NJ  
111 <sup>68</sup> Université de Montréal, Département de géographie, Université de Montréal, Montréal, QC H2V 0B3, Canada  
112 <sup>69</sup> Department of Ecology and Evolution, Cornell  
113 <sup>70</sup> U.S. Geological Survey, California Water Science Center, 6000 J Street, Placer Hall, Sacramento, CA, 95819  
114 <sup>71</sup> National Ecological Observatory Network, Battelle, 1685 38th St Ste 100, Boulder, Colorado, 80301, USA  
115 <sup>72</sup> Environmental Science Division, Argonne National Laboratory, Lemont, IL, USA  
116 <sup>73</sup> Space Sciences and Engineering Center, University of Wisconsin-Madison, Madison, WI 53706 USA  
117 <sup>74</sup> School of Forest Sciences, University of Eastern Finland, Joesnuu, Finland  
118 <sup>75</sup> Freshwater and Marine Science, University of Wisconsin-Madison  
119 <sup>76</sup> Graduate School of Life and Environmental Sciences, Osaka Prefecture University  
120 <sup>77</sup> Department of Plant and Soil Sciences, University of Delaware, Newark, DE, USA  
121 <sup>78</sup> A.N. Severtsov Institute of Ecology and Evolution, Russian Academy of Sciences  
122 <sup>79</sup> California State University San Marcos, San Marcos, CA, USA  
123 <sup>80</sup> University of Innsbruck, Department of Ecology, Sternwartestr. 15, 6020 Innsbruck, AUSTRIA  
124 <sup>81</sup> Sarawak Tropical Peat Research Institute, Sarawak, Malaysia  
125 <sup>82</sup> Department of Geographical Sciences, University of Maryland, College Park, MD 20740, USA  
126 <sup>83</sup> Department of Animal and Plant Sciences, University of Sheffield, Western Bank, Sheffield, S10 2TN, United  
127 Kingdom  
128 <sup>84</sup> U.S. Geological Survey, Water Mission Area, 345 Middlefield Road, Menlo Park, CA, 94025  
129 <sup>85</sup> Biospheric Sciences Laboratory, NASA Goddard Space Flight Center, Greenbelt, Maryland  
130 <sup>86</sup> Precourt Institute for Energy, Stanford University, Stanford, California  
131  
132  
133  
134 *Correspondence to:* Kyle B. Delwiche (delwiche@stanford.edu)

135  
136 **Abstract.** Methane (CH<sub>4</sub>) emissions from natural landscapes constitute roughly half of global CH<sub>4</sub> contributions to  
137 the atmosphere, yet large uncertainties remain in the absolute magnitude and the seasonality of emission quantities  
138 and drivers. Eddy covariance (EC) measurements of CH<sub>4</sub> flux are ideal for constraining ecosystem-scale CH<sub>4</sub>  
139 emissions due to quasi-continuous and high temporal resolution of CH<sub>4</sub> flux measurements, coincident carbon dioxide,  
140 water, and energy flux measurements, lack of ecosystem disturbance, and increased availability of datasets over the  
141 last decade. Here, we 1) describe the newly published dataset, FLUXNET-CH<sub>4</sub> Version 1.0, the first, open source  
142 global dataset of CH<sub>4</sub> EC measurements (available at <https://fluxnet.org/data/fluxnet-ch4-community-product/>).  
143 FLUXNET-CH<sub>4</sub> includes half-hourly and daily gap-filled and non gap-filled aggregated CH<sub>4</sub> fluxes and  
144 meteorological data from 79 sites globally: 42 freshwater wetlands, 6 brackish and saline wetlands, 7 formerly drained  
145 ecosystems, 7 rice paddy sites, 2 lakes, and 15 uplands. Then, we 2) evaluate FLUXNET-CH<sub>4</sub> representativeness for  
146 freshwater wetland coverage globally, because the majority of sites in FLUXNET-CH<sub>4</sub> Version 1.0 are freshwater  
147 wetlands which are a substantial source of total atmospheric CH<sub>4</sub> emissions; and 3) provide the first global estimates  
148 of the seasonal variability and seasonality predictors of freshwater wetland CH<sub>4</sub> fluxes. Our representativeness analysis  
149 suggests that the freshwater wetland sites in the dataset cover global wetland bioclimatic attributes (encompassing  
150 energy, moisture, and vegetation-related parameters) in arctic, boreal, and temperate regions, but only sparsely cover  
151 humid tropical regions. Seasonality metrics of wetland CH<sub>4</sub> emissions vary considerably across latitudinal bands. In  
152 freshwater wetlands (except those between 20° S to 20° N) the spring onset of elevated CH<sub>4</sub> emissions starts three  
153 days earlier, and the CH<sub>4</sub> emission season lasts 4 days longer, for each degree C increase in mean annual air

154 temperature. On average, the spring onset of increasing CH<sub>4</sub> emissions lags soil warming by one month, with very  
155 few sites experiencing increased CH<sub>4</sub> emissions prior to the onset of soil warming. In contrast, roughly half of these  
156 sites experience the spring onset of rising CH<sub>4</sub> emissions prior to the spring increase in gross primary productivity  
157 (GPP). The timing of peak summer CH<sub>4</sub> emissions does not correlate with the timing for either peak summer  
158 temperature or peak GPP. Our results provide seasonality parameters for CH<sub>4</sub> modeling, and highlight seasonality  
159 metrics that cannot be predicted by temperature or GPP (i.e., seasonality of CH<sub>4</sub> peak). FLUXNET-CH<sub>4</sub> is a powerful  
160 new resource for diagnosing and understanding the role of terrestrial ecosystems and climate drivers in the global CH<sub>4</sub>  
161 cycle; and future additions of sites in tropical ecosystems and site-years of data collection will provide added value to  
162 this database. All seasonality parameters are available at <https://doi.org/10.5281/zenodo.4672601>. Additionally, raw  
163 FLUXNET-CH<sub>4</sub> data used to extract seasonality parameters can be downloaded from [https://fluxnet.org/data/fluxnet-](https://fluxnet.org/data/fluxnet-ch4-community-product/)  
164 [ch4-community-product/](https://fluxnet.org/data/fluxnet-ch4-community-product/), and a complete list of the 79 individual site data DOIs is provided in Table 2 in the Data  
165 Availability section of this document.

166  
167  
168  
169  
170

## 171 **1 Introduction**

172 Methane (CH<sub>4</sub>) has a global warming potential that is 28 times larger than carbon dioxide (CO<sub>2</sub>) on a 100-  
173 year time scale (Myhre et al., 2013), and its atmospheric concentration has increased by >1000 ppb since 1800  
174 (Etheridge et al., 1998). While atmospheric CH<sub>4</sub> concentrations are substantially lower than those of CO<sub>2</sub>, CH<sub>4</sub> has  
175 contributed 20-25% as much radiative forcing as CO<sub>2</sub> since 1750 (Etminan et al., 2016). Despite its importance to  
176 global climate change, natural CH<sub>4</sub> sources and sinks remain poorly constrained, and with uncertain attribution to the  
177 various biogenic and anthropogenic sources (Saunio et al., 2016, 2020). Bottom-up and top-down estimates differ  
178 by 154 Tg/yr (745 versus 591 Tg/yr, respectively); much of this difference arises from natural sources (Saunio et al.,  
179 2020). Vegetated wetlands and inland water bodies account for most natural CH<sub>4</sub> emissions, as well as the majority  
180 of uncertainty in bottom-up emissions estimates (Saunio et al., 2016). Better diagnosis and prediction of terrestrial  
181 CH<sub>4</sub> sources to the atmosphere requires high frequency and continuous measurements of CH<sub>4</sub> exchange across a  
182 continuum of time (hours to years) and space (meters to kilometers) scales.

183 Tower-based eddy covariance (EC) measurements provide ecosystem-scale CH<sub>4</sub> fluxes at high temporal  
184 resolution across years, are coupled with measurements of key CH<sub>4</sub> drivers such as temperature, water and recent  
185 substrate input (inferred from CO<sub>2</sub> flux), and thus help constrain bottom-up CH<sub>4</sub> budgets and improve CH<sub>4</sub> predictions.  
186 Although EC towers began measuring CO<sub>2</sub> fluxes in the late 1970s (Desjardins 1974; Anderson et al., 1984), and  
187 some towers began measuring CH<sub>4</sub> in the 1990s (Verma et al., 1992), most CH<sub>4</sub> flux EC measurements began within  
188 the last decade (2010s). Given that many EC CH<sub>4</sub> sites are relatively new, the flux community has only recently  
189 compiled them for global synthesis efforts (e.g., Chang et al., in press) and is still working to standardize CH<sub>4</sub> flux  
190 measurements and establish gap-filling protocols (Nemitz et al., 2018; Knox et al., 2019). Furthermore, the growth of  
191 EC networks for CH<sub>4</sub> fluxes has sometimes taken place in a relatively *ad hoc* fashion, often at sites that were already  
192 measuring CO<sub>2</sub> fluxes or where higher CH<sub>4</sub> fluxes were expected, potentially introducing bias. The representativeness  
193 and spatial distribution of CO<sub>2</sub> flux tower networks have been assessed to evaluate its ability to upscale fluxes  
194 regionally (Hargrove et al., 2003; Hoffman et al., 2013; Papale et al., 2015; Villarreal et al., 2018, 2019) and globally  
195 (Jung et al., 2009; 2020). However, a relatively sparse coverage of CH<sub>4</sub> flux towers prompts the question of how well  
196 the current observation network provides a sufficient sampling of global or ecosystem-specific bioclimatic conditions.

197 Broad-scale wetland CH<sub>4</sub> seasonality estimates, such as when fluxes increase, peak, and decrease and the  
198 predictors of seasonality, remain relatively unconstrained across wetlands globally. These key seasonality metrics  
199 vary considerably across high-emitting systems such as wetlands and other aquatic systems (Desjardins, 1974; Dise,  
200 1992; Melloh and Crill 1996; Wik et al., 2013; Zona et al., 2016; Treat et al., 2018). Few continuous CH<sub>4</sub> flux datasets  
201 across representative site-years make it difficult to establish trends in seasonal dynamics, though monthly or annually  
202 aggregated estimates of CH<sub>4</sub> fluxes from different seasons do exist for high latitudes (Zona et al., 2016; Treat et al.,  
203 2018). Seasonal variability in freshwater wetland CH<sub>4</sub> fluxes is expected to be driven by changes in air and soil  
204 temperature, soil moisture (including water table dynamics), and recent carbon substrate availability, which influence  
205 the rates of CH<sub>4</sub> production and consumption (Lai, 2009; Bridgham et al., 2013; Dean et al., 2018). Temperature has  
206 widely been found to strongly affect CH<sub>4</sub> flux (Chu et al., 2014; Yvon-Durocher et al., 2014; Sturtevant et al., 2016),  
207 but the relationship is complex (Chang et al., 2020) and varies seasonally (Koebsch et al., 2015; Helbig et al., 2017).  
208 CH<sub>4</sub> flux is also driven by inundation depth since anoxic conditions are typically necessary for methanogenesis (Lai,  
209 2009; Bridgham et al., 2013), though CH<sub>4</sub> production under bulk-oxic conditions has been observed (Angle et al.,  
210 2017). Substrate availability influences CH<sub>4</sub> production potential and is linked with gross primary productivity (GPP)  
211 because recent photosynthate fuels methanogenesis though this relationship can vary by ecosystem type, plant  
212 functional type and biome (Meronigal et al., 1999; Chanton et al., 2008; Hatala et al., 2012; Lai et al., 2014; Malhotra  
213 and Roulet, 2015; Sturtevant et al., 2016). In process models, the seasonality of CH<sub>4</sub> emissions from wetlands globally  
214 is primarily constrained by inundation (Poulter et al., 2017), with secondary within-wetland influences from  
215 temperature and availability of carbon (C) substrates (Melton et al., 2013; Castro-Morales et al., 2018). Bottom-up  
216 and top-down global CH<sub>4</sub> estimates continue to disagree on total CH<sub>4</sub> flux magnitudes and seasonality, including the  
217 timing of annual peak emissions (Spahni et al., 2011; Saunio et al., 2020). Thus, the variability and predictors of  
218 wetland CH<sub>4</sub> seasonality globally remain a knowledge gap that high-frequency and long-term EC data can help fill.

219 Here, we first describe Version 1.0 of the FLUXNET-CH<sub>4</sub> dataset (available at  
220 <https://fluxnet.org/data/fluxnet-ch4-community-product/>). Version 1.0 of the dataset expands and formalizes the  
221 publication of data scattered among regional flux networks as described previously in Knox et al. (2019). FLUXNET-  
222 CH<sub>4</sub> includes half-hourly and daily gap-filled and non gap-filled aggregated CH<sub>4</sub> fluxes and meteorological data from  
223 79 sites globally: 42 freshwater wetlands, 6 brackish and saline wetlands, 7 formerly drained ecosystems, 7 rice paddy  
224 sites, 2 lakes, and 15 upland ecosystems. FLUXNET-CH<sub>4</sub> includes an additional 2 wetland sites (RU-Vrk and SE-  
225 St1), but they are not available under the CC BY 4.0 data policy and thus are excluded from this analysis. Since the  
226 majority of sites in FLUXNET-CH<sub>4</sub> Version 1.0 (hereafter referred to solely as “FLUXNET-CH<sub>4</sub>”) are freshwater  
227 wetlands, which are a substantial source of total atmospheric CH<sub>4</sub> emissions, we use the subset of data from freshwater  
228 wetlands to evaluate the representativeness of freshwater wetland coverage in the FLUXNET-CH<sub>4</sub> dataset relative to  
229 wetlands globally, and provide the first assessment of global variability and predictors of freshwater wetland CH<sub>4</sub> flux  
230 seasonality. We quantify a suite of CH<sub>4</sub> seasonality metrics and evaluate temperature and GPP (a proxy for recent  
231 substrate input) as predictors of seasonality across four latitudinal bands (northern, temperate, subtropical, and  
232 tropical). Due to a lack of high-temporal resolution water table data at all sites, our analyses are unable to evaluate the  
233 critical role of water table on CH<sub>4</sub> seasonality. Here we provide parameters for better understanding and modeling  
234 seasonal variability in freshwater wetland CH<sub>4</sub> fluxes and generate new hypotheses and data resources for future  
235 syntheses.

## 236 2. Methods

### 237 2.1 FLUXNET-CH<sub>4</sub> dataset

#### 238 2.1.1 History and data description

239 The FLUXNET-CH<sub>4</sub> dataset was initiated by the Global Carbon Project (GCP) in 2017 to better constrain  
240 the global CH<sub>4</sub> budget (<https://www.globalcarbonproject.org/methanebudget/index.htm>). Beginning with a kick off

241 meeting in May 2018 in Washington DC, hosted by Stanford University, we coordinated with the AmeriFlux  
242 Management Project, the European Ecosystem Fluxes Database, and the ICOS Ecosystem Thematic Centre (ICOS-  
243 ETC) to avoid duplication of efforts, as most sites are part of different regional networks (albeit with different data  
244 products). We collected and standardized data for FLUXNET-CH<sub>4</sub> with assistance from the regional flux networks,  
245 AmeriFlux's "Year of Methane", FLUXNET, the EU's Readiness of ICOS for Necessities of Integrated Global  
246 Observations (RINGO) project, and a U.S. Geological Survey Powell Center working group. FLUXNET-CH<sub>4</sub> is a  
247 community-led project, so while we developed it with assistance from FLUXNET, we do not necessarily use standard  
248 FLUXNET data variables, formats, or methods.

249 FLUXNET-CH<sub>4</sub> includes gap-filled half-hourly CH<sub>4</sub> fluxes and meteorological variables. Gaps in  
250 meteorological variables (TA - air temperature, SW\_IN - incoming shortwave radiation, LW\_IN - incoming longwave  
251 radiation, VPD - vapor pressure deficient, PA - pressure, P - precipitation, WS - wind speed) were filled with the  
252 ERA-Interim (ERA-I) reanalysis product (Vuichard and Papale, 2015). We used the REdDyProc package (Wutzler et  
253 al., 2018) to filter flux values with low friction velocity ( $u^*$ ) based on relating nighttime  $u^*$ , to fill gaps in CO<sub>2</sub>, latent  
254 heat, and sensible heat fluxes, and to partition net CO<sub>2</sub> fluxes into gross primary production (GPP) and ecosystem  
255 respiration (RECO) using both the daytime (Lasslop et al., 2010) and nighttime (Reichstein et al., 2005) approaches.  
256 Data gaps of CH<sub>4</sub> flux were filled using artificial neural network (ANN) methods first described in Knox et al. (2015)  
257 and in Knox et al. (2019), and summarized here in Sect. 2.1.2. Gap-filled data for gaps exceeding two months are  
258 provided and flagged for quality. Please see Table B1 for variable description and units, as well as quality flag  
259 information. For the seasonality analysis in this paper we excluded data from gaps exceeding two months, and we  
260 encourage future users of FLUXNET-CH<sub>4</sub> to critically evaluate gap-filled values from long data gaps before including  
261 them in analyses (Dengel et al., 2013; Kim et al., 2020).

262 In addition to half-hourly data, the FLUXNET-CH<sub>4</sub> Version 1.0 release also contains a full set of daily mean  
263 values for all parameters except wind direction and precipitation. Daily precipitation is included as the daily sum of  
264 the half-hourly data, and daily average wind direction is not included.

### 265 2.1.2 Gap-filling methods and uncertainty estimates

266 As described in Knox et al. (2015) and in Knox et al. (2019), the ANN routine used to gap-fill the CH<sub>4</sub> data  
267 was optimized for generalizability and representativeness. To avoid biasing the ANN toward environmental conditions  
268 with typically better data coverage (e.g., summer-time and daytime measurements), the explanatory data were divided  
269 into a maximum of 15 clusters using a k-means clustering algorithm. Data used to train, test, and validate the ANN  
270 were proportionally sampled from these clusters. For generalizability, the simplest ANN architecture with good  
271 performance (<5% gain in model accuracy for additional increases in architecture complexity) was selected for 20  
272 extractions of the training, test, and validation data. Within each extraction, each tested ANN architecture was  
273 reinitialized 10 times, and the initialization with the lowest root-mean-square-error was selected to avoid local minima.  
274 The median of the 20 predictions was used to fill each gap. A standard set of variables available across all sites was  
275 used to gap-fill CH<sub>4</sub> fluxes (Dengel et al., 2013), which included the previously mentioned meteorological variables  
276 TA, SW\_IN, WS, PA, and sine and cosine functions to represent seasonality. These meteorological variables were  
277 selected for their relevance to CH<sub>4</sub> exchange and were gap-filled using the ERA-I reanalysis data. Other variables  
278 related to CH<sub>4</sub> flux (e.g., water table depth [WTD] and soil temperature [TS]) were not included as explanatory  
279 variables as they were not available across all sites or had large gaps that could not be filled using the ERA-I reanalysis  
280 data (Knox et al., 2019). The ANN gap-filling was performed using MATLAB (MathWorks 2018, version 9.4.0).

281 While the median of the 20 predictions was used to fill each gap, the spread of the predictions was used to  
282 provide a measure of uncertainty resulting from the ANN gap-filling procedure. Specifically, the combined annual  
283 gap-filling and random uncertainty was calculated from the variance of the cumulative sums of the 20 ANN predictions  
284 (Knox et al., 2015; Anderson et al., 2016; Oikawa et al., 2017). The (non-cumulative) variance of the 20 ANN

285 predictions was also used to provide gap-filling uncertainty for each half-hourly gap-filled value. While this output is  
286 useful for data-model comparisons, it cannot be used to estimate cumulative annual gap-filling error because gap-  
287 filling error is not random, which is why the cumulative sums of the 20 ANN predictions are used to estimate annual  
288 gap-filling error.

289 Random errors in EC fluxes follow a double exponential (Laplace) distribution with the standard deviation  
290 varying with flux magnitude (Richardson et al., 2006; Richardson et al., 2012). For half-hourly CH<sub>4</sub> flux  
291 measurements, random error was estimated using the residuals of the median ANN predictions, providing a  
292 conservative “upper limit” estimate of the random flux uncertainty (Moffat et al., 2007; Richardson et al., 2008). The  
293 annual cumulative uncertainty at 95% confidence was estimated by adding the cumulative gap-filling and random  
294 measurement uncertainties in quadrature (Richardson and Hollinger, 2007; Anderson et al., 2016). Annual  
295 uncertainties in CH<sub>4</sub> flux for individual site-years are provided in Table B2. Throughout this paper, we include  
296 uncertainties on individual site years when discussing single years of data. In sites with multiple years of data, we  
297 report the standard deviation of the multiple years.

### 298 2.1.3 Dataset structure and site metadata

299 FLUXNET-CH<sub>4</sub> contains two comma-separated data files per site at half-hourly and daily resolutions which  
300 are available for download at <https://fluxnet.org/data/fluxnet-ch4-community-product/>, along with a file containing  
301 select site metadata. Each site has a unique FLUXNET-CH<sub>4</sub> DOI. All data from the 79 sites used in this analysis are  
302 available under CC BY 4.0 (<https://creativecommons.org/licenses/by/4.0/>) copyright license (FLUXNET-CH<sub>4</sub> has an  
303 additional 2 sites available under the FLUXNET Tier 2 license (<https://fluxnet.org/data/data-policy/>), though these  
304 sites are not included in our analysis).

305 Metadata (Table B3) include site coordinates, ecosystem classification based on site literature,  
306 presence/absence and dominance for specific vegetation types, and DOI link, as well as calculated data such as annual  
307 and quarterly CH<sub>4</sub> flux values. FLUXNET-CH<sub>4</sub> Version 1.0 sites were classified based on site-specific literature as  
308 fen, bog, swamp, marsh, salt marsh, lake, mangrove, rice paddy/field, wet tundra, upland, or drained ecosystems that  
309 previously could have been wetlands, seasonally flooded pastures, or agricultural areas. To the extent possible, we  
310 followed classification systems of previous wetland CH<sub>4</sub> syntheses (Olefeldt et al., 2013; Turetsky et al., 2014; Treat  
311 et al., 2018). Drained systems are former wetlands that have subsequently been drained but may maintain a relatively  
312 shallow water table, which can contribute to occasional methane emissions, although we do not have specific water  
313 table depth information at all drained sites. Upland ecosystems are further divided into alpine meadows, grasslands,  
314 needleleaf forests, mixed forest, crops, tundra, and urban. Freshwater wetland classifications follow hydrological  
315 definitions of bog (ombrotrophic), fen (minerotrophic), wet tundra, marshes and swamps, and were designated as per  
316 primary literature on the site. For all sites, vegetation was classified for presence or absence of brown mosses (all  
317 species from the division Bryophyta except those in the class Sphagnopsida), *Sphagnum* mosses (any species from  
318 class Sphagnopsida), ericaceous shrubs, trees (of any height) and aerenchymatous species (mostly Order Poales but  
319 includes exceptions). These categories closely follow Treat et al., (2018), except that aerenchymatous species had to  
320 be expanded beyond Cyperaceae to incorporate wetlands globally. Presence/absence of vegetation groups was  
321 designated based on species lists in primary literature from the site. Out of the vegetation groups present, the dominant  
322 (most abundant) group is also reported and is based on information provided by lead site investigators.

323 In addition to the variable description table (Table B1) and the site metadata (Table B3), we provide several  
324 more tables to complement our analysis. Table B4 includes the climatic data used in the representativeness analysis.  
325 Table 5 provides seasonality parameters for CH<sub>4</sub> flux, air temperature, soil temperature (from the probe closest to the  
326 ground surface), and GPP. For sites with multiple soil temperature probes, the full set of soil temperature parameters  
327 are in Table B6. Table B7 contains the soil temperature probe depths. Table B2 contains the annual CH<sub>4</sub> flux and  
328 uncertainty. All Appendix B tables are also available at <https://doi.org/10.5281/zenodo.4672601>.

329

#### 330 2.1.4 Annual CH<sub>4</sub> fluxes

331 Annual CH<sub>4</sub> fluxes were calculated from gap-filled data for site-years with data gaps shorter than two  
332 consecutive months, or for sites above 20° N where >2 month data gaps occurred outside of the highest CH<sub>4</sub>-emission  
333 months of May 1 through October 31. Since we did not sum gap-filled values for >2 month gaps during the winter,  
334 annual sums from these years will be an underestimate since winter fluxes can be important (Zona et al., 2016; Treat  
335 et al., 2018). Several sites had less than one year of data, and we report gap-filled CH<sub>4</sub> flux annual sums for sites with  
336 between six months and one year of data (BW-Gum = 228 days, CH-Oe2 = 200 days, JP-Swl = 210 days, US-EDN =  
337 182 days). While these sums will be an underestimate of annual CH<sub>4</sub> flux since they do not span a full year (and we  
338 therefore do not use them in the seasonality analysis), their relative magnitude can still be informative. For example,  
339 site JP-SWL is a lake site, and even with less than a year of data the summed CH<sub>4</sub> flux of 66 g C m<sup>-2</sup> is relatively high  
340 (Taoka et al., 2020). In addition to sites with short time series, the annual CH<sub>4</sub> sum for site ID-Pag represents 365 days  
341 spanning June 2016 to June 2017.

#### 342 2.1.5 Subset analysis on freshwater wetland CH<sub>4</sub> flux

343 In addition to the FLUXNET-CH<sub>4</sub>-wide description of site class distributions and annual CH<sub>4</sub> fluxes, we  
344 also include a subset analysis on freshwater wetlands, given that it is the dominant ecosystem type in our dataset and  
345 an important global CH<sub>4</sub> source (Saunio et al., 2016). First, we analyze freshwater wetland representativeness, and  
346 subsequently the seasonality of their CH<sub>4</sub> emissions. Freshwater wetlands included in the seasonality and  
347 representativeness analysis are indicated in Table B3, column “IN\_SEASONALITY\_ANALYSIS”.

348

### 349 2.2 Wetland representativeness

#### 350 2.2.1 Principal Component Analysis

351 To compare the FLUXNET-CH<sub>4</sub> site distribution to the global wetland distribution, we evaluated their  
352 representativeness in the entire global wetland cover along four bioclimatic gradients. Only freshwater wetland sites  
353 were included in this analysis. Coastal sites were excluded because salinity, an important control on CH<sub>4</sub> production,  
354 could not be evaluated across the tower network due to a lack of global gridded salinity data (Bartlett et al., 1987;  
355 Poffenbarger et al., 2011). The four bioclimatic variables used were: mean annual air temperature (MAT), latent heat  
356 flux (LE), enhanced vegetation index (EVI), and simple ratio water index (SRWI; data sources in Table B4). We use  
357 EVI because it is a more direct measurement than GPP from global gridded products and is considered a reasonable  
358 proxy for GPP (Sims et al., 2006). Together, these environmental variables account for, or are, proxies for key controls  
359 of CH<sub>4</sub> production, oxidation at the surface, and transport (Bridgman et al., 2013). We use a principal components  
360 analysis (PCA) to visualize the site distribution across the four environmental drivers at once. For this analysis, we  
361 consider the annual average bioclimatic conditions over 2003-2015. In the PCA output, we evaluate the coverage of  
362 the 42 freshwater sites over 0.25° grid cells containing >5% wetland mean cover in Wetland Area and Dynamics for  
363 Methane Modeling (WAD2M; Zhang et al., 2020; Zhang et al., 2021) for the same time period.

#### 364 2.2.2 Global Dissimilarity and Constituency Analysis

365 To further identify geographical gaps in the coverage of the FLUXNET-CH<sub>4</sub> Version 1.0 network, we  
366 quantified the dissimilarity of global wetlands from the tower network, using a similar approach to that taken for CO<sub>2</sub>  
367 flux towers (Meyer and Pebesma 2020). We calculated the 4-dimensional Euclidean distance from the four bioclimatic  
368 variables between every point at the land surface to every tower location at the FLUXNET-CH<sub>4</sub> network. We then  
369 divided these distances by the average distance between towers to produce a dissimilarity index. Dissimilarity scores

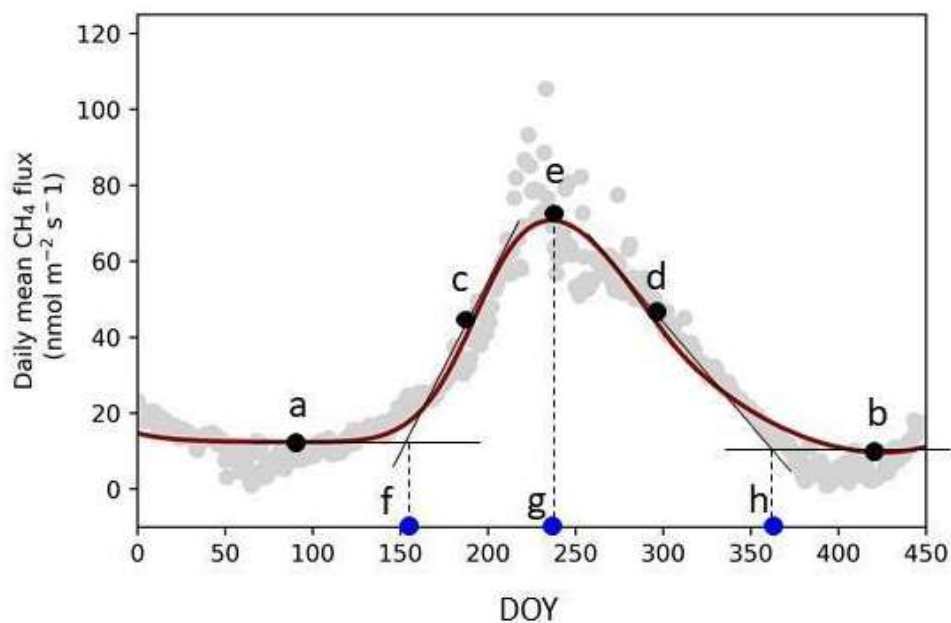
370 <1 represent areas whose nearest tower is closer than the average distance among towers, while areas with scores >1  
371 are more distant. Lastly, we identified the importance of an individual tower in the network by estimating the  
372 geographical area to which it is most analogous in bioclimate space. We divided the world's land surface according  
373 to closest towers in bioclimatic space. The area to which each tower is nearest is defined as the tower's constituency.

### 374 2.3 Wetland CH<sub>4</sub> seasonality

375 To examine freshwater wetland CH<sub>4</sub> seasonality across the global range of sites in FLUXNET-CH<sub>4</sub>, we  
376 extracted seasonality parameters for CH<sub>4</sub>, temperature, and GPP using Timesat, a software package designed to  
377 analyze seasonality of environmental systems (Jönsson and Eklundh, 2002; Jönsson and Eklundh, 2004; Eklundh  
378 and Jönsson, 2015). Timesat calculates several seasonality parameters, including baseline flux, peak flux, and the  
379 slope of spring flux increase and fall decrease (Fig. 1). We also calculate parameters such as amplitude (peak flux -  
380 baseline, which is the average of spring and fall baselines;  $(“e” - ((“a” + “b”)/2))$  in Fig. 1), and relative peak timing ( $(“g” - “f”) / (“h” - “f”)$  in Fig. 1). Timesat uses a double-logistic fitting function to create a series of localized fits  
381 centered on data minima and maxima. Localized fits are minimized using a merit function and the Levenberg-  
382 Marquardt method (Madsen et al., 2004; Nielsen, 1999). These localized fits are then merged using a global  
383 function to create a smooth fit over the full time interval. To fit CH<sub>4</sub> time-series in Timesat, we used gap-filled data  
384 after removing gaps exceeding two months. We do not report Timesat parameters when large gaps occur during CH<sub>4</sub>  
385 emissions spring increase, peak, or fall decrease.  
386

387 We estimate ‘start of elevated emissions season’ when CH<sub>4</sub> emissions begin to increase in the spring (“f”  
388 in Fig. 1), and ‘end of elevated emissions season’ when the period of elevated CH<sub>4</sub> flux ends in the fall (“h” in Fig.  
389 1), as the intercept between the Timesat fitted baseline parameter and shoulder-season slope (similar to Gu et al.,  
390 2009). To extract seasonality parameters with Timesat, sites need a sufficiently pronounced seasonality, a  
391 sufficiently long time period, and minimal data gaps (we note that while Timesat is capable of fitting two peaks per  
392 year, all the freshwater wetland sites have a single annual peak). We excluded site-years in restored wetlands when  
393 wetlands were still under construction. Of the 42 freshwater wetland sites in FLUXNET-CH<sub>4</sub> Version 1.0, 36 had  
394 sufficient data series to extract seasonality parameters. These 36 wetlands had 141 site-years of data total, which we  
395 fit with the double-logistic fitting method which followed site data well (representative examples in Fig. 2). For  
396 extratropical sites in the Southern Hemisphere, we shifted all data by 182 days so that maximum solar insolation  
397 seasonality would be congruent across the globe.

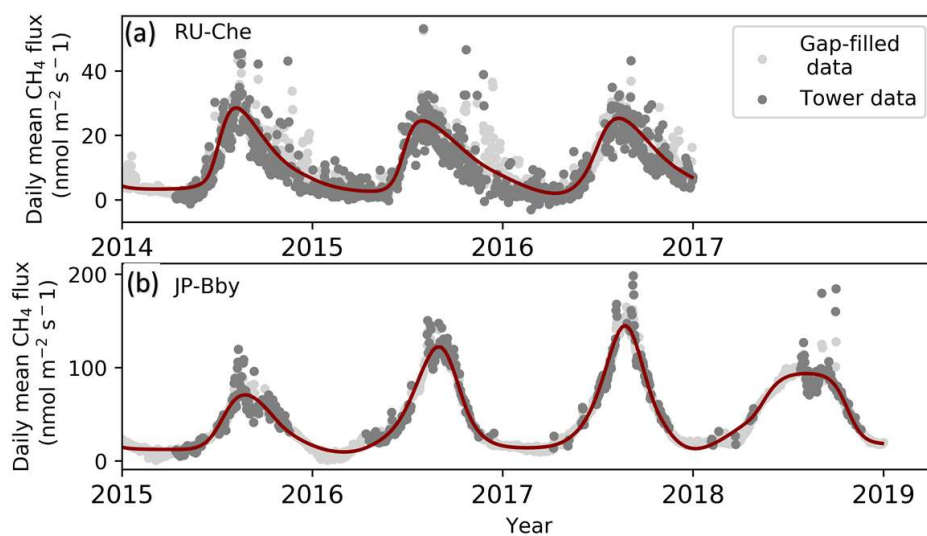
398 We also used Timesat to extract seasonality metrics for GPP, partitioned using the daytime-based approach  
399 (Lasslop et al., 2010) (GPP\_DT), air temperature (TA), and soil temperature (TS\_1, TS\_2, etc). For sites where  
400 winter soil temperatures fall significantly below 0 °C, Timesat fits a soil temperature “start of elevated season” date  
401 to periods when the soil is still frozen. In order for Timesat to define the soil temperature seasonality within the  
402 thawed season, we converted all negative soil temperatures to zero (simply removing these values results in too  
403 many missing values for Timesat to fit). Many sites have more than one soil temperature probe, so we extracted  
404 separate seasonality metrics from each individual probe (although we used the metrics from the shallowest  
405 temperature probe in our analysis). Tables B4 contain the Timesat seasonality parameters used in the seasonality  
406 analysis. We did not include water table depth in the seasonality analysis because many sites either lack water table  
407 depth measurements or have sparse data.



408  
 409 **Figure 1: TIMESAT parameter description.** (a) and (b) base values (Timesat reports the average of these two values), (c)  
 410 and (d) slopes of seasonal curves (lines drawn between 20% and 80% of the amplitude), (e) peak value, and day of year  
 411 (DOY) for the start (f), peak (g), and end (h) of the elevated methane (CH<sub>4</sub>) emissions season. Data points are the mean  
 412 daily gap-filled CH<sub>4</sub> fluxes from site JP-Bby in 2015.

413

414



415  
 416 **Figure 2: Examples of Timesat fits for two FLUXNET-CH<sub>4</sub> sites, (a) RU-Che and (b) JP-Bby. Methane (CH<sub>4</sub>) flux data**  
 417 **showing daily average flux tower data, with several high outliers excluded to improve the plot (dark gray), gap-filled**

418 values (light gray), and Timesat-fitted curve (dark red line) for sites JP-Bby and RU-Che. Timesat captures the size and  
419 shape of peaks (note different scale on y-axes). CH<sub>4</sub> = methane.

420

421 We regressed the CH<sub>4</sub> seasonality parameters from Timesat against annual temperature, annual water table  
422 depth, and Timesat seasonality parameters for air temperature, soil temperature, and GPP (proxy for recent carbon  
423 input available as substrate) using linear mixed-effect modeling with the *lmer* command (with site as a random  
424 effect) from the R (R Core Team 2018, version 3.6.2) package lmerTest (Kuznetsova et al., 2017). For these  
425 regressions we present the marginal R<sup>2</sup> outputs from *lmer*, which represent the variance explained only by the fixed  
426 effects. Mixed-effect modeling was necessary to account for the non-independence between measurements taken at  
427 the same site during different years (Zona et al., 2016; Treat et al., 2018). We also compared how seasonality  
428 metrics varied across latitudinal bands by dividing sites into northern (> 60° N), temperate (between 40° N and 60°  
429 N), subtropical (absolute value between 20° and 40° latitude, with site NZ-KOP being the only Southern hemisphere  
430 site), and tropical (absolute value below 20°). Site-year totals for the northern, temperate, subtropical, and tropical  
431 bands were  $n = 57, 36, 39,$  and  $9,$  respectively. We used the Kruskal-Wallis test to establish whether groups (either  
432 across quarters or across latitudes) were from similar distributions, and the post hoc multiple comparison “Dwass,  
433 Steel, Critchlow, and Fligner” procedure for inter-group comparisons. Kruskal-Wallis and post-hoc tests were  
434 implemented in Python Version 3.7.4, using stats from *scipy* for Kruskal-Wallis and *posthoc\_dscf* from  
435 *scikit\_posthocs*.

436 We also compared quarterly CH<sub>4</sub> flux sums by dividing data into quarterly periods:  
437 January/February/March (JFM), April/May/June (AMJ), July/August/September (JAS), and  
438 October/November/December (OND). For the sake of simplicity, we chose to compare quarterly periods rather than  
439 site-specific growing/non-growing season periods so that all time periods would be the same length. Quarterly sums  
440 were computed from the gap-filled CH<sub>4</sub> fluxes when the longest continuous data gap within the quarter did not  
441 exceed 30 days, leading to site-year counts of 67, 92, 95, 72 for JFM, AMJ, JAS, and OND, respectively. We  
442 compared quarterly CH<sub>4</sub> fluxes across latitudinal bands both for the total CH<sub>4</sub> flux, and for the quarterly percentage  
443 of the annual CH<sub>4</sub> flux. Quarterly statistics were also conducted with the Kruskal-Wallis test and the post hoc  
444 multiple comparison “Dwass, Steel, Critchlow, and Fligner” procedure implemented in Python. Quarterly values  
445 are provided in Table B3, and the sum of mean quarterly CH<sub>4</sub> flux does not always equal mean annual CH<sub>4</sub> flux  
446 because some quarters either do not have data, or have data gaps that exceed 30 days.  
447

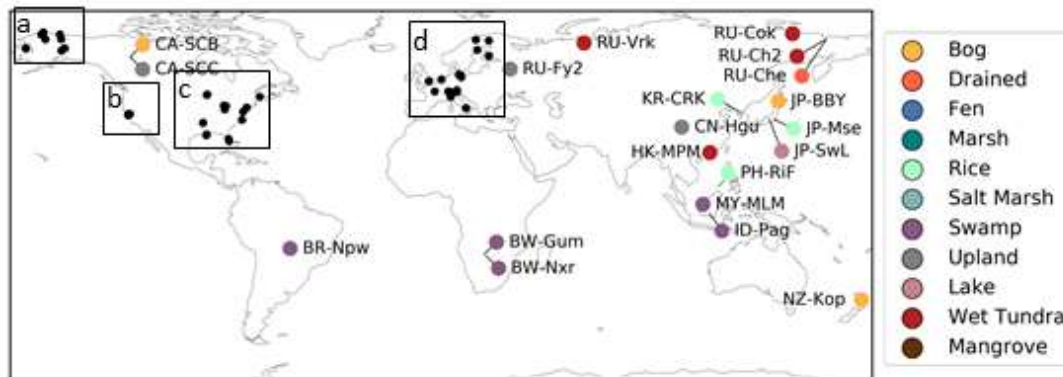
## 448 3. Results and Discussion

### 449 3.1 FLUXNET-CH<sub>4</sub> dataset

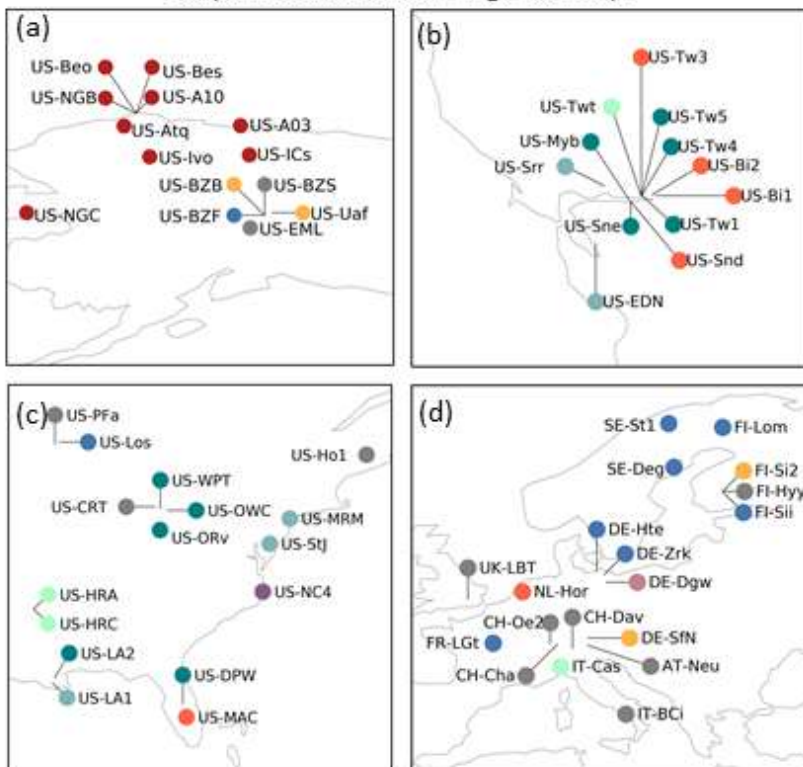
#### 450 3.1.1 Dataset description

451 Version 1.0 of the FLUXNET-CH<sub>4</sub> dataset contains 79 unique sites, 293 total site-years of data, and 201  
452 site-years with sufficient data to estimate annual CH<sub>4</sub> emissions. A synthesis paper, published prior to the public data  
453 release of FLUXNET-CH<sub>4</sub> Version 1.0, had 60 unique sites and 139 site-years with annual CH<sub>4</sub> emissions estimates  
454 (Knox et al., 2019). Freshwater wetlands make up the majority of sites ( $n = 42$ ), and the dataset also includes five salt  
455 marshes and one mangrove wetland. Notable additions to FLUXNET-CH<sub>4</sub> from the previous unpublished dataset  
456 used in Knox et al., (2019) include six tropical sites (between 20° S and 20° N), including one site in South America,  
457 two sites in southern Africa, and three sites in Southeast Asia. The 15 upland sites include six needleleaf forests, three  
458 crop sites (excluding rice), two alpine meadows, one grassland, one mixed forest, one tundra, and one urban site. The  
459 drained sites represent former wetlands that have been artificially drained for use as grasslands ( $n = 3$ ) or croplands

460 (n = 3). FLUXNET-CH4 sites span the globe, though are concentrated in North America and Europe (Fig. 3). Table  
 461 B3 includes characteristics of all sites in the dataset.

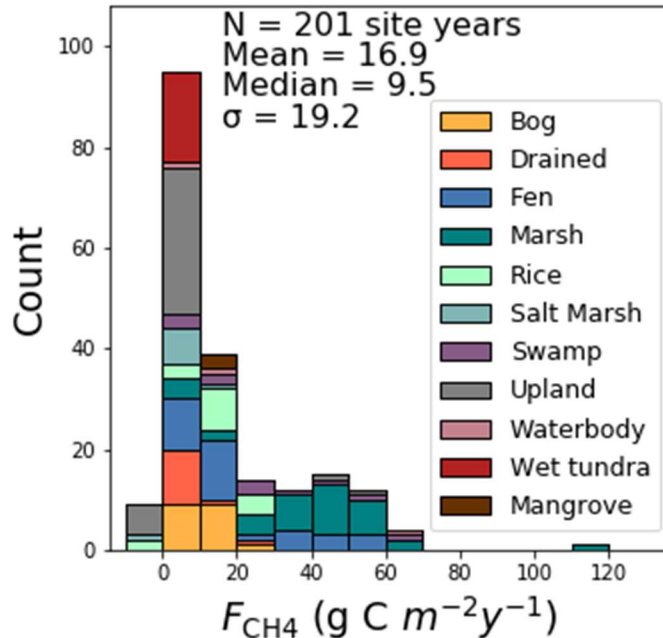


Subpanels as defined on global map:



462

463 Figure 3. Global map of FLUXNET-CH4 Version 1.0 site locations colored by site type. Insets (a)-(d) show sites that were  
 464 too closely located to distinguish in the global map.



465

466 **Figure 4. Histogram of annual methane fluxes ( $F_{CH_4}$ ,  $g C m^{-2} yr^{-1}$ ) grouped by site type.**

467 Sites represent a range of ecosystem types, latitudes, median fluxes, and seasonality patterns (Table 1).  
 468 Across all FLUXNET-CH<sub>4</sub> sites, mean average annual CH<sub>4</sub> flux is positively skewed with a median flux of 9.5 g C  
 469 m<sup>-2</sup> yr<sup>-1</sup>, a mean flux of 16.9 g C m<sup>-2</sup> yr<sup>-1</sup>, and numerous annual CH<sub>4</sub> fluxes exceeding 60 g C m<sup>-2</sup> yr<sup>-1</sup>. Marshes and  
 470 swamps have the highest median flux, and upland, salt marsh, and tundra sites have the lowest (Fig. 4). Lake  
 471 emissions are highly variable due to one high-flux lake site (JP-SWL). Flux data at many sites show strong  
 472 seasonality in CH<sub>4</sub> emissions, but data coverage is also lower outside the growing season (Table 1). Data coverage  
 473 is lowest during the JFM quarter (on average 20% of half-hourly time periods contain flux data) reflecting the  
 474 predominance of Northern hemisphere sites and the practical difficulties in maintaining EC tower sites during colder  
 475 winter months (Table 1). Bogs, fens, and marshes have pronounced seasonality, with fluxes being highest in the  
 476 AMJ and JAS quarters. In contrast, CH<sub>4</sub> fluxes from uplands, drained sites, and salt marshes are more uniform and  
 477 low year-round.

478 **Table 1: Summary table of sites grouped by ecosystem class reporting annual mean flux (Ann\_Flux) and standard**  
 479 **deviation from inter-annual variability (Ann\_Flux\_SD), site-years of data, % data cover per quarter, and median (med.)**  
 480 **flux across site class. JFM= January, February, March; AMJ = April, May, June; JAS = July, August, September; OND**  
 481 **= October, November, December.**

	# of Sites	# of Site-Years	Ann_Flux g C m <sup>-2</sup> year <sup>-1</sup>	Ann_Flux_SD g C m <sup>-2</sup> year <sup>-1</sup>	JFM coverage (%)	AMJ coverage (%)	JAS coverage (%)	OND coverage (%)	JFM flux (med.)	AMJ flux (med.)	JAS flux (med.)	OND flux (med.)
Salt marsh	5	10	2.9	4.7	7	42	50	37	1.5	1.7	2.1	1.6
Wet tundra	11	39	3.8	1.8	8	28	40	18	0.4	2.6	8.1	3.2

Upland	15	47	4.0	10.5	23	35	39	28	1.2	0.5	1.4	0.8
Drained	7	20	6.3	7.1	22	39	39	29	4.6	3.6	5.1	3.6
Bog	7	32	10.5	6.4	8	27	37	18	7.2	11.0	24.8	9.5
Mangrove	1	3	11.1	0.5	46	28	30	41	3.2	7.2	22.5	14.1
Rice	7	20	14.4	8.8	16	37	45	27	3.2	11.9	43.1	4.2
Fen	8	40	20.5	16.0	29	43	40	30	2.8	14.2	26.0	6.4
Swamp	6	15	26.4	19.9	24	34	29	19	14.7	24.9	31.0	24.4
Lake	2	4	28.2	33.4	15	13	27	36	0.2	47.6	90.2	40.3
Marsh	10	42	40.8	20.7	22	43	53	30	13.5	55.0	85.8	36.1

482

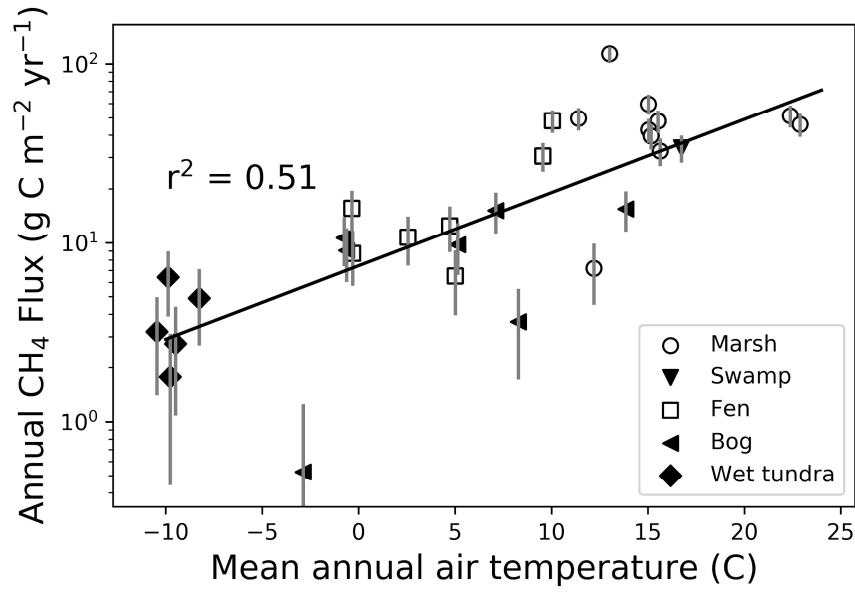
483

### 484 3.1.2 Freshwater wetland CH<sub>4</sub> characteristics

485 The FLUXNET-CH<sub>4</sub> Version 1.0 dataset contains 42 freshwater wetlands that span 37°S to 69°N, including  
486 bogs, fens, wet tundra, marshes, and swamps, and a range of annual CH<sub>4</sub> emission rates (Fig. 4). The majority of  
487 freshwater wetlands in our dataset emit 0-20 g C m<sup>-2</sup> yr<sup>-1</sup>, with 10 emitting 20-60 g C m<sup>-2</sup> yr<sup>-1</sup>, and one more than 60 g  
488 C m<sup>-2</sup> yr<sup>-1</sup>. Differences in annual CH<sub>4</sub> flux among wetland types is partially driven by temperature (which is often  
489 linked to site type), with mean annual air temperature explaining 51% of the variance between sites (Fig. 5, exponential  
490 relationship). The global relationship between annual methane emissions and temperature can be described using a  
491 Q<sub>10</sub> relationship where  $Q_{10} = R_2/R_1^{((T_2-T_1)/10)}$ , with R<sub>2</sub> and R<sub>1</sub> being the CH<sub>4</sub> emission rates at temperatures T<sub>2</sub> and T<sub>1</sub>,  
492 respectively (temperature in degrees C). The Q<sub>10</sub> based on Fig. 5 data is 2.57. We also note that annual CH<sub>4</sub> flux from  
493 individual biomes may have different relationships with temperature, as previous work has shown biome-specific  
494 trends in CH<sub>4</sub> flux with environmental drivers (Abdalla et al., 2016). However, there currently are not enough data  
495 points in each biome category to compare relationships between mean annual CH<sub>4</sub> flux and temperature. Annual CH<sub>4</sub>  
496 flux is not correlated with mean annual water table depth in FLUXNET-CH<sub>4</sub>, unlike in Knox et al., (2019), which  
497 used a subset of the FLUXNET-CH<sub>4</sub> sites where CH<sub>4</sub> flux was correlated with water table depth only for sites with  
498 water table below ground for 90% of measured days ( $r^2 = 0.31$ ,  $p < 0.05$ ,  $n = 27$  site years). Freshwater wetland  
499 seasonality is further described in Sect. 3.3.

500

501



502  
 503 **Figure 5: Relationship between mean annual wetland methane (CH<sub>4</sub>) flux (g C m<sup>-2</sup> yr<sup>-1</sup>, logarithmic scale) and mean**  
 504 **annual air temperature (°C) for each freshwater wetland site, with wetland type indicated by symbol. Markers represent**  
 505 **individual site means, with vertical error bars representing the standard deviation of interannual variability.**

506

507

508 **3.1.3 Upland, rice and urban CH<sub>4</sub> characteristics**

509 Upland agricultural sites are characterized by a lack of seasonal pattern in CH<sub>4</sub> emissions, relatively low flux,  
 510 and sometimes negative daily flux (i.e., CH<sub>4</sub> uptake) averages. All of the upland non-agricultural sites in FLUXNET-  
 511 CH<sub>4</sub> Version 1.0 are net (albeit weak) CH<sub>4</sub> sources except for the needleleaf forest site US-Ho1, which has mean  
 512 annual CH<sub>4</sub> flux of  $-0.1 \pm 0.1$  g C m<sup>-2</sup> yr<sup>-1</sup> (see Table B3 for site acronyms and metadata). The average agricultural site  
 513 emissions are  $1.3 \pm 0.8$  g C m<sup>-2</sup> yr<sup>-1</sup> and non-agricultural site emissions are  $1.6 \pm 1.2$  g C m<sup>-2</sup> yr<sup>-1</sup> across sites.

514 Rice sites (n = 7) have average annual emissions across all sites of  $16.7 \pm 7.7$  g C m<sup>-2</sup> yr<sup>-1</sup> and are characterized  
 515 by strong seasonal patterns, with either one or more CH<sub>4</sub> emission peaks per year depending on the number of rice  
 516 seasons and field water management. One peak is typically observed during the reproductive period for the  
 517 continuously flooded sites with one rice season (i.e., US-HRC, JP-MSE) (Iwata et al., 2018; Runkle et al., 2019;  
 518 Hwang et al., 2020). For sites with only one rice season but with single or multiple drainage and re-flooding periods,  
 519 a secondary peak may appear before the reproductive peak (i.e., KR-CRK, IT-Cas, and US-HRA; Meijide et al., 2011;  
 520 Runkle et al., 2019; Hwang et al., 2020). Two reproductive peaks appear for sites with two rice seasons (i.e., PH-RiF),  
 521 and each reproductive peak may be accompanied by a secondary peak due to drainage events (Alberto et al., 2015).  
 522 Even sites with one, continuously flooded rice season may experience a second peak if the field is flooded during the  
 523 fallow season to provide habitat for migrating birds (e.g., US-Twt; Knox et al., 2016).

524 The dataset has one year of urban data from site UK-LBT in London, England. UK-LBT observes CH<sub>4</sub> fluxes  
 525 from a 190 m tall communications tower in the center of London, and has a mean annual CH<sub>4</sub> flux of  $46.5 \pm 5.6$  g C  
 526 m<sup>-2</sup> yr<sup>-1</sup>. This flux is more than twice as high as the mean annual CH<sub>4</sub> flux across all FLUXNET-CH<sub>4</sub> sites,  $16.9$  g C  
 527 m<sup>-2</sup> yr<sup>-1</sup>. The London site has higher CH<sub>4</sub> emissions in the winter compared to summer, which is attributed to a seasonal  
 528 increase in natural gas usage (Helfter et al., 2016.)

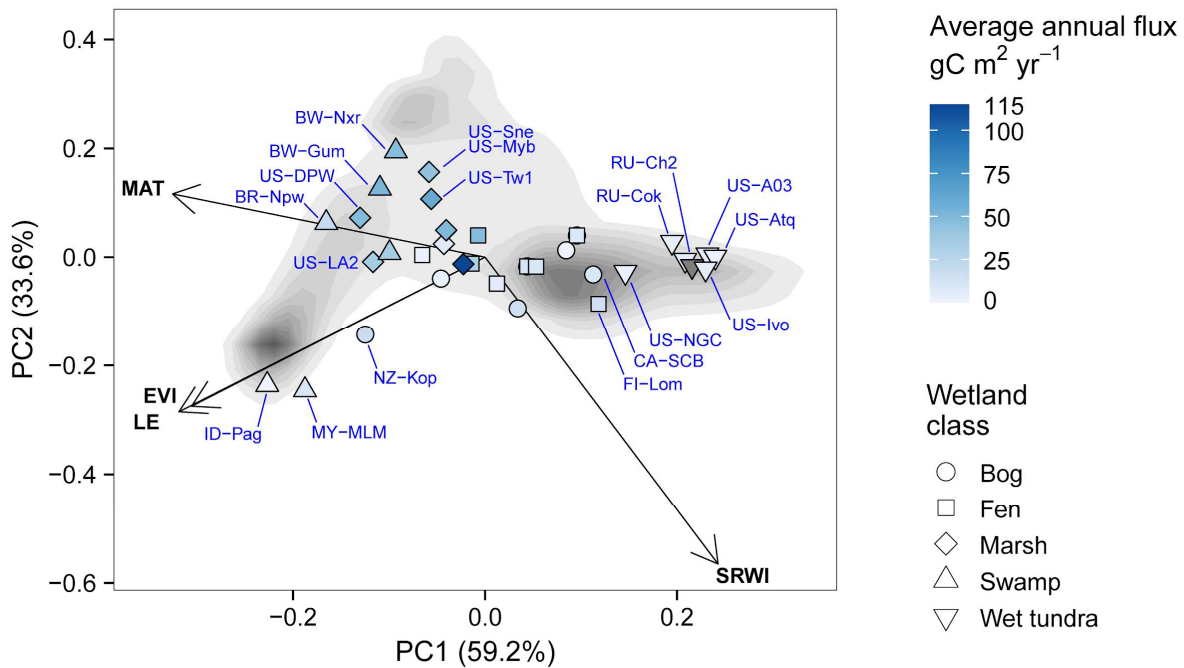
### 529 3.1.4 Saltwater and mangrove wetland CH<sub>4</sub> characteristics

530 Three of the five saltwater wetlands in FLUXNET-CH<sub>4</sub> (US-Edn, US-MRM, and US-Srr) have a very low  
531 mean annual CH<sub>4</sub> flux (see Table B2 for individual site-year CH<sub>4</sub> flux sums and associated uncertainty) and minimal  
532 seasonality. Two other FLUXNET-CH<sub>4</sub> saltwater sites (US-La1 and US-StJ) have significantly higher fluxes, with  
533 annual sums of  $12.6 \pm 0.6$  and  $9.6 \pm 1.0$  g C m<sup>-2</sup> yr<sup>-1</sup>, respectively, while the mangrove site HK-MPM has annual mean  
534 fluxes of  $11.1 \pm 0.5$  g C m<sup>-2</sup> yr<sup>-1</sup>. This range of CH<sub>4</sub> fluxes across different saltwater ecosystems could be valuable for  
535 exploring the effect of salinity and different biogeochemical pathways of CH<sub>4</sub> production, oxidation, and transport of  
536 CH<sub>4</sub> (Bartlett et al., 1987; Poffenbarger et al., 2011). Saltwater wetlands along the coast have unique CH<sub>4</sub> dynamics  
537 attributable to the presence of abundant electron acceptors, most importantly sulphates, which inhibit methanogenesis  
538 (Pattnaik et al., 2000; Mishra et al., 2003; Weston et al., 2006), but at low concentrations can have no effect (Chambers  
539 et al., 2011) or even increase methanogenesis (Weston et al., 2011). In fact, estuarine wetlands with moderate salinity  
540 can still be significant sources of CH<sub>4</sub> (Liu et al., 2020). Even under sulfate-rich conditions, high CH<sub>4</sub> production can  
541 be found via methylotrophic methanogenesis (Dalcin Martins et al. 2017; Seyfferth et al., 2020,) or because the  
542 processes of sulfate reduction and methanogenesis are spatially separated (Koebsch et al., 2019). Consequently,  
543 representing the biophysical drivers of ecosystem-scale CH<sub>4</sub> fluxes in non-freshwater wetlands is challenging and may  
544 represent a combination of competing or confounding effects (Vazquez-Lule and Vargas 2021).  
545

### 546 3.2 Wetland Representativeness

547 We evaluated the representativeness of freshwater wetland sites in the FLUXNET-CH<sub>4</sub> Version 1.0 dataset  
548 against wetlands globally based on bioclimatic conditions of our sites. When evaluating bioclimatic variables  
549 individually, the distribution across the network was significantly different from the global distribution ( $\alpha > 0.05$ ;  
550 two-tailed Kolmogorov-Smirnov tests; see Table B4).

551 When considering the four bioclimatic variables, MAT, LE, EVI and SRWI in a PCA, we found that our  
552 tower network generally samples the bioclimatic conditions of global wetland cover, but some noticeable gaps remain  
553 (Fig. 6). Three clusters of the world's wetland-dense regions are identified, but are not equally sampled by the network.  
554 A cluster of low temperature wetlands is sampled by a large number of high-latitude sites. The other two wetland  
555 clusters are not as well sampled: a high temperature and LE cluster is represented only by two towers (ID-Pag and  
556 MY-MLM), while drier and temperate and subtropical wetlands including large swathes of the Sahel in Africa only  
557 have a site in Botswana (BW-Npw) as their closest-analog tower.  
558



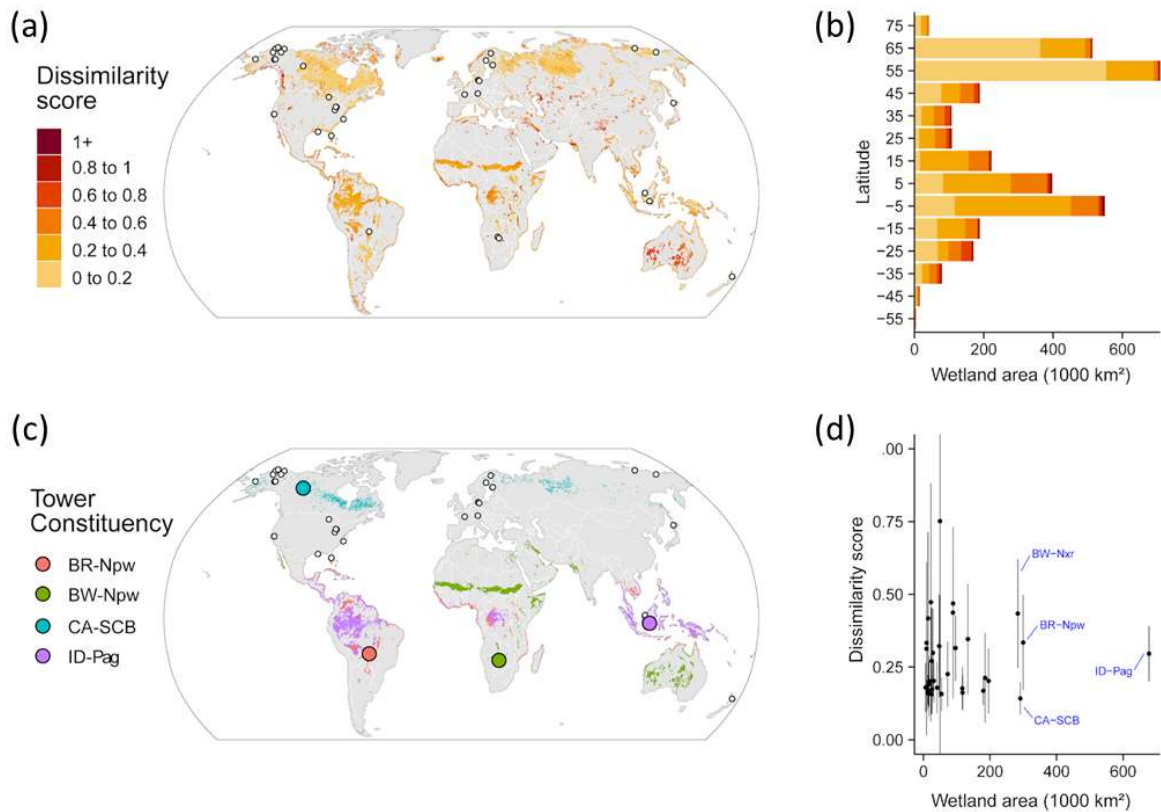
559

560 **Figure 6: Principal Component Analysis displaying the distribution of freshwater wetland sites (points) along the two main**  
 561 **principal components together accounting for 91.9% of variance. Tower sites are represented as points with shapes**  
 562 **indicating their wetland type and color shade representing the annual methane (CH<sub>4</sub>) flux (gray points represent sites for**  
 563 **which <6 months of flux data was available to estimate annual budget). Sites codes are labeled in blue text for selected sites**  
 564 **deviating from average conditions. Loading variables are represented by the arrows: mean annual temperature (MAT),**  
 565 **simple ratio water index (SRWI), latent heat flux (LE) and enhanced vegetation index (EVI). The background shades of**  
 566 **gray are a qualitative representation of the density of global wetland pixels and their distribution in the PCA climate-space,**  
 567 **with darker color representing higher densities (excluding Greenland and Antarctica). Only grid cells with >5% average**  
 568 **wetland fraction according to the WAD2M over 2000-2018 are included (Zhang et al., 2020). The loading variables are**  
 569 **represented by the arrows: mean annual temperature (MAT), simple ratio water index (SRWI), latent heat flux (LE) and**  
 570 **enhanced vegetation index (EVI).**

571

572 Evaluating the bioclimatic dissimilarity of global wetlands to the FLUXNET-CH<sub>4</sub> network shows the least  
 573 captured regions are in the tropics (Fig. 7A). Sparse coverage in the tropics also means that the few existing towers  
 574 occupy a critical place in the network, particularly as tropical wetlands are the largest CH<sub>4</sub> emitters (Bloom et al.,  
 575 2017; Poulter et al., 2017). Highly dissimilar wetlands are limited in extent and distributed across all latitudes, but the  
 576 average dissimilarity is higher in north temperate (55° to 65°) and tropical (-5° to 5°) latitudes (Fig. 7B). To evaluate  
 577 the importance of individual towers in the network, we estimated the geographical area to which it is most analogous  
 578 in bioclimate-space (Fig. 7C). We found that some towers have disproportionately large constituencies (i.e., wetland  
 579 areas that share the same closest bioclimatic analog tower). Towers in Indonesia (ID-Pag), Brazilian Pantanal (BR-  
 580 Npw), and Botswana floodplains (BW-Nxr) represent the closest climate analog for much of the tropics (678, 300 and  
 581 284 thousand km<sup>2</sup>, respectively) while CA-SCB represents a vast swath (291 thousand km<sup>2</sup>) of boreal/arctic regions  
 582 (Fig. 7D).

583



584

585 **Figure 7: (a) Distance in bioclimatic space between global land surface and the FLUXNET-CH4 Version 1.0 tower network**  
 586 **(gray areas indicate no mapped wetlands). The Euclidean distance was computed on the four bioclimatic variables and was**  
 587 **then standardized by the average distance within-network. Most of the land surface has a dissimilarity score lower than 1,**  
 588 **meaning these areas are closer than the average tower distance (lower dissimilarity score means a similar bioclimate to that**  
 589 **represented by towers in the network). However, this pattern reflects more the sparsity of the tower network than a**  
 590 **similarity of the land surface to the network. Areas with <5% coverage by wetlands were excluded to focus on wetland-**  
 591 **dense regions. (b) Latitudinal distribution of dissimilarity score, (c) Map of the four largest tower constituencies, (d)**  
 592 **Scatterplot of wetland area in each tower constituency plotted against the average dissimilarity score (point) and +/-**  
 593 **standard deviation (error bar).**

594 Our assessment of wetland CH<sub>4</sub> tower coverage determines the ability of our dataset to represent global  
 595 wetland distributions and highlights some clear representation gaps in the network, particularly in tropical and humid  
 596 regions. Other geographic regions such as India, China and Australia, where towers exist but are not included in the  
 597 current network should be prioritized when expanding the network, even though they are not among the most distant  
 598 areas to the current network. Similar representativeness assessments have been developed for CO<sub>2</sub> tower networks to  
 599 identify gaps and priorities for expansion (Jung et al., 2009). To improve the geographic coverage of the network for  
 600 representing global-scale fluxes, locations for new tower sites can be targeted to cover bio-climatically distant areas  
 601 from the current network (Villarreal et al., 2019). Candidate regions for expansion that are both high CH<sub>4</sub> emitting  
 602 (Saunio et al., 2020) as well as located in under-sampled climates are: African Sahel, Amazon basin, Congo basin,  
 603 South-East Asia. Climatic conditions over boreal and arctic biomes are generally better represented (primarily at lower  
 604 elevations), but there is scope to expand the network in wetland-dense regions like the Hudson Bay Lowlands and  
 605 Northern Siberian Lowlands. Moreover, establishing sites in other ecosystem types, especially lakes and reservoirs  
 606 (see Deemer et al. 2016, Bastviken et al. 2011, Matthews et al. 2020) in most climatic zones would help capture CH<sub>4</sub>  
 607 fluxes from these ecosystems.

608 Understanding the representativeness of the network is essential when inferring general patterns of flux  
 609 magnitude, seasonality, and drivers from the tower data (Villarreal et al., 2018). We produced a first-order

610 representativeness of average bioclimatic conditions, but temporal representativeness (across seasons, climate  
611 anomalies and extreme events) is particularly needed given the episodic nature of CH<sub>4</sub> fluxes (Chu et al., 2017;  
612 Mahecha et al., 2017; Göckede et al., 2019).

613 Assessing representation of wetland CH<sub>4</sub> sites is complicated by the fact that wetlands occupy only a fraction  
614 of most landscapes (except wetland dense regions such as Northern Siberian Lowlands, Hudson Bay Lowlands, Congo  
615 basin, etc.) and that not all relevant factors affecting CH<sub>4</sub> production and consumption could be considered in our  
616 analysis. For instance, our assessment of representation did not consider wetland types as such maps are limited by  
617 the inherent difficulties in remotely sensing wetland features (Gallant, 2015). The attribution of representativeness is  
618 further complicated by the fact that many EC tower locations are subject to small-scale variability within the field of  
619 view, or footprint, of the sensor. Consequently, the individual time steps within EC flux time series may represent a  
620 mixture of different wetland types, or different fractions of wetland contribution to the total CH<sub>4</sub> flux, varying with  
621 wind direction, atmospheric stability, or season (Chu et al 2021). This further complicates upscaling efforts.  
622 Additionally, this representativeness analysis did not apply weights to the drivers to reflect their varying influence on  
623 CH<sub>4</sub> flux. Such weights can be included in future versions as they are generated by a cross-validated machine learning  
624 approach (Jung et al., 2020). Future efforts could include the dissimilarity index from this analysis as a metric of  
625 extrapolation in a CH<sub>4</sub> flux upscaling effort.

626

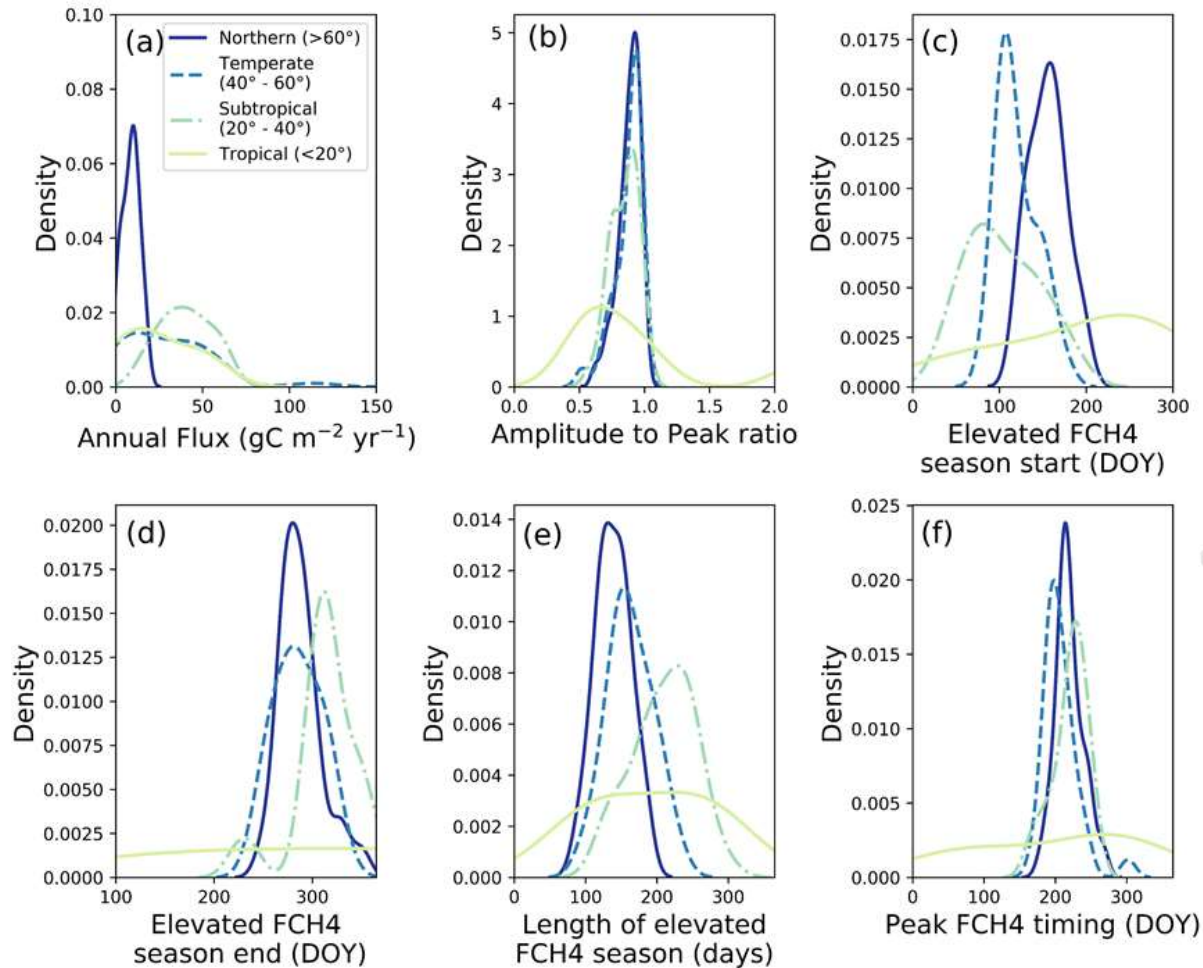
### 627 3.3 Freshwater wetland flux seasonality

#### 628 3.3.1 Seasonal flux comparisons by latitudinal bands

629 CH<sub>4</sub> flux and seasonality varied substantially across latitudinal bands (northern, temperate, subtropical, and  
630 tropical) (Fig. 8). Annual CH<sub>4</sub> fluxes for temperate, and subtropical sites were significantly higher than for northern  
631 sites ( $8.7 \pm 5.0$ ,  $29.7 \pm 25.2$ ,  $40.1 \pm 14.6$ , and  $24.5 \pm 20.7$  g C m<sup>-2</sup> yr<sup>-1</sup> for northern, temperate, subtropical, and tropical,  
632 respectively,  $p < 0.0001$  using Kruskal Wallis and post hoc comparisons; Fig. 8a), and tropical sites were similar to all  
633 other latitudinal bands likely because of their small sample size. The ratio of seasonal amplitude to peak flux provides  
634 a measure of the relative seasonal increase in emissions compared with baseline, where a ratio of zero indicates no  
635 seasonal change in amplitude, a ratio of one indicates the off-season flux is zero, and values over one means the off-  
636 season baseline CH<sub>4</sub> fluxes were negative (i.e., uptake). Average amplitude to peak flux ratios were similar across all  
637 latitudinal bands ( $0.9 \pm 0.1$ ,  $0.9 \pm 0.1$ ,  $0.9 \pm 0.1$ ,  $1.0 \pm 0.7$ , for northern, temperate, subtropical, and tropical,  
638 respectively; Fig. 8b). The spring increase in CH<sub>4</sub> emissions began later in northern sites compared with temperate  
639 and subtropical sites (end of May versus April, respectively,  $p = 0.001$ ; Fig. 8c), while tropical sites vary widely in  
640 elevated emission season start date. Northern sites also had shorter elevated CH<sub>4</sub> flux season lengths ( $138 \pm 24$  days)  
641 compared to temperate sites ( $162 \pm 32$  days), and both were shorter than subtropical sites ( $209 \pm 43$  days;  $p < 0.0001$ ;  
642 Fig. 8e). On average, CH<sub>4</sub> flux peaked earlier for temperate sites compared to northern ( $p = 0.008$ ) and subtropical  
643 sites ( $p = 0.02$ ; mid to late July compared with early August; Fig. 8f), while tropical sites again vary widely. Given  
644 their unique seasonality, and low number of site-years ( $n = 9$ ), tropical systems are discussed separately in Sect. 3.3.3,  
645 and not included in the comparisons in the remainder of this section. While our results on CH<sub>4</sub> seasonality corroborate  
646 expected trends for these latitudinal bands, they provide some of the first estimates of CH<sub>4</sub> seasonality parameters and  
647 ranges across a global distribution of sites.

648

649

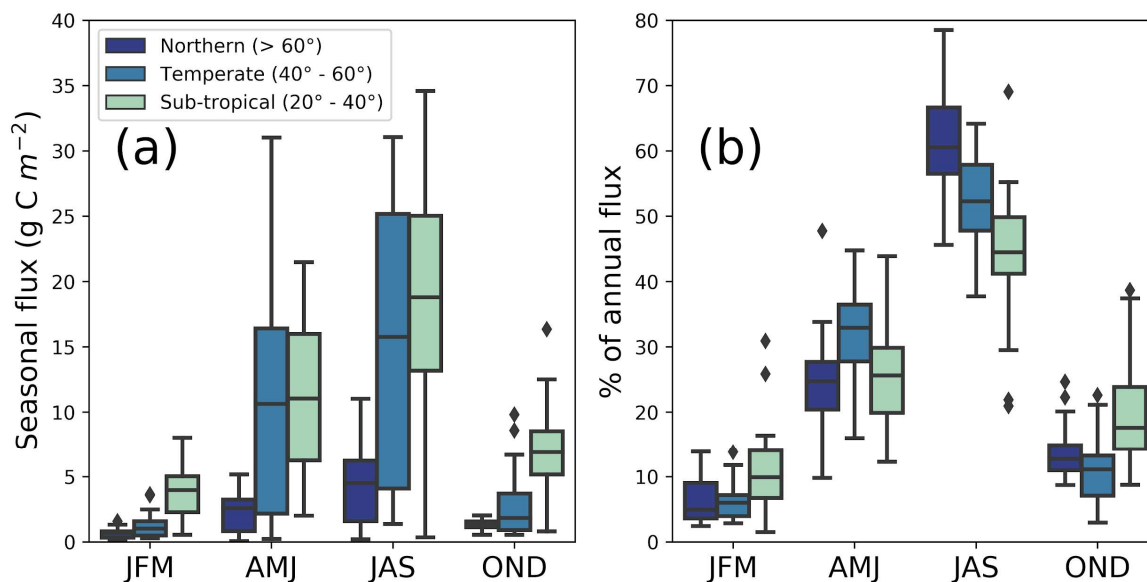


650  
 651  
 652 **Figure 8: (a) Annual methane (CH<sub>4</sub>) flux (g C m<sup>-2</sup> yr<sup>-1</sup>), (b) Ratio of seasonal amplitude to seasonal peak, where values of 0**  
 653 **indicate uniform annual CH<sub>4</sub> flux, values of one indicate zero off-season fluxes, and values exceeding one indicate negative**  
 654 **off-season fluxes, (c) CH<sub>4</sub> flux (FCH<sub>4</sub>) elevated emissions season start by day of year (DOY), (d) FCH<sub>4</sub> elevated emissions**  
 655 **season end by DOY, (e) Length of elevated CH<sub>4</sub> flux season (days), and (f) DOY of peak FCH<sub>4</sub>. Northern (dark blue, solid**  
 656 **line), Temperate (blue, dashed line), Sub-tropical (green, dot-dash line) and Tropical (light green, solid line) wetlands**  
 657 **plotted using the kernel density function. Each panel has lines that represent latitudinal bands as follows: northern (> 60°),**  
 658 **temperate (between 40° and 60°), subtropical (between 20° and 40°), and tropical (< 20°), though the site-year totals vary**  
 659 **between these groups (n = 57, n = 36, n = 39, and n = 9 respectively). All total CH<sub>4</sub> flux values and elevated season start**  
 660 **values are positive, and the apparent continuation of the data distribution into negative values is an artifact of the kernel**  
 661 **density function. Southern Hemisphere sites below 20° S were shifted by 182 days to make summer the middle of the year**  
 662 **for comparability with Northern Hemisphere sites.**  
 663

664 We found that latitudinal groups showed strong differences in absolute CH<sub>4</sub> flux across quarters, and narrower  
 665 differences in percentage of annual CH<sub>4</sub> flux (Fig. 9a versus 9b). Thus, the AMJ quarter had a similar relative  
 666 contribution to the annual CH<sub>4</sub> flux across latitudes, regardless of the absolute annual CH<sub>4</sub> flux. CH<sub>4</sub> fluxes (Fig. 9a)  
 667 were highest during JAS for northern, temperate, and subtropical sites and highest in AMJ and JAS for temperate sites  
 668 (p<0.01). Though CH<sub>4</sub> fluxes in northern sites are most commonly measured during warm summer months (Sachs et  
 669 al., 2010; Parmentier et al., 2011), fluxes in JFM and OND (50% of the yearly duration) on average make up 18.1 ±  
 670 3.6%, 15.3 ± 0.1%, and 31.2 ± 0.1% (northern, temperate, subtropical, respectively) of annual emissions. This pattern  
 671 indicates that a substantial fraction of annual CH<sub>4</sub> fluxes occurs during cooler months. The contribution of non-

672 growing season CH<sub>4</sub> emissions to annual CH<sub>4</sub> fluxes has previously been described for arctic and boreal regions (Zona  
 673 et al., 2016; Treat et al., 2018) and our analysis suggests comparable contributions in temperate and subtropical  
 674 systems for the same quarterly periods.

675  
 676  
 677



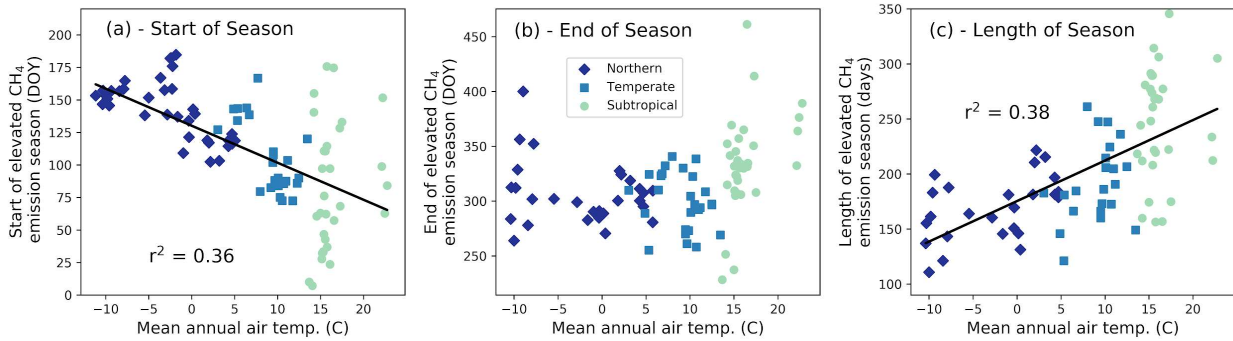
678  
 679  
 680  
 681  
 682  
 683  
 684  
 685  
 686

**Figure 9: (a) Quarterly contribution to total annual CH<sub>4</sub> flux in g C m<sup>-2</sup>, and (b) percentage of annual CH<sub>4</sub> flux. Sites were divided into northern (> 60° N), temperate (40° N - 60° N), and subtropical (20° N - 40° N). Quarters with continuous data gaps exceeding 30 days were excluded. We used the following quarterly periods: January/February/March (JFM), April/May/June (AMJ), July/August/September (JAS), and October/November/December (OND). Tropical sites are discussed separately in Sect. 3.3.3 because of their unique seasonality and low number of sites.**

### 687 3.3.2 Predictors of CH<sub>4</sub> flux phenology

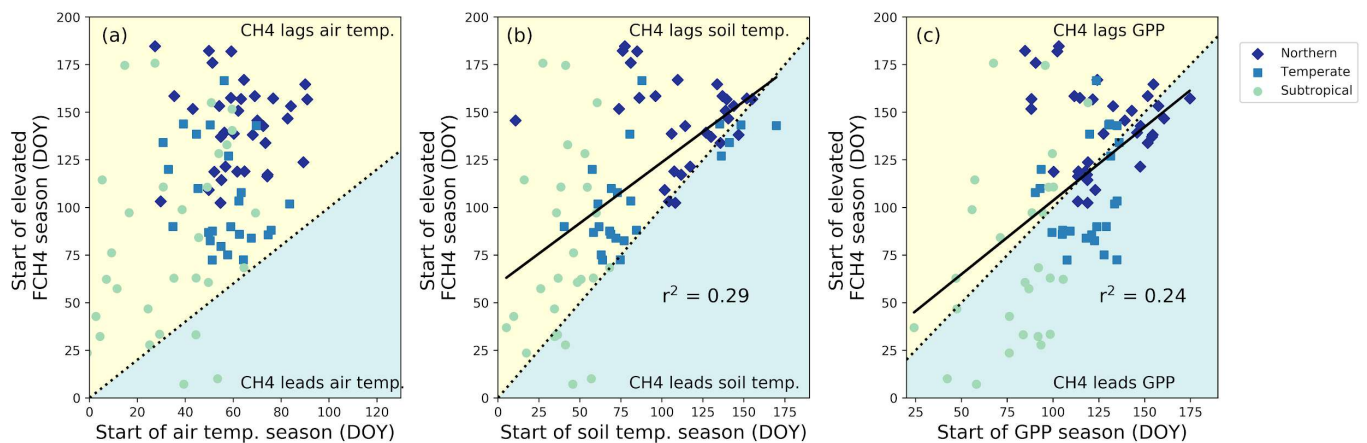
688 The start of the elevated CH<sub>4</sub> flux season, and how long the elevated flux season lasts, correlated strongly  
 689 with mean annual air temperature (Fig. 10; p<0.0001 for each). Methane flux began to increase roughly two months  
 690 earlier in the warmest systems (mean annual temperature > 20 °C) compared to the coldest (mean annual  
 691 temperature near -10 °C), though several of the warmer sites had high variability. Our data suggest that the CH<sub>4</sub>  
 692 season started  $2.8 \pm 0.5$  days earlier for every degree Celsius increase in mean annual temperature (Fig. 10a). In  
 693 contrast, the end of the CH<sub>4</sub> emission season was not correlated with mean annual temperature, but a positive trend  
 694 existed despite high variability in warmest and coldest sites (Fig. 10b). The high variability seen in the end of CH<sub>4</sub>  
 695 season at northern sites is important to note and would likely be better resolved by incorporating other seasonality or  
 696 phenological characteristics, such as moisture, active layer depth, and plant community composition (e.g., Kittler et  
 697 al., 2017). Plants with aerenchymatous tissue, for example, influence the timing of plant-mediated CH<sub>4</sub> flux and are  
 698 a key source of uncertainty while predicting CH<sub>4</sub> seasonality for northern wetlands (Xu et al., 2016, Kwon et al.,  
 699 2017). Despite the relative lack of trend with season end date, the season length was still positively correlated with  
 700 mean annual temperature, with the warmest sites having roughly three more months of seasonally elevated CH<sub>4</sub>  
 701 emissions than the coldest sites (Fig. 10c). CH<sub>4</sub> season length increased  $3.6 \pm 0.6$  days for every degree Celsius  
 702 increase in mean annual temperature (note that these relationships are correlations, and we cannot disentangle

703 causality with this analysis). Temperature is highly correlated with other parameters (i.e., radiation, days of snow  
 704 cover, etc.), so CH<sub>4</sub> flux is also likely to correlate with other environmental parameters.



705  
 706 **Figure 10.** The (a) start of the elevated methane (CH<sub>4</sub>) emission season ( $y = -2.8x + 130$ , with ‘x’ in °C and ‘y’ in day of  
 707 year (DOY)), (b) the end of the elevated emission season in DOY, and (c) the length of the emission season with mean  
 708 annual site air temperature ( $y = 3.6x + 176.6$ , with ‘x’ in °C and ‘y’ in days). Each point represents a site-year of data and  
 709 all reported  $r^2$  are significant to  $p < 0.0001$ . Tropical sites are discussed separately in Sect. 3.3.3.

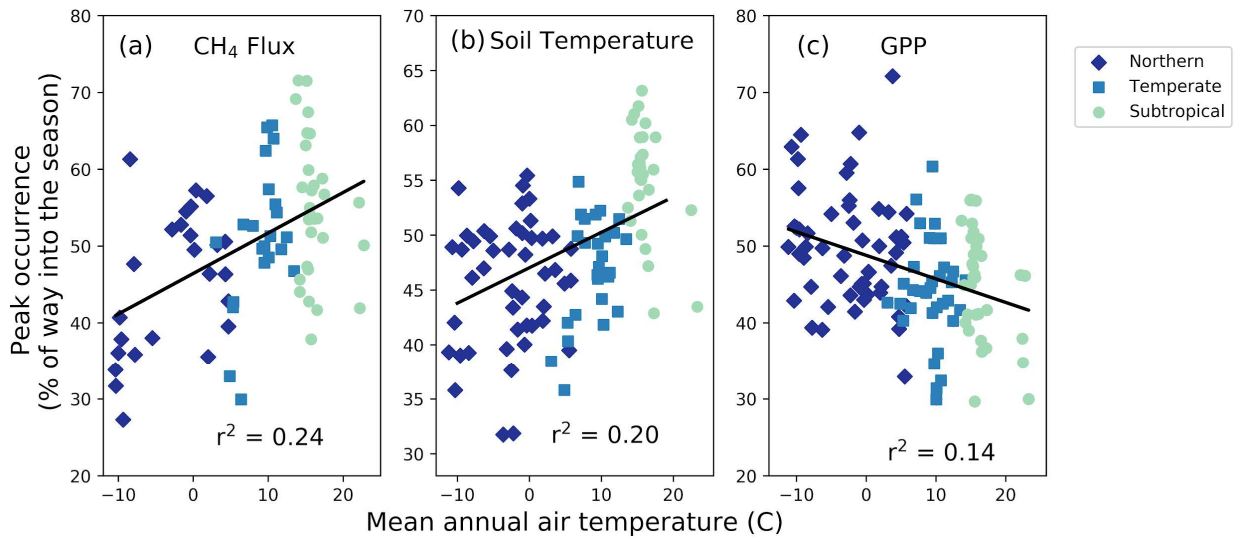
710 Although the spring onset of increasing CH<sub>4</sub> emissions correlated with mean annual air temperature, on  
 711 average it lagged the spring increase in the shallowest soil temperatures by  $31 \pm 40$  days (Fig. 11, lag is significantly  
 712 different than zero,  $p < 0.001$ ), with very few instances of CH<sub>4</sub> emissions beginning before seasonal soil  
 713 temperatures increase (and by  $20 \pm 50$  days for the deepest temperature probes). In contrast, for roughly half of the  
 714 sites, CH<sub>4</sub> emission increased prior to seasonal GPP (a proxy for fresh substrate availability) increases. This  
 715 suggests that the initiation of increased CH<sub>4</sub> fluxes at the beginning of the season was not limited by availability of  
 716 substrate derived from recent photosynthate. Additionally, the onset of CH<sub>4</sub> fluxes tended to occur closer to the  
 717 onset of soil temperature increase for cooler temperature sites (sites with later start dates tend to be cooler; Fig. 11a).  
 718 This result is likely attributable to the direct influence of increased temperature on microbial processes (Chadburn et  
 719 al., 2020), as well as the indirect influences of snow melt, both via release of CH<sub>4</sub> from the snowpack as well as a  
 720 higher water table leading to more CH<sub>4</sub> production (Hargreaves et al., 2001; Tagesson et al., 2012; Mastepanov et  
 721 al., 2013; Helbig et al., 2017). These observed trends hold for the entire temperature or GPP range of freshwater  
 722 wetland sites, but are not necessarily applicable within individual latitudinal bands.



723  
 724

725 **Figure 11. Relationship between the onset of the methane (CH<sub>4</sub>) emission season to (a) the beginning of the air**  
 726 **warming by day of year (DOY), (b) soil warming at the shallowest probe depth per site by DOY, and (c) gross primary**  
 727 **productivity (GPP) increase for the subset of sites with soil temperature data by DOY. Each point represents a site-year**  
 728 **of data. Dashed lines represent a 1:1 relationship, solid lines are significant (p < 0.05) regression fits. On average, the**  
 729 **CH<sub>4</sub> emission season lags the soil temperature increase by 31 ± 40 days, and is more synchronous with GPP.**

730 In contrast with the CH<sub>4</sub> season-start timing, the timing of the CH<sub>4</sub> peak did not correlate with either the  
 731 timing of the soil temperature peak or the GPP peak (Fig. A1). For 63% of the sites, the average timing of peak CH<sub>4</sub>  
 732 emissions lagged the soil temperature peak, and at 83% of the sites average peak CH<sub>4</sub> lagged peak GPP (Fig. A1).  
 733 Although there was no simple relationship between absolute CH<sub>4</sub> peak timing and the environmental drivers we  
 734 investigated, there was a correlation (p = 0.0005) between the relative timing of peak CH<sub>4</sub> compared to season onset  
 735 (calculated as described in Section 2.3) and mean annual air temperature (Fig. 12a). For cooler sites, the peak of  
 736 seasonal CH<sub>4</sub> emissions occurred closer to the onset of the CH<sub>4</sub> emission season than the end of the season, resulting  
 737 in an asymmetrical seasonal CH<sub>4</sub> flux shape that is illustrated in Fig. 2a. Soil temperature also peaked earlier in the  
 738 season for cooler wetlands, though the relationship is not as pronounced (p = 0.009, Fig. 12b). In contrast, GPP  
 739 peaked later in the season for cooler wetlands (p = 0.009, Fig. 12c). Previous work on Arctic sites (sites US-Ivo,  
 740 US-Beo, US-Atq, US-Bes, and RU-CH2) highlighted the asymmetrical annual CH<sub>4</sub> peak, with higher fall emissions  
 741 being attributed to the “zero curtain” period when soil below the surface remains thawed for an extended period of  
 742 time due to snow insulation (Zona et al., 2016; Kittler et al., 2017). Furthermore, soils can stay above the “zero  
 743 curtain” range for an extended time into the fall and winter (Helbig et al., 2017), which may also be caused by snow  
 744 insulation. The rapid onset of emissions in the spring following snowmelt could be attributed to the release of  
 745 accumulated CH<sub>4</sub> (Friborg et al., 1997), and other high latitude sites have seen similarly sharp increases in CH<sub>4</sub>  
 746 emissions at snowmelt (Dise, 1992, Windsor, 1992). However, not all studies in high latitudes have observed  
 747 asymmetrical CH<sub>4</sub> emission peaks, pointing to the inherent complexity of these ecosystems (Rinne et al., 2007;  
 748 Tagesson et al., 2012).



749  
 750 **Figure 12. Site-year peak methane (CH<sub>4</sub>) emission (a) and peak soil temperature (b) occur earlier in the season for sites**  
 751 **with lower mean annual temperatures. (c) Gross primary productivity (GPP) tends to peak earlier in the season for**  
 752 **warmer sites, though the trend is weak. All r<sup>2</sup> values are significant at p < 0.001. Each point represents a site-year of**  
 753 **data.**

### 754 3.3.3 Uniqueness of tropical wetlands

755 Tropical wetlands typically do not experience the large swings in temperature and GPP that contribute to  
756 CH<sub>4</sub> flux seasonality in temperate and northern sites. Indeed, the relatively constant high temperatures and high  
757 GPP in tropical ecosystems may lead to the lower ratio between seasonal amplitude and peak CH<sub>4</sub> flux compared  
758 with temperate and northern sites (Fig. 8b). Tropical flux sites have historically been under-studied, leading to a  
759 lack of synthesized information about these ecosystems. FLUXNET-CH<sub>4</sub> has five tropical wetland sites (latitude  
760 between 20° S and 20° N), and one tropical rice site, representing 13 site-years of data. These sites are especially  
761 insightful as they provide the first estimates of CH<sub>4</sub> fluxes from tropical, large seasonal floodplain systems.  
762

763 We found a broad range of annual CH<sub>4</sub> fluxes across tropical sites in FLUXNET-CH<sub>4</sub> Version 1.0. Annual  
764 CH<sub>4</sub> flux emissions from two Southeast Asian flooded peat forests were relatively low,  $0.01 \pm 0.1$  and  $9.5 \pm 0.6$  g C  
765 m<sup>-2</sup> yr<sup>-1</sup> for ID-PAG and MY-MLM, respectively, which is consistent with annual CH<sub>4</sub> fluxes measured at another  
766 peat forest in Indonesia (Deshmukh et al., 2020). In contrast, mean annual CH<sub>4</sub> flux for a seasonally flooded swamp  
767 in the Brazilian Pantanal region (BR-NPW) was over twice as high as MY-MLM, at  $19.2 \pm 2.5$  g C m<sup>-2</sup> yr<sup>-1</sup>.  
768 Similarly high annual CH<sub>4</sub> fluxes were observed at the two Botswana swamp sites in the Okavango Delta ( $51.7 \pm$   
769  $10.6$  and  $47.3 \pm 3.7$  g C m<sup>-2</sup> yr<sup>-1</sup> for BW-GUM and BW-NXR, respectively), one of which is seasonally inundated  
770 and surrounded by grassland (BW-NXR) and the other is a permanently flooded lagoon covered in a floating  
771 papyrus mat (BW-GUM). The relatively low fluxes found at the two Southeast Asian peat forest sites indicate that  
772 these ecosystems may be smaller CH<sub>4</sub> sources than expected, given their location in the humid tropics. Even the  
773 higher-emitting tropical sites in Brazil and Botswana are still well within the range of annual CH<sub>4</sub> flux typical in  
774 cooler latitudes (Fig. 1).

775 In addition to having highly variable CH<sub>4</sub> flux magnitudes, the tropical sites differ from each other in their  
776 seasonality. CH<sub>4</sub> flux hit a minimum around July for two sites (BW-GUM, latitude 18.965 °S and MY-MLM, latitude  
777 1.46 °N), while CH<sub>4</sub> flux increased through July and the subsequent months for the other Botswana site, BW-NXR  
778 (latitude 19.548 °S). Site ID-Pag (latitude 2.32 °S) had minimal seasonality, whereas the flooded forest site in Brazil  
779 (BR-NPW, latitude 16.49 °S) had near-zero fluxes from approximately July to January, and consistently high fluxes  
780 for the remainder of the year. The rice site PH-RiF (latitude 14.14 °N) had two annual CH<sub>4</sub> flux peaks, which is  
781 consistent with some other rice sites and likely reflects management practices. Baseline CH<sub>4</sub> flux values also differed,  
782 with the two Botswana sites having the highest off-season fluxes (29 and 133 nmol m<sup>-2</sup> s<sup>-1</sup> for BW-NXR and BW-  
783 GUM, respectively, estimated by Timesat), MY-MLM having an intermediate baseline CH<sub>4</sub> flux (16 nmol m<sup>-2</sup> s<sup>-1</sup>,  
784 estimated by Timesat), and the remainder of the sites having essentially zero flux at baseline. While more tropical  
785 wetland data will be needed to extract broad scale conclusions about these ecosystems, the six tropical sites in  
786 FLUXNET-CH<sub>4</sub> provide an important starting point for synthesis studies and highlight tropical wetland CH<sub>4</sub>  
787 variability.

788

### 789 4.0 Data Availability

790 Half-hourly and daily aggregations are available for download at [https://fluxnet.org/data/fluxnet-ch4-](https://fluxnet.org/data/fluxnet-ch4-community-product/)  
791 [community-product/](https://fluxnet.org/data/fluxnet-ch4-community-product/), along with a table containing site metadata compiled from Table B3. Variable descriptions and  
792 units are provided in Table B1, and at <https://fluxnet.org/data/fluxnet-ch4-community-product/>. Each site has a unique  
793 FLUXNET-CH<sub>4</sub> DOI as listed in Table B3. All site data used in this analysis are available under the CC BY 4.0  
794 (<https://creativecommons.org/licenses/by/4.0/>) copyright policy (2 additional sites in FLUXNET-CH<sub>4</sub> are available  
795 under the more restrictive Tier 2 data policy, <https://fluxnet.org/data/data-policy/>; these sites are not used in our  
796 analysis). The individual site DOIs are provided below in Table 2. All seasonality parameters used in these analyses  
797 are available at <https://doi.org/10.5281/zenodo.4672601>.

799 **Table 2: Site identification (SITE\_ID), data DOI, and DOI reference for each FLUXNET-CH4 site.**

SITE_ID	DOI	DOI_REFERENCE
AT-Neu	10.18140/FLX/1669365	Wohlfahrt et al., 2020.
BR-Npw	10.18140/FLX/1669368	Vourlitis et al., 2020.
BW-Gum	10.18140/FLX/1669370	Helfter, 2020a.
BW-Nxr	10.18140/FLX/1669518	Helfter, 2020b.
CA-SCB	10.18140/FLX/1669613	Sonnentag and Helbig, 2020a.
CA-SCC	10.18140/FLX/1669628	Sonnentag and Helbig, 2020b.
CH-Cha	10.18140/FLX/1669629	Hörtnagl et al., 2020a.
CH-Dav	10.18140/FLX/1669630	Hörtnagl et al., 2020b.
CH-Oe2	10.18140/FLX/1669631	Hörtnagl, et al., 2020c.
CN-Hgu	10.18140/FLX/1669632	Niu and Chen, 2020.
DE-Dgw	10.18140/FLX/1669633	Sachs et al, 2020a.
DE-Hte	10.18140/FLX/1669634	Koebisch and Jurasinski, 2020.
DE-SfN	10.18140/FLX/1669635	Klatt et al., 2020.
DE-Zrk	10.18140/FLX/1669636	Sachs et al., 2020b.
FI-Hyy	10.18140/FLX/1669637	Mammarella et al. 2020.
FI-Lom	10.18140/FLX/1669638	Aurela et al., 2020.
FI-Si2	10.18140/FLX/1669639	Vesala et al., 2020a.
FI-Sii	10.18140/FLX/1669640	Vesala et al., 2020b
FR-LGt	10.18140/FLX/1669641	Jacotot et al., 2020.
HK-MPM	10.18140/FLX/1669642	Lai and Liu, 2020.
ID-Pag	10.18140/FLX/1669643	Sakabe et al., 2020.
IT-BCi	10.18140/FLX/1669644	Magliulo et al., 2020.

IT-Cas	10.18140/FLX/1669645	Manca and Goded, 2020.
JP-BBY	10.18140/FLX/1669646	Ueyama et al., 2020.
JP-Mse	10.18140/FLX/1669647	Iwata, 2020a.
JP-SwL	10.18140/FLX/1669648	Iwata, 2020b.
KR-CRK	10.18140/FLX/1669649	Ryu et al., 2020.
MY-MLM	10.18140/FLX/1669650	Tang et al., 2020.
NL-Hor	10.18140/FLX/1669651	Dolman et al., 2020a.
NZ-Kop	10.18140/FLX/1669652	Campbell and Goodrich, 2020.
PH-RiF	10.18140/FLX/1669653	Alberto and Wassmann, 2020.
RU-Ch2	10.18140/FLX/1669654	Goeckede, 2020.
RU-Che	10.18140/FLX/1669655	Merbold et al., 2020.
RU-Cok	10.18140/FLX/1669656	Dolman et al., 2020b.
RU-Fy2	10.18140/FLX/1669657	Varlagin, 2020.
SE-Deg	10.18140/FLX/1669659	Nilsson and Peichl, 2020.
UK-LBT	10.18140/FLX/1670207	Helfter, 2020c.
US-A03	10.18140/FLX/1669661	Billesbach and Sullivan, 2020a.
US-A10	10.18140/FLX/1669662	Billesbach and Sullivan, 2020b.
US-Atq	10.18140/FLX/1669663	Zona and Oechel, 2020a.
US-Beo	10.18140/FLX/1669664	Zona and Oechel, 2020b.
US-Bes	10.18140/FLX/1669665	Zona and Oechel, 2020c.
US-Bi1	10.18140/FLX/1669666	Rey-Sanchez et al., 2020a.
US-Bi2	10.18140/FLX/1669667	Rey-Sanchez et al., 2020b.
US-BZB	10.18140/FLX/1669668	Euskirchen and Edgar, 2020a.
US-BZF	10.18140/FLX/1669669	Euskirchen and Edgar, 2020b.
US-BZS	10.18140/FLX/1669670	Euskirchen and Edgar, 2020c.

US-CRT	10.18140/FLX/1669671	Chen and Chu, 2020a.
US-DPW	10.18140/FLX/1669672	Hinkle and Bracho, 2020.
US-EDN	10.18140/FLX/1669673	Oikawa, 2020.
US-EML	10.18140/FLX/1669674	Schuur, 2020.
US-Ho1	10.18140/FLX/1669675	Richardson and Hollinger, 2020.
US-HRA	10.18140/FLX/1669676	Runkle et al., 2020.
US-HRC	10.18140/FLX/1669677	Reba et al., 2020.
US-ICs	10.18140/FLX/1669678	Euskirchen et al., 2020d.
US-Ivo	10.18140/FLX/1669679	Zona and Oechel, 2020d.
US-LA1	10.18140/FLX/1669680	Holm et al., 2020a.
US-LA2	10.18140/FLX/1669681	Holm et al., 2020b.
US-Los	10.18140/FLX/1669682	Desai and Thom, 2020a.
US-MAC	10.18140/FLX/1669683	Sparks, 2020.
US-MRM	10.18140/FLX/1669684	Schafer, 2020.
US-Myb	10.18140/FLX/1669685	Matthes et al., 2020.
US-NC4	10.18140/FLX/1669686	Noormets et al., 2020.
US-NGB	10.18140/FLX/1669687	Torn and Dengel, 2020a.
US-NGC	10.18140/FLX/1669688	Torn and Dengel, 2020b.
US-ORv	10.18140/FLX/1669689	Bohrer and Morin, 2020a.
US-OWC	10.18140/FLX/1669690	Bohrer et al., 2020b.
US-PFa	10.18140/FLX/1669691	Desai and Thom, 2020b.
US-Snd	10.18140/FLX/1669692	Detto et al., 2020.
US-Sne	10.18140/FLX/1669693	Short et al., 2020.
US-Srr	10.18140/FLX/1669694	Windham-Myers et al., 2020.
US-StJ	10.18140/FLX/1669695	Vazquez-Lule and Vargas, 2020.

US-Tw1	10.18140/FLX/1669696	Valach et al., 2020a.
US-Tw3	10.18140/FLX/1669697	Chamberlain et al., 2020.
US-Tw4	10.18140/FLX/1669698	Eichelmann et al., 2020.
US-Tw5	10.18140/FLX/1669699	Valach et al., 2020b.
US-Twt	10.18140/FLX/1669700	Knox et al., 2020.
US-Uaf	10.18140/FLX/1669701	Iwata et al., 2020c.
US-WPT	10.18140/FLX/1669702	Chen and Chu, 2020b.

800

801

802

## 803 5.0 Conclusions

804 The breadth and scope of CH<sub>4</sub> flux data in the FLUXNET-CH<sub>4</sub> dataset make it possible to study the global  
805 patterns of CH<sub>4</sub> fluxes, particularly for global freshwater wetlands which release a substantial fraction of  
806 atmospheric CH<sub>4</sub>. To help data users understand seasonal patterns within the dataset, we provide the first global  
807 estimates of CH<sub>4</sub> flux patterns and predictors in CH<sub>4</sub> seasonality using freshwater wetland data. In the seasonality  
808 analysis, we find that, on average, the seasonal increase in CH<sub>4</sub> emissions begins about three months earlier and lasts  
809 about four months longer at the warmest sites compared with the coolest sites. We also find that the beginning of the  
810 CH<sub>4</sub> emission season lags the beginning of seasonal soil warming by approximately one month, with almost no  
811 instances of CH<sub>4</sub> emissions increasing before temperature increases. Additionally, roughly half the sites have CH<sub>4</sub>  
812 emissions increasing prior to GPP increase; highlighting the importance of substrate versus temperature limitations  
813 on wetland CH<sub>4</sub> emissions. Furthermore, relative to warmer climates, wetland CH<sub>4</sub> emissions in cooler climates  
814 increase faster in the warming season and decrease slower in the cooling season. This phenomenon has previously  
815 been noted on a regional scale and we show that it persists at the global scale. Constraining the seasonality of CH<sub>4</sub>  
816 fluxes on a global scale can help improve the accuracy of global wetland models.

817 FLUXNET-CH<sub>4</sub> is an important new resource for the research community, but critical data gaps and  
818 opportunities remain. The current FLUXNET-CH<sub>4</sub> dataset is biased towards sites in boreal and temperate regions,  
819 which influence the relationships presented in our analyses. Tropical ecosystems are estimated to account for 64% of  
820 potential natural CH<sub>4</sub> emissions (<30° N, Saunio et al., 2020) but only account for 13% of the FLUXNET-CH<sub>4</sub>  
821 sites in the dataset. Unsurprisingly, tropical sites in our network do not represent the range of bioclimatic wetland  
822 conditions present in the tropics. Therefore, while maintaining flux towers in tropical ecosystems is challenging, it is  
823 necessary to further constrain the global CH<sub>4</sub> cycle. Coastal wetlands are also poorly represented in FLUXNET-CH<sub>4</sub>  
824 even though there is evidence of substantial CH<sub>4</sub> emissions from these ecosystems, so better representation across  
825 salinity gradients is warranted. Lastly, the average time series for FLUXNET-CH<sub>4</sub> Version 1.0 is relatively short,  
826 only 3.7 site-years on average compared with 7.2 for CO<sub>2</sub> sites in FLUXNET (Pastorello et al., 2020). Adding  
827 additional site-years of data from existing sites, as a complement to adding new sites, will increase the community's  
828 ability to explain interannual variability in CH<sub>4</sub> emission and seasonality. Nevertheless, FLUXNET-CH<sub>4</sub> is an  
829 important and unprecedented resource with which to diagnose and understand drivers of the global CH<sub>4</sub> cycle.

830 **Author contribution**

831 Kyle B. Delwiche oversaw the data release, performed the seasonality analysis, gathered metadata, and  
832 prepared the manuscript with contributions from all co-authors. Sara Helen Knox gathered and standardized the  
833 data, and gap-filled the CH<sub>4</sub> flux data. Avni Malhotra prepared the manuscript and gathered metadata. Etienne  
834 Fluet-Chouinard did the representativeness analysis and prepared the manuscript. Gavin McNicol gathered data and  
835 prepared the manuscript. Robert B. Jackson oversaw the data collection, processing, analysis, and release. Danielle  
836 Christianson and You-Wei Cheah oversaw the FLUXNET-CH<sub>4</sub> dataset release on fluxnet.org. Dario Papale,  
837 Eleonora Canfora, and Carlo Trotta did the data collection, curation, and pre-processing for all of the sites outside  
838 North and South America. Remaining co-authors contributed eddy-covariance data to FLUXNET-CH<sub>4</sub> dataset  
839 and/or participated in editing the manuscript.

840 **Competing interests**

841 The authors declare that they have no conflict of interest.

842 **Acknowledgements**

843 We acknowledge primary support from the Gordon and Betty Moore Foundation (Grant GBMF5439, “Advancing  
844 Understanding of the Global Methane Cycle”; Stanford University) and from the John Wesley Powell Center for  
845 Analysis and Synthesis of the U.S. Geological Survey (“Wetland FLUXNET Synthesis for Methane” working  
846 group). Benjamin R. K. Runkle was supported by the U.S. National Science Foundation CBET CAREER Award  
847 1752083. Ankur R. Desai acknowledges support of the DOE AmeriFlux Network Management Project. Masahito  
848 Ueyama was supported by ArCS II (JPMXD1420318865) and JSPS KAKENHI (20K21849). Dario Papale and Nina  
849 Buchmann acknowledge the support of the RINGO (GA 730944) H2020 EU project. Nina Buchmann and Kathrin  
850 Fuchs acknowledge the SNF project M4P (40FA40\_154245/1) and InnoFarm (407340\_172433). Nina Buchmann  
851 acknowledges support from the SNF for ICOS-CH Phases 1 and 2 (20FI21\_148992, 20FI20\_173691). Carlo Trotta  
852 acknowledges the support of the E-SHAPE (GA 820852) H2020 EU project. William J. Riley was supported by the  
853 US Department of Energy, BER, RGCM, RUBISCO project under contract no. DEAC02-05CH11231. Jessica  
854 Turner acknowledges support from NSF GRFP (DGE-1747503) and NTL LTER (DEB-1440297). Minseok Kang  
855 was supported by the National Research Foundation of Korea (NRF-2018 R1C1B6002917). Carole Helfter  
856 acknowledges the support of the UK Natural Environment Research Council (the Global Methane Budget project,  
857 grant number NE/N015746/1). Rodrigo Vargas acknowledges support from the National Science Foundation  
858 (1652594). Dennis Baldocchi acknowledges the California Department of Water Resources for a funding contract  
859 from the California Department of Fish and Wildlife and the United States Department of Agriculture (NIFA grant  
860 #2011-67003-30371), as well as the U.S. Department of Energy’s Office of Science (AmeriFlux contract #7079856)  
861 for funding the AmeriFlux core sites. US-A03 and US-A10 are operated by the Atmospheric Radiation  
862 Measurement (ARM) user facility, a U.S. Department of Energy Office of Science user facility managed by the  
863 Biological and Environmental Research Program (doi:10.5439/1025039, doi:10.5439/1025274,  
864 doi:10.5439/1095578). Work at ANL was supported by the U.S. Department of Energy, Office of Science, Office of  
865 Biological and Environmental Research, under contract DE-AC02-06CH11357. Any use of trade, firm, or product  
866 names is for descriptive purposes only and does not imply endorsement by the U.S. Government. The CH-Dav, DE-  
867 SfN, FI-Hyy, FI-Lom, FI-Sii, FR-LGt, IT-BCi, SE-Deg and SE-Sto sites are part of the ICOS European Research  
868 Infrastructure. Oliver Sonntag acknowledges funding by the Canada Research Chairs, Canada Foundation for  
869 Innovation Leaders Opportunity Fund, and Natural Sciences and Engineering Research Council Discovery Grant  
870 Programs for work at CA-SCC and CA-SCB. Benjamin Poulter acknowledges support from the NASA Carbon  
871 Cycle and Ecosystems Program. Derrick Lai acknowledges the support of the Research Grants Council of the Hong  
872 Kong Special Administrative Region, China (Project No. CUHK 458913). We thank Nathaniel Goenawan for his  
873 help with the representativeness analysis.

874 **References**

- 875 Abdalla, M., Hastings, A., Truu, J., Espenberg, M., Mander, Ü, Smith, P. Emissions of methane from northern  
 876 peatlands: a review of management impacts and implications for future management options. *Ecol. Evol.*, 6,  
 877 7080–7102. <https://doi.org/10.1002/ece3.2469>.
- 878 Alberto, M. C. R., Wassmann, R., Gummert, M., Buresh, R. J., Quilty, J. R., Correa, T. Q., Centeno, C. A. R., &  
 879 Oca, G. M. Straw incorporated after mechanized harvesting of irrigated rice affects net emissions of CH<sub>4</sub> and  
 880 CO<sub>2</sub> based on eddy covariance measurements. *Field Crop. Res.*, 184, 162–175.  
 881 <https://doi.org/10.1016/j.fcr.2015.10.004>. 2015.
- 882 Alberto, M., & Wassmann, R. FLUXNET-CH<sub>4</sub> PH-RiF Philippines Rice Institute flooded. Philippines.  
 883 <https://doi:10.18140/FLX/1669653>. 2020.
- 884 Anderson, D. E., Verma, S. B., & Rosenberg, N. J. Eddy correlation measurements of CO<sub>2</sub>, latent heat, and sensible  
 885 heat fluxes over a crop surface. *Bound. Lay. Meteorol.*, 29(3), 263–272. <https://doi.org/10.1007/bf00119792>.  
 886 1984.
- 887 Anderson, F. E., Bergamaschi, B., Sturtevant, C., Knox, S., Hastings, L., Windham-Myers, L., Detto, M., Hestir, E.  
 888 L., Drexler, J., Miller, R. L., Matthes, J. H., Verfaillie, J., Baldocchi, D., Snyder, R. L., & Fujii R. Variation of  
 889 energy and carbon fluxes from a restored temperate freshwater wetland and implications for carbon market  
 890 verification protocols. *J. of Geophys. Res. – Biogeo.*, 121(3), 777–795. <https://doi.org/10.1002/2015JG003083>.  
 891 2016.
- 892 Angle, J. C., Morin, T. H., Solden, L. M., Narrowe, A. B., Smith, G. J., Borton, M. A., Rey-Sanchez, C., Daly, R.  
 893 A., Mirfenderesgi, G., Hoyt, D. W., Riley, W. J., Miller, C. S., Bohrer, G., & Wrighton, K. C. Methanogenesis  
 894 in oxygenated soils is a substantial fraction of wetland methane emissions. *Nat. Comm.*, 8(1), 1567.  
 895 <https://doi.org/10.1038/s41467-017-01753-4>. 2017.
- 896 Aurela, M., Lohila, A., J.-P., Hatakka, J., Rainne, J., Mäkelä, T., & Lauria, T. FLUXNET-CH<sub>4</sub> FI-Lom  
 897 Lompolojankka. Finland. <https://doi:10.18140/FLX/1669638>. 2020.
- 898 Bartlett, K. B., Bartlett, D. S., Harriss, R. C., & Sebacher, D. I. Methane emissions along a salt marsh salinity  
 899 gradient. *Biogeochemistry*, 4(3), 183–202. <https://doi.org/10.1007/bf02187365>. 1987.
- 900 Bastviken, D., Tranvik, L. J., Downing, J. A., Crill, P. M., & Enrich-Prast, A. Freshwater methane emissions offset  
 901 the continental carbon sink. *Science*, 331(6013), 50. <https://doi.org/10.1126/science.1196808>. 2011.
- 902 Billesbach, D., & Sullivan, R. FLUXNET-CH<sub>4</sub> US-A03 ARM-AMF3-Oliktok. United States. <https://doi:10.18140/FLX/1669661>. 2020a.
- 903 Billesbach, D., & Sullivan, R. FLUXNET-CH<sub>4</sub> US-A10 ARM-NSA-Barrow. United States.  
 904 <https://doi:10.18140/FLX/1669662>. 2020b.
- 905 Bloom, A. A., Bowman, K. W., Lee, M., Turner, A. J., Schroeder, R., Worden, J. R., Weidner, R., McDonald, K.  
 906 C., & Jacob, D. J. A global wetland methane emissions and uncertainty dataset for atmospheric chemical  
 907 transport models (WetCHARTs version 1.0). *Geosci. Model Dev.*, 10, 2141–2156.  
 908 <https://doi.org/10.5194/gmd-10-2141-2017>. 2017.
- 909 Bridgham, S. D., Cadillo-Quiroz, H., Keller, J. K., & Zhuang, Q. Methane emissions from wetlands:  
 910 biogeochemical, microbial, and modeling perspectives from local to global scales. *Glob. Change Biol.*, 19(5),  
 911 1325–1346. <https://doi.org/10.1111/gcb.12131>. 2013.
- 912 Bohrer, G., & Morin, T. H. FLUXNET-CH<sub>4</sub> US-ORv Olentangy River Wetland Research Park. United States.  
 913 <https://doi:10.18140/FLX/1669689>. 2020a.
- 914 Bohrer, G., Kerns, J., Morin, T. H., Rey-Sanchez, A. C., Villa, J., & Ju, Y. FLUXNET-CH<sub>4</sub> US-OWC Old Woman  
 915 Creek. United States. <https://doi:10.18140/FLX/1669690>. 2020b.
- 916 Campbell, D., & Goodrich, J. FLUXNET-CH<sub>4</sub> NZ-Kop Kopuatai. New Zealand.  
 917 <https://doi:10.18140/FLX/1669652>. 2020.
- 918 Castro-Morales, K., Kleinen, T., Kaiser, S., Zaehle, S., Kittler, F., Kwon, M. J., Beer, C., & Göckede, M. Year-  
 919 round simulated methane emissions from a permafrost ecosystem in Northeast Siberia. *Biogeosciences*, 15(9),  
 920 2691–2722. <https://doi.org/10.5194/bg-15-2691-2018>. 2018.
- 921 Chadburn, S. E., Aalto, T., Aurela, M., Baldocchi, D., Biasi, C., Boike, J., Burke, E. J., Comyn-Platt, E., Dolman,  
 922 A. J., Duran-Rojas, & Others. Modeled microbial dynamics explain the apparent temperature sensitivity of  
 923 wetland methane emissions. *Global Biogeochemical Cycles*, 34(11). <https://doi.org/10.1029/2020gb006678>.  
 924 2020.
- 925

926 Chamberlain, S. D., Oikawa, P., Sturtevant, C., Szutu, D., Verfaillie, J., & Baldocchi, D. FLUXNET-CH4 US-Tw3  
927 Twitchell Alfalfa. United States. <https://doi:10.18140/FLX/1669697>. 2020.

928 Chambers, L. G., Ramesh Reddy, K., & Osborne, T. Z. Short-Term Response of Carbon Cycling to Salinity Pulses  
929 in a Freshwater Wetland. *Soil Sci. Soc. Am. J.*, 75(5), 2000–2007. <https://doi.org/10.2136/sssaj2011.0026>.  
930 2011.

931 Chang, K. Y., W. J. Riley, S. H. Knox, R. B. Jackson, G. McNicol, B. Poulter, M. Aurela, D. Baldocchi, S. Bansal,  
932 G. Bohrer, D. I. Campbell, A. Cescatti, H. Chu, K. B. Delwiche, A. Desai, E. Euskirchen, T. Friborg, M.  
933 Goeckede, G. Holm, M. Kang, T. Keenan, K. W. Krauss, A. Lohila, I. Mammarella, A. Miyata, M. B. Nilsson,  
934 A. Noormets, D. Papale, B. R. K. Runkle, Y. Ryu, T. Sachs, K. V. R. Schäfer, H. P. Schmid, N. Shurpali, O.  
935 Sonnentag, A. C. I. Tang, M. S. Torn, C. Trotta, M. Ueyama, R. Vargas, T. Vesala, L. Windham-Myers, Z.  
936 Zhang, & D. Zona. Global wetland methane emissions have hysteretic responses to seasonal temperature.  
937 *Nature Communications* [In press]. 2021

938 Chanton, J. P., Glaser, P. H., Chasar, L. S., Burdige, D. J., Hines, M. E., Siegel, D. I., Tremblay, L. B., & Cooper,  
939 W. T. Radiocarbon evidence for the importance of surface vegetation on fermentation and methanogenesis in  
940 contrasting types of boreal peatlands. *Global Biogeochem. Cy.*, 22(4). <https://doi.org/10.1029/2008gb003274>.  
941 2008.

942 Chen, J., & Chu, H. FLUXNET-CH4 US-CRT Curtice Walter-Berger cropland. United States.  
943 <https://doi:10.18140/FLX/1669671>. 2020a.

944 Chen, J., & Chu, H. FLUXNET-CH4 US-WPT Winous Point North Marsh. United States.  
945 <https://doi:10.18140/FLX/1669702>. 2020b.

946 Chu, H., Chen, J., Gottgens, J. F., Ouyang, Z., John, R., Czajkowski, K., & Becker, R. Net ecosystem methane and  
947 carbon dioxide exchanges in a Lake Erie coastal marsh and a nearby cropland. *J. Geophys. Res.: Biogeo.*,  
948 119(5), 722–740. <https://doi.org/10.1002/2013JG002520>. 2014.

949 Chu, H., Baldocchi, D. D., John, R., Wolf, S., & Reichstein, M. Fluxes all of the time? A primer on the temporal  
950 representativeness of FLUXNET. *Journal of Geophysical Research: Biogeosciences*, 122(2), 289–307.  
951 <https://doi.org/10.1002/2016JG003576>. 2017.

952 Chu, H., Luo, X., Ouyang, Z., Chan, W. S., Dengel, S., Biraud, S. C., Torn, M. S., Metzger, S., Kumar, J., Arain, M.  
953 A., & Others. Representativeness of Eddy-Covariance flux footprints for areas surrounding AmeriFlux sites.  
954 *Agricultural and Forest Meteorology*, 301-302, 108350. <https://doi.org/10.1016/j.agrformet.2021.108350>.  
955 2021.

956 Dalcin Martins, P., Hoyt, D. W., Bansal, S., Mills, C. T., Tfaily, M., Tangen, B. A., Finocchiaro, R. G., Johnston,  
957 M. D., McAdams, B. C., Solensky, M. J., Smith, G. J., Chin, Y.-P., & Wilkins, M. J. Abundant carbon  
958 substrates drive extremely high sulfate reduction rates and methane fluxes in Prairie Pothole Wetlands. *Global*  
959 *Change Biology*, 23(8), 3107–3120. <https://doi.org/10.1111/gcb.13633>. 2017.

960 Dean, J. F., Middelburg, J. J., Röckmann, T., Aerts, R., Blauw, L. G., Egger, M., Jetten, M. S. M., de Jong, A. E. E.,  
961 Meisel, O. H., Rasigraf, O., Slomp, C. P., in't Zandt, M. H., & Dolman, A. J. Methane Feedbacks to the Global  
962 Climate System in a Warmer World. *Rev. Geophys.*, 56(1), 207–250. <https://doi.org/10.1002/2017rg000559>.  
963 2018.

964 Deemer, B. R., Harrison, J. A., Li, S., Beaulieu, J. J., DelSontro, T., Barros, N., Bezerra-Neto, J. F., Powers, S. M.,  
965 Dos Santos, M. A., & Vonk, J. A. Greenhouse Gas Emissions from Reservoir Water Surfaces: A New Global  
966 Synthesis. *Bioscience*, 66(11), 949–964. <https://doi.org/10.1093/biosci/biw117>. 2016.

967 Dengel, S., Zona, D., Sachs, T., Aurela, M., Jammot, M., Parmentier, F.-J. W., Oechel, W., & Vesala, T. Testing the  
968 applicability of neural networks as a gap-filling method using CH4 flux data from high latitude wetlands.  
969 *Biogeosciences*, 10, 8185–8200. <https://doi.org/10.5194/bg-10-8185-2013>. 2013.

970 Deshmukh, C. S., Julius, D., Evans, C. D., Nardi, Susanto, A. P., Page, S. E., Gauci, V., Laurén, A., Sabiham, S.,  
971 Agus, F., Asyhari, A., Kurnianto, S., Suardiwierianto, Y., & Desai, A. R. Impact of forest plantation on  
972 methane emissions from tropical peatland. *Glob. Change Biol.*, 26, 2477-2495.  
973 <https://doi.org/10.1111/gcb.15019>. 2020.

974 Desai, A. R., & Thom, J. FLUXNET-CH4 US-Los Lost Creek. United States. <https://doi:10.18140/FLX/1669682>.  
975 2020a.

976 Desai, A. R., & Thom, J. FLUXNET-CH4 US-PFa Park Falls/WLEF. United States.  
977 <https://doi:10.18140/FLX/1669691>. 2020b.

978 Desjardins, R. L. A technique to measure CO2 exchange under field conditions. *Int. J. Biometeorol.*, 18(1), 76–83.  
979 <https://doi.org/10.1007/bf01450667>. 1974.

980 Detto, M., Sturtevant, C., Oikawa, P., Verfaillie, J., & Baldocchi, D. FLUXNET-CH4 US-Snd Sherman Island.  
981 United States. <https://doi:10.18140/FLX/1669692>. 2020.

982 Dise, N. Winter fluxes of methane from Minnesota peatlands. *Biogeochemistry*, 17(2).  
983 <https://doi.org/10.1007/bf00002641>. 1992.

984 Dolman, H., Hendriks, D., Parmentier, F.-J., Marchesini, L. B., Dean, J., & van Huissteden, K. FLUXNET-CH4  
985 NL-Hor Horstermeer. Netherlands. <https://doi:10.18140/FLX/1669651>. 2020a.

986 Dolman, H., van der Molen, H., Parmentier, F.-J., Marchesini, L. B., Dean, J., van Huissteden, K., & Maximov, T.  
987 FLUXNET-CH4 RU-Cok Chokurdakh. Russian Federation. <https://doi:10.18140/FLX/1669656>. 2020b.

988 Eichelmann, E., Knox, S., Rey Sanchez, C., Valach, A., Sturtevant, C., Szutu, D., Verfaillie, J., & Baldocchi, D.  
989 FLUXNET-CH4 US-Tw4 Twitchell East End Wetland. United States. <https://doi:10.18140/FLX/1669698>.  
990 2020.

991 Eklundh, L., & Jönsson, P. TIMESAT: A Software Package for Time-Series Processing and Assessment of  
992 Vegetation Dynamics. *Remote Sensing Time Series* (pp. 141–158). [https://doi.org/10.1007/978-3-319-15967-](https://doi.org/10.1007/978-3-319-15967-6_7)  
993 [6\\_7](https://doi.org/10.1007/978-3-319-15967-6_7). 2015.

994 Etheridge, D. M., Steele, L. P., Francey, R. J., & Langenfelds, R. L. Atmospheric methane between 1000 A.D. and  
995 present: Evidence of anthropogenic emissions and climatic variability. *J. Geophys. Res. – Atmos.*, 103(D13),  
996 15979–15993. <https://doi.org/10.1029/98jd00923>. 1998.

997 Etminan, M., Myhre, G., Highwood, E. J., & Shine, K. P. Radiative forcing of carbon dioxide, methane, and nitrous  
998 oxide: A significant revision of the methane radiative forcing. *Geophys. Res. Lett.*, 43(24), 12,614–12,623.  
999 <https://doi.org/10.1002/2016gl071930>. 2016.

1000 Euskirchen, E., & Edgar, C. FLUXNET-CH4 US-BZB Bonanza Creek Thermokarst Bog. United States.  
1001 <https://doi:10.18140/FLX/1669668>. 2020a.

1002 Euskirchen, E., & Edgar, C. FLUXNET-CH4 US-BZF Bonanza Creek Rich Fen. United States.  
1003 <https://doi:10.18140/FLX/1669669>. 2020b.

1004 Euskirchen, E., & Edgar, C. FLUXNET-CH4 US-BZS Bonanza Creek Black Spruce. United States.  
1005 <https://doi:10.18140/FLX/1669670>. 2020c.

1006 Euskirchen, E., Bret-Harte, M., & Edgar, C. Marion Bret-Harte. FLUXNET-CH4 US-ICs Imnavait Creek  
1007 Watershed Wet Sedge Tundra. United States. <https://doi:10.18140/FLX/1669678>. 2020d.

1008 Gallant, A. The Challenges of Remote Monitoring of Wetlands. *Remote Sensing*, 7(8), 10938–10950.  
1009 <https://doi.org/10.3390/rs70810938>. 2015.

1010 Göeckede, M., Kittler, F., & Schaller, C. Quantifying the impact of emission outbursts and non-stationary flow on  
1011 eddy covariance CH4 flux measurements using wavelet techniques. *Biogeosciences*, 16(16), 3113–3131.  
1012 <https://doi.org/10.5194/bg-16-3113-2019>. 2019.

1013 Goeckede, M. FLUXNET-CH4 RU-Ch2 Chersky reference. Russian Federation.  
1014 <https://doi:10.18140/FLX/1669654>. 2020.

1015 Gu, L., Post, W. M., Baldocchi, D. D., Andrew Black, T., Suyker, A. E., Verma, S. B., Vesala, T., & Wofsy, S. C.  
1016 Characterizing the Seasonal Dynamics of Plant Community Photosynthesis Across a Range of Vegetation  
1017 Types. In: Noormets A. (eds) *Phenology of Ecosystem Processes*. Springer, New York, NY. pp. 35–58.  
1018 [https://doi.org/10.1007/978-1-4419-0026-5\\_2](https://doi.org/10.1007/978-1-4419-0026-5_2). 2009.

1019 Hargreaves, K. J., Fowler, D., Pitcairn, C. E. R., & Aurela, M. Annual methane emission from Finnish mires  
1020 estimated from eddy covariance campaign measurements. *Theor. Appl. Climatol.*, 70, 203–213.  
1021 <https://doi.org/10.1007/s007040170015>. 2001.

1022 Hargrove, W. W., Hoffman, F. M., & Law, B. E. New analysis reveals representativeness of the AmeriFlux  
1023 network. *Eos, Transactions American Geophysical Union*, 84(48), 529.  
1024 <https://doi.org/10.1029/2003EO480001>. 2003.

1025 Hatala, J. A., Detto, M., & Baldocchi, D. D. Gross ecosystem photosynthesis causes a diurnal pattern in methane  
1026 emission from rice. *Geophys. Res. Lett.*, 39(6). <https://doi.org/10.1029/2012gl051303>. 2012.

1027 Helbig, M., Quinton, W. L., & Sonnentag, O. Warmer spring conditions increase annual methane emissions from a  
1028 boreal peat landscape with sporadic permafrost. *Environ. Res. Lett.*, 12(11), 115009.  
1029 <https://doi.org/10.1088/1748-9326/aa8c85>. 2017.

1030 Helfter, C., Tremper, A. H., Halios, C. H., Kotthaus, S., Björkegren, A., Grimmond, C. S. B., Barlow, J. F., &  
1031 Nemitz, E. Spatial and temporal variability of urban fluxes of methane, carbon monoxide and carbon dioxide  
1032 above London, UK. *Atmos. Chem. Phys.* 16, 10543–10557. <https://doi.org/10.5194/acp-2016-216-ac1>. 2016.

1033 Helfter, C. FLUXNET-CH4 BW-Gum Guma. Botswana. <https://doi:10.18140/FLX/1669370>. 2020a.

1034 Helfter, C. FLUXNET-CH4 BW-Nxr Nxaraga. Botswana. <https://doi:10.18140/FLX/1669518>. 2020b.

1035 Helfter, C. FLUXNET-CH4 UK-LBT London BT. United Kingdom. <https://doi:10.18140/FLX/1670207>. 2020c.

1036 Hinkle, C. R., & Bracho, R. FLUXNET-CH4 US-DPW Disney Wilderness Preserve Wetland. United States.  
1037 <https://doi:10.18140/FLX/1669672>. 2020.

1038 Hoffman, F. M., Kumar, J., Mills, R. T., & Hargrove, W. W. Representativeness-based sampling network design for  
1039 the State of Alaska. *Landscape Ecol.*, 28(8), 1567–1586. <https://doi.org/10.1007/s10980-013-9902-0>. 2013.

1040 Hollinger, D. Y., and A. D. Richardson. Uncertainty in Eddy Covariance Measurements and Its Application to  
1041 Physiological Models. *Tree Physiology* 25 (7): 873–85. <https://doi.org/10.1093/treephys/25.7.873>. 2005.

1042 Holm, G. O., Perez, B. C., McWhorter, D. E., Krauss, K. W., Raynie, R. C., & Killebrew, C. J. FLUXNET-CH4  
1043 US-LA1 Pointe-aux-Chenes Brackish Marsh. United States. <https://doi:10.18140/FLX/1669680>. 2020a.

1044 Holm, G. O., Perez, B. C., McWhorter, D. E., Krauss, K. W., Raynie, R. C., & Killebrew, C. J. FLUXNET-CH4  
1045 US-LA2 Salvador WMA Freshwater Marsh. United States. <https://doi:10.18140/FLX/1669681>. 2020b.

1046 Hörtnagl, L., Feigenwinter, I. Fuchs, K., Merbold, L., Buchmann, N., Eugster, W., Zeeman, M., Pluess, P., Käslin,  
1047 F., Meier, P., Koller, P., & Baur, T. FLUXNET-CH4 CH-Cha Chamau. Switzerland.  
1048 <https://doi:10.18140/FLX/1669629>. 2020a.

1049 Hörtnagl, Lukas, Werner Eugster, Lutz Merbold, Nina Buchmann, Mana Gharun, Sophia Etzold, Rudolf Haesler,  
1050 Matthias Haeni, Philip Meier, Florian Käslin, Thomas Baur, & Peter Pluess. FLUXNET-CH4 CH-Dav Davos.  
1051 Switzerland. <https://doi:10.18140/FLX/1669630>. 2020b.

1052 Hörtnagl, Lukas, Regine Maier, Werner Eugster, Nina Buchmann, Carmen Emmel, Patrick Koller, Thomas Baur,  
1053 Peter Pluess, Florian Käslin, & Philip Meier. FLUXNET-CH4 CH-Oe2 Oensingen crop. Switzerland.  
1054 <https://doi:10.18140/FLX/1669631>. 2020c.

1055 Hwang, Y., Ryu, Y., Huang, Y., Kim, J., Iwata, H., & Kang, M. Comprehensive assessments of carbon dynamics in  
1056 an intermittently-irrigated rice paddy. *Agr. Forest Met.*, 285–286, 107933.  
1057 <https://doi.org/10.1016/j.agrformet.2020.107933>. 2020.

1058 Iwata, H., Mano, M., Ono, K., Tokida, T., Kawazoe, T., Kosugi, Y., Sakabe, A., Takahashi, K., & Miyata, A.  
1059 Exploring sub-daily to seasonal variations in methane exchange in a single-crop rice paddy in central Japan.  
1060 *Atmos. Environ.*, 179, 156–165. <https://doi.org/10.1016/j.atmosenv.2018.02.015>. 2018.

1061 Iwata, Hiroki. FLUXNET-CH4 JP-Mse Mase rice paddy field. Japan. <https://doi:10.18140/FLX/1669647>. 2020a.

1062 Iwata, Hiroki. FLUXNET-CH4 JP-SwL Suwa Lake. Japan. <https://doi:10.18140/FLX/1669648>. 2020b.

1063 Iwata, Hiroki, Masahito Ueyama, & Yoshinobu Harazono. FLUXNET-CH4 US-Uaf University of Alaska,  
1064 Fairbanks. United States. <https://doi:10.18140/FLX/1669701>. 2020c.

1065 Jacotot, Adrien, Sébastien Gogo, & Fatima Laggoun-Déforge. FLUXNET-CH4 FR-LGt La Guette. France.  
1066 <https://doi:10.18140/FLX/1669641>. 2020.

1067 Jung, M., Reichstein, M., & Bondeau, A. Towards global empirical upscaling of FLUXNET eddy covariance  
1068 observations: validation of a model tree ensemble approach using a biosphere model. *Biogeosciences*, 6(10),  
1069 2001–2013. <https://doi.org/10.5194/bg-6-2001-2009>. 2009.

1070 Jung, M., Schwalm, C., Migliavacca, M., Walther, S., Camps-Valls, G., Koirala, S., Anthoni, P., Besnard, S.,  
1071 Bodesheim, P., Carvalhais, N., Chevallier, F., Gans, F., Goll, D. S., Haverd, V., Kohler, P., Ichii, K., Jain, A.  
1072 K., Liu, J., Lombardozzi, D., Nabel, J. E. M. S., Nelson, J. A., O’Sullivan, M., Pallandt, M., Papale, D., Peters,  
1073 W., Pongrats, J., Rodenbeck, C., Sitch, S., Tramontana, G., Walker, A., Weber, U., & Reichstein, M. Scaling  
1074 carbon fluxes from eddy covariance sites to globe: synthesis and evaluation of the FLUXCOM approach.  
1075 *Biogeosciences*, 17(5), 1343–1365. <https://doi.org/10.5194/bg-17-1343-2020>. 2020.

1076 Kim, Y., Johnson, M. S., Knox, S. H., Andrew Black, T., Dalmagro, H. J., Kang, M., Kim, J., & Baldocchi, D. Gap-  
1077 filling approaches for eddy covariance methane fluxes: A comparison of three machine learning algorithms and  
1078 a traditional method with principal component analysis. *Glob. Change Biol.*, 26(3), 1499–1518.  
1079 <https://doi.org/10.1111/gcb.14845>. 2020.

1080 Kittler, F., Heimann, M., Kolle, O., Zimov, N., Zimov, S., & Göckede, M. Long-Term Drainage Reduces CO<sub>2</sub>  
1081 Uptake and CH<sub>4</sub> Emissions in a Siberian Permafrost Ecosystem: Drainage impact on Arctic carbon cycle.  
1082 *Global Biogeochem. Cy.*, 31(12), 1704–1717. <https://doi.org/10.1002/2017GB005774>. 2017.

1083 Klatt, Janina, Hans Peter Schmid, Matthias Mauder, & Rainer Steinbrecher. FLUXNET-CH4 DE-SfN Schechenfilz  
1084 Nord. Germany. <https://doi:10.18140/FLX/1669635>. 2020.

1085 Knox, S. H., Sturtevant, C., Matthes, J. H., Koteen, L., Verfaillie, J., & Baldocchi, D. Agricultural peatland  
1086 restoration: effects of land-use change on greenhouse gas (CO<sub>2</sub> and CH<sub>4</sub>) fluxes in the Sacramento-San  
1087 Joaquin Delta. *Glob. Change Biol.*, 21(2), 750–765. <https://doi.org/10.1111/gcb.12745>. 2015.

1088 Knox, S. H., Matthes, J. H., Sturtevant, C., Oikawa, P. Y., Verfaillie, J., & Baldocchi, D. Biophysical controls on  
1089 interannual variability in ecosystem-scale CO<sub>2</sub> and CH<sub>4</sub> exchange in a California rice paddy. *J. Geophys. Res.-*  
1090 *Biogeo.*, 121(3), 978–1001. <https://doi.org/10.1002/2015jg003247>. 2016.

1091 Knox, S. H., Jackson, R. B., Poulter, B., McNicol, G., Fluet-Chouinard, E., Zhang, Z., Hugelius, G., Bousquet, P.,  
1092 Canadell, J. G., Saunois, M., Papale, D., Chu, H., Keenan, T. F., Baldocchi, D., Torn, M. S., Mammarella, I.,  
1093 Trotta, C., Aurela, M., Bohrer, G., Campbell, D.I., Cescatti, A., Chamberlain, S., Chen, J., Chen, W., Dengel,

1094 S., Desai, A.R., Euskirchen, E., Friborg, T., Gasbarra, D., Goded, I., Goeckede, M., Heimann, M., Helbig, M.,  
1095 Hirano, T., Hollinger, D.Y., Iwata, H., & Others. FLUXNET-CH4 Synthesis Activity: Objectives,  
1096 Observations, and Future Directions. *B. Am. Meteorol. Soc.*, 100(12), 2607–2632. [https://doi.org/10.1175/bams-](https://doi.org/10.1175/bams-d-18-0268.1)  
1097 [d-18-0268.1](https://doi.org/10.1175/bams-d-18-0268.1). 2019.

1098 Knox, Sara, Jaclyn Hatala Matthes, Joseph Verfaillie, & Dennis Baldocchi. FLUXNET-CH4 US-Twt Twitchell  
1099 Island. United States. <https://doi.org/10.18140/FLX/1669700>. 2020.

1100 Koebsch, F., Jurasinski, G., Koch, M., Hofmann, J., & Glatzel, S. Controls for multi-scale temporal variation in  
1101 ecosystem methane exchange during the growing season of a permanently inundated fen. *Agr. Forest*  
1102 *Meteorol.*, 204, 94–105. <https://doi.org/10.1016/j.agrformet.2015.02.002>. 2015.

1103 Koebsch, F., Winkel, M., Liebner, S., Liu, B., Westphal, J., Schmiedinger, I., Spitz, A., Gehre, M., Jurasinski, G.,  
1104 Köhler, S., & Others. Sulfate deprivation triggers high methane production in a disturbed and rewetted coastal  
1105 peatland. *Biogeosciences*, 16, 1937–1953. <https://doi.org/10.5194/bg-16-1937-2019>. 2019.

1106 Koebsch, Franziska, & Gerald Jurasinski. FLUXNET-CH4 DE-Hte Huetelmoor. Germany.  
1107 <https://doi.org/10.18140/FLX/1669634>. 2020.

1108 Kuznetsova A., Brockhoff P.B., & Christensen R. H. B. “lmerTest Package: Tests in Linear Mixed  
1109 Effects Models.” *Journal of Statistical Software*, 82(13), 1-26.  
1110 <https://doi.org/10.18637/jss.v082.i13>. 2017.

1111 Kwon, M. J., Beulig, F., Ilie, I., Wildner, M., Küsel, K., Merbold, L., Mahecha, M. D., Zimov, N., Zimov, S. A.,  
1112 Heimann, M., Schuur, E. A. G., Kostka, J. E., Kolle, O., Hilke, I., & Goeckede, M. Plants, microorganisms, and  
1113 soil temperatures contribute to a decrease in methane fluxes on a drained Arctic floodplain. *Global Change*  
1114 *Biology*, 23(6), 2396–2412. <https://doi.org/10.1111/gcb.13558>. 2017.

1115 Lai, D. Y. F. Methane Dynamics in Northern Peatlands: A Review. *Pedosphere*, 19(4), 409–421.  
1116 [https://doi.org/10.1016/s1002-0160\(09\)00003-4](https://doi.org/10.1016/s1002-0160(09)00003-4). 2009.

1117 Lai, D. Y. F., Roulet, N. T., & Moore, T. R. The spatial and temporal relationships between CO2 and CH4  
1118 exchange in a temperate ombrotrophic bog. *Atmos. Environ.*, 89, 249–259.  
1119 <https://doi.org/10.1016/j.atmosenv.2014.02.034>. 2014.

1120 Lai, Derrick Y.F., & Jiangong Liu. FLUXNET-CH4 HK-MPM Mai Po Mangrove. Hong Kong.  
1121 <https://doi.org/10.18140/FLX/1669642>. 2020.

1122 Lasslop, G., Reichstein, M., Papale, D., Richardson, A. D., Arneeth, A., Barr, A., Stoy, P., & Wohlfahrt, G.  
1123 Separation of net ecosystem exchange into assimilation and respiration using a light response curve approach:  
1124 critical issues and global evaluation. *Glob. Change Biol.*, 16(1), 187–208. [https://doi.org/10.1111/j.1365-](https://doi.org/10.1111/j.1365-2486.2009.02041.x)  
1125 [2486.2009.02041.x](https://doi.org/10.1111/j.1365-2486.2009.02041.x). 2010.

1126 Liu, J., Zhou, Y., Valach, A., Shortt, R., Kasak, K., Rey-Sanchez, C., Hemes, K. S., Baldocchi, D., & Lai, D. Y. F.  
1127 Methane emissions reduce the radiative cooling effect of a subtropical estuarine mangrove wetland by half.  
1128 *Glob. Change Biol.*, 26(9), 4998–5016. <https://doi.org/10.1111/gcb.15247>. 2020.

1129 Madsen, K., Nielsen, H. B., & Tingleff, O. Methods for non-linear least squares problems. Informatics and  
1130 Mathematical Modelling, Technical University of Denmark. 2<sup>nd</sup> Edition. 2004.

1131 Magliulo, Vincenzo, Paul Di Tommasi, Daniela Famulari, Daniele Gasbarra, Luca Vitale, Antonio Manco,  
1132 Ferdinando di Matteo, Andrea Esposito, & Maurizio Tosca. FLUXNET-CH4 IT-BCi Borgo Cioffi. Italy.  
1133 <https://doi.org/10.18140/FLX/1669644>. 2020.

1134 Mahecha, M. D., Gans, F., Sippel, S., Donges, J. F., Kaminski, T., Metzger, S., Migliavacca, M., Papale, D.,  
1135 Rammig, A., & Zscheischler, J. Detecting impacts of extreme events with ecological in situ monitoring  
1136 networks. *Biogeosciences*, 14(18), 4255–4277. <https://doi.org/10.5194/bg-14-4255-2017>. 2017.

1137 Malhotra, A., & Roulet, N. T. Environmental correlates of peatland carbon fluxes in a thawing landscape: do  
1138 transitional thaw stages matter? *Biogeosciences*, 12(10), 3119–3130. <https://doi.org/10.5194/bg-12-3119-2015>.  
1139 2015.

1140 Mammarella, Ivan, Timo Vesala, Petri Keronen, Pasi Kolari, Samuli Launiainen, Jukka Pumpanen, Üllar Rannik,  
1141 Erkki Siivola, Janne Levula, & Toivo Pohja. FLUXNET-CH4 FI-Hyy Hyytiala. Finland.  
1142 <https://doi.org/10.18140/FLX/1669637>. 2020.

1143 Manca, Giovanni, & Ignacio Goded. FLUXNET-CH4 IT-Cas Castellaro. Italy. <https://doi.org/10.18140/FLX/1669645>.  
1144 2020.

1145 Mastepanov, M., Sigsgaard, C., Tagesson, T., Ström, L., Tamstorf, M. P., Lund, M., & Christensen, T. R.  
1146 Revisiting factors controlling methane emissions from high-Arctic tundra. *Biogeosciences*, 10(7), 5139–5158.  
1147 <https://doi.org/10.5194/bg-10-5139-2013>. 2013.

1148 Matthes, Jaclyn Hatala, Cove Sturtevant, Patty Oikawa, Samuel D Chamberlain, Daphne Szutu, Ariane Arias Ortiz,  
1149 Joseph Verfaillie, & Dennis Baldocchi. FLUXNET-CH4 US-Myb Mayberry Wetland. United States.  
1150 <https://doi.org/10.18140/FLX/1669685>. 2020.

1151 Matthews, E., Johnson, M. S., Genovese, V., Du, J., & Bastviken, D. Methane emission from high latitude lakes:  
1152 methane-centric lake classification and satellite-driven annual cycle of emissions. *Sci. Rep.*- UK, 10(1), 12465.  
1153 <https://doi.org/10.1038/s41598-020-68246-1>. 2020.

1154 Megonigal, J. P., Whalen, S. C., Tissue, D. T., Bovard, B. D., Allen, A. S., & Albert, D. B. A Plant-Soil-  
1155 Atmosphere Microcosm for Tracing Radiocarbon from Photosynthesis through Methanogenesis. *Soil Sci. Soc.*  
1156 *Am. J.* 63(3), 665–671. <https://doi.org/10.2136/sssaj1999.03615995006300030033x>. 1999.

1157 Meijide, A., Manca, G., Goded, I., Magliulo, V., Di Tommasi, P., Seufert, G., & Cescatti, A. Seasonal trends and  
1158 environmental controls of methane emissions in a rice paddy field in Northern Italy. *Biogeosciences*, 8(12),  
1159 3809. <https://doi.org/10.5194/bg-8-3809-2011>. 2011.

1160 Melloh, R. A., & Crill, P. M. Winter methane dynamics in a temperate peatland. *Global Biogeochem. Cy.*, 10(2),  
1161 247–254. <https://doi.org/10.1029/96gb00365>. 1996.

1162 Melton, J. R., Wania, R., Hodson, E. L., Poulter, B., Ringeval, B., Spahni, R., Bohn, T., Avis, C. A., Beerling, D. J.,  
1163 Chen, G., Eliseev, A. V., Denisov, S. N., Hopcroft, P. O., Lettenmaier, D. P., Riley, W. J., Singarayer, J. S.,  
1164 Subin, Z. M., Tian, H., Zürcher, S., & Others. Present state of global wetland extent and wetland methane  
1165 modelling: conclusions from a model inter-comparison project (WETCHIMP). *Biogeosciences*, 10(2), 753–  
1166 788. <https://doi.org/10.5194/bg-10-753-2013>. 2013.

1167 Merbold, Lutz, Corinna Rebmann, & Chiara Corradi. FLUXNET-CH4 RU-Che Cherski. Russian Federation.  
1168 <https://doi.org/10.18140/FLX/1669655>. 2020.

1169 Meyer, H., & Pebesma, E. Predicting into unknown space? Estimating the area of applicability of spatial prediction  
1170 models. *arXiv [stat.ML]*. arXiv. <http://arxiv.org/abs/2005.07939>. 2020.

1171 Mishra, S. R., Pattnaik, P., Sethunathan, N., & Adhya, T. K. Anion-Mediated Salinity Affecting Methane  
1172 Production in a Flooded Alluvial Soil. *Geomicrobiol. J.*, 20(6), 579–586. <https://doi.org/10.1080/713851167>.  
1173 2003.

1174 Moffat, A. M., Papale, D., Reichstein, M., Hollinger, D. Y., Richardson, A. D., Barr, A. G., Beckstein, C., Braswell,  
1175 B. H., Churkina, G., Desai, A. R., Falge, E., Gove, J. H., Heimann, M., Hui, D., Jarvis, A. J., Kattge, J.,  
1176 Noormets, A., & Stauch, V. J. Comprehensive comparison of gap-filling techniques for eddy covariance net  
1177 carbon fluxes. *Agr. Forest Meteorol.*, 147(3), 209–232. <https://doi.org/10.1016/j.agrformet.2007.08.011>. 2007.

1178 Myhre, G., D. Shindell, F.-M. Bréon, W. Collins, J. Fuglestedt, J. Huang, D. Koch, J.-F. Lamarque, D. Lee, B.  
1179 Mendoza, T. Nakajima, A. Robock, G. Stephens, T. Takemura and H. Zhang. Anthropogenic and Natural  
1180 Radiative Forcing Supplementary Material. In Stocker, T.F., D. Qin, G.-K. Plattner, M. Tignor, S.K. Allen, J.  
1181 Boschung, A. Nauels, Y. Xia, V. Bex and P.M. Midgley (Ed.), *Climate Change 2013: The Physical Science*  
1182 *Basis. Contribution of Working Group I to the Fifth Assessment Report of the Intergovernmental Panel on*  
1183 *Climate Change*. 2013.

1184 Nemitz, E., Mammarella, I., Ibrom, A., Aurela, M., Burba, G. G., Dengel, S., Gielen, B., Grelle, A., Heinesch, B.,  
1185 Herbst, M., Hörtnagl, L., Klemedtsson, L., Lindroth, A., Lohila, A., McDermitt, D. K., Meier, P., Merbold, L.,  
1186 Nelson, D., Nicolini, G., & Others. Standardisation of eddy-covariance flux measurements of methane and  
1187 nitrous oxide. *Int. Agrophys.*, 32(4), 517–549. <https://doi.org/10.1515/intag-2017-0042>. 2018.

1188 Nielsen, H. B. Damping parameter in Marquardt's method. Department of Mathematical Modeling, IMM, Technical  
1189 University of Denmark. Technical Report, IMM-REP-1999-05. 1999.

1190 Nilsson, Mats B., & Matthias Peichl. FLUXNET-CH4 SE-Deg Degero. Sweden.  
1191 <https://doi.org/10.18140/FLX/1669659>. 2020.

1192 Niu, Shuli, & Weinan Chen. FLUXNET-CH4 CN-Hgu Hongyuan. China. <https://doi.org/10.18140/FLX/1669632>. 2020.

1193 Noormets, Asko, John King, Bhaskar Mitra, Guofang Miao, Maricar Aguilos, Kevan Minick, Prajaya Prajapati,  
1194 Jean-Christophe Domec, Jonathan Furst, & Maxwell Wightman. FLUXNET-CH4 US-NC4  
1195 NC\_AlligatorRiver. United States. <https://doi.org/10.18140/FLX/1669686>. 2020.

1196 Oikawa, P. Y., Jenerette, G. D., Knox, S. H., Sturtevant, C., Verfaillie, J., Dronova, I., Poindexter, C. M.,  
1197 Eichelmann, E., & Baldocchi, D. D. Evaluation of a hierarchy of models reveals importance of substrate  
1198 limitation for predicting carbon dioxide and methane exchange in restored wetlands. *J. Geophys. Res.-Biogeo.*,  
1199 122(1), 145–167. <https://doi.org/10.1002/2016JG003438>. 2017.

1200 Oikawa, Patty. FLUXNET-CH4 US-EDN Eden Landing Ecological Reserve. United States.  
1201 <https://doi.org/10.18140/FLX/1669673>. 2020.

1202 Olefeldt, D., Turetsky, M. R., Crill, P. M., & McGuire, A. D. Environmental and physical controls on northern  
1203 terrestrial methane emissions across permafrost zones. *Glob. Change Biol.*, 19(2), 589–603.  
1204 <https://doi.org/10.1111/gcb.12071>. 2013.

1205 Papale, D., Andrew Black, T., Carvalhais, N., Cescatti, A., Chen, J., Jung, M., Kiely, G., Lasslop, G., Mahecha, M.  
1206 D., Margolis, H., Merbold, L., Montagnani, L., Moors, E., Olesen, J. E., Reichstein, M., Tramontana, G., van  
1207 Gorsel, E., Wohlfahrt, G., & Ráduly, B. Effect of spatial sampling from European flux towers for estimating  
1208 carbon and water fluxes with artificial neural networks. *J. Geophys. Res.-Biogeo.*, 120(10), 1941–1957.  
1209 <https://doi.org/10.1002/2015jg002997>. 2015.

1210 Parmentier, F. J. W., van Huissteden, J., van der Molen, M. K., Schaepman-Strub, G., Karsanaev, S. A., Maximov,  
1211 T. C., & Dolman, A. J. Spatial and temporal dynamics in eddy covariance observations of methane fluxes at a  
1212 tundra site in northeastern Siberia. *J. Geophys. Res.*, 116(G3), 1368. <https://doi.org/10.1029/2010JG001637>.  
1213 2011.

1214 Pastorello, G., Trotta, C., Canfora, E., Chu, H., Christianson, D., Cheah, Y.-W., Poindexter, C., Chen, J.,  
1215 Elbashandy, A., Humphrey, M., Isaac, P., Polidori, D., Ribeca, A., van Ingen, C., Zhang, L., Amiro, B.,  
1216 Ammann, C., Arain, M. A., Ardö, J., & Others. The FLUXNET2015 dataset and the ONEFlux processing  
1217 pipeline for eddy covariance data. *Scientific Data*, 7(1), 225. <https://doi.org/10.1038/s41597-020-0534-3>. 2020.

1218 Pattnaik, P., Mishra, S. R., Bharati, K., Mohanty, S. R., Sethunathan, N., & Adhya, T. K. Influence of salinity on  
1219 methanogenesis and associated microflora in tropical rice soils. *Microbiol. Res.*, 155(3), 215–220.  
1220 [https://doi.org/10.1016/S0944-5013\(00\)80035-X](https://doi.org/10.1016/S0944-5013(00)80035-X). 2000.

1221 Poffenbarger, H. J., Needelman, B. A., & Patrick Megonigal, J. Salinity Influence on Methane Emissions from  
1222 Tidal Marshes. *Wetlands*, 31(5), 831–842. <https://doi.org/10.1007/s13157-011-0197-0>. 2011.

1223 Poulter, B., Bousquet, P., Canadell, J. G., Ciais, P., Peregón, A., Saunois, M., Arora, V. K., Beerling, D. J., Brovkin,  
1224 V., Jones, C. D., Joos, F., Gedney, N., Ito, A., Kleinen, T., Koven, C. D., McDonald, K., Melton, J. R., Peng,  
1225 C., Peng, S., & Others. Global wetland contribution to 2000–2012 atmospheric methane growth rate dynamics.  
1226 *Environ. Res. Lett.*, 12(9), 094013. <https://doi.org/10.1088/1748-9326/aa8391>. 2017.

1227 Reba, Michele, Benjamin Runkle, & Kosana Suvocarev. FLUXNET-CH4 US-HRC Humnoke Farm Rice Field –  
1228 Field C. United States. <https://doi:10.18140/FLX/1669677>. 2020.

1229 Reichstein, M., Falge, E., Baldocchi, D., Papale, D., Aubinet, M., Berbigier, P., Bernhofer, C., Buchmann, N.,  
1230 Gilmanov, T., Granier, A., Grunwald, T., Havrankova, K., Ilvesniemi, H., Janous, D., Knohl, A., Laurila, T.,  
1231 Lohila, A., Loustau, D., Matteucci, G., & Others. On the separation of net ecosystem exchange into  
1232 assimilation and ecosystem respiration: review and improved algorithm. *Glob. Change Biol.*, 11(9), 1424–  
1233 1439). <https://doi.org/10.1111/j.1365-2486.2005.001002.x>. 2005.

1234 Rey-Sanchez, Camilo, Daphne Szutu, Robert Shortt, Samuel D. Chamberlain, Joseph Verfaillie, & Dennis  
1235 Baldocchi. FLUXNET-CH4 US-Bi1 Bouldin Island Alfalfa. United States. <https://doi:10.18140/FLX/1669666>.  
1236 2020a.

1237 Rey-Sanchez, Camilo, Daphne Szutu, Kyle Hemes, Joseph Verfaillie, & Dennis Baldocchi. FLUXNET-CH4 US-  
1238 Bi2 Bouldin Island corn. United States. <https://doi:10.18140/FLX/1669667>. 2020b.

1239 Richardson, A. D., Hollinger, D. Y., Burba, G. G., Davis, K. J., Flanagan, L. B., Katul, G. G., William Munger, J.,  
1240 Ricciuto, D. M., Stoy, P. C., Suyker, A. E., Verma, S. B., & Wofsy, S. C. A multi-site analysis of random error  
1241 in tower-based measurements of carbon and energy fluxes. *Agr. Forest Meteorol.*, 136(1), 1–18.  
1242 <https://doi.org/10.1016/j.agrformet.2006.01.007>. 2006.

1243 Richardson, A. D., & Hollinger, D. Y. A method to estimate the additional uncertainty in gap-filled NEE resulting  
1244 from long gaps in the CO2 flux record. *Agr. Forest Meteorol.*, 147(3), 199–208.  
1245 <https://doi.org/10.1016/j.agrformet.2007.06.004>. 2007.

1246 Richardson, A. D., Mahecha, M. D., Falge, E., Kattge, J., Moffat, A. M., Papale, D., Reichstein, M., Stauch, V. J.,  
1247 Braswell, B. H., Churkina, G., Kruijt, B., & Hollinger, D. Y. Statistical properties of random CO2 flux  
1248 measurement uncertainty inferred from model residuals. *Agr. Forest Meteorol.*, 148(1), 38–50.  
1249 <https://doi.org/10.1016/j.agrformet.2007.09.001>. 2008.

1250 Richardson, A. D., Aubinet, M., Barr, A. G., Hollinger, D. Y., Ibrom, A., Lasslop, G., & Reichstein, M. Uncertainty  
1251 quantification. *Eddy Covariance: A Practical Guide to Measurement and Data Analysis*. (eds) Aubinet, M.,  
1252 Vesala, T., Papale, D. Springer Atmospheric Sciences. 2012.

1253 Richardson, Andrew D, & David Y Hollinger. FLUXNET-CH4 US-Ho1 Howland Forest (main tower). United  
1254 States. <https://doi:10.18140/FLX/1669675>. 2020.

1255 Rinne, J., Riutta, T., Pihlatie, M., Aurela, M., Haapanala, S., Tuovinen, J.-P., Tuittila, E.-S., & Vesala, T. Annual  
1256 cycle of methane emission from a boreal fen measured by the eddy covariance technique. *Tellus B*, 59(3), 449–  
1257 457. <https://doi.org/10.1111/j.1600-0889.2007.00261.x>. 2007.

1258 Runkle, B. R. K., Suvočarev, K., Reba, M. L., Reavis, C. W., Smith, S. F., Chiu, Y.-L., & Fong, B. Methane  
1259 Emission Reductions from the Alternate Wetting and Drying of Rice Fields Detected Using the Eddy  
1260 Covariance Method. *Envir. Sci. Tech.*, 53(2), 671–681. <https://doi.org/10.1021/acs.est.8b05535>. 2019.

1261 Runkle, Benjamin, Michele Reba, & Kosana Suvocarev. FLUXNET-CH4 US-HRA Humnoke Farm Rice Field –  
1262 Field A. United States. <https://doi:10.18140/FLX/1669676>. 2020.

1263 Ryu, Youngryel, Minseok Kang, & Jongho Kim. FLUXNET-CH4 KR-CRK Cheorwon Rice paddy. Korea,  
1264 Republic of. <https://doi:10.18140/FLX/1669649>. 2020.

1265 Sachs, T., Giebels, M., Boike, J., & Kutzbach, L. Environmental controls on CH4 emission from polygonal tundra  
1266 on the microsite scale in the Lena river delta, Siberia: CONTROLS ON TUNDRA CH4 FLUX AND  
1267 SCALING. *Glob. Change Biol.*, 16(11) 3096 – 3110. <https://doi.org/10.1111/j.1365-2486.2010.02232.x>. 2010.

1268 Sachs, Torsten, Christian Wille, & Eric Larmanou. FLUXNET-CH4 DE-Dgw Dagowsee. Germany.  
1269 <https://doi:10.18140/FLX/1669633>. 2020a.

1270 Sachs, Torsten, Christian Wille, Eric Larmanou, & Daniela Franz. FLUXNET-CH4 DE-Zrk Zarnekow. Germany.  
1271 <https://doi:10.18140/FLX/1669636>. 2020b.

1272 Sakabe, Ayaka, Masayuki Itoh, Takashi Hirano, & Kitso Kusin. FLUXNET-CH4 ID-Pag Palangkaraya undrained  
1273 forest. Indonesia. <https://doi:10.18140/FLX/1669643>. 2020.

1274 Saunio, M., Bousquet, P., Poulter, B., Peregon, A., Ciais, P., Canadell, J. G., Dlugokencky, E. J., Etiope, G.,  
1275 Bastviken, D., Houweling, S., Janssens-Maenhout, G., Tubiello, F. N., Castaldi, S., Jackson, R. B., Alexe, M.,  
1276 Arora, V. K., Beerling, D. J., Bergamaschi, P., Blake, D. R., & Others. The global methane budget 2000–2012.  
1277 *Earth Syst. Sci. Data*, 8, 697-751. <https://doi.org/10.5194/essd-8-697-2016>. 2016.

1278 Saunio, M., Stavert, A. R., Poulter, B., Bousquet, P., Canadell, J. G., Jackson, R. B., Raymond, P. A.,  
1279 Dlugokencky, E. J., Houweling, S., Patra, P. K., Ciais, P., Arora, V. K., Bastviken, D., Bergamaschi, P., Blake,  
1280 D. R., Brailsford, G., Bruhwiler, L., Carlson, K. M., Carrol, M., & Others. The Global Methane Budget 2000–  
1281 2017. *Earth Syst. Sci. Data*, 12, 1561-1623. <https://doi.org/10.5194/essd-12-1561-2020>. 2020.

1282 Schafer, Karina. FLUXNET-CH4 US-MRM Marsh Resource Meadowlands Mitigation Bank. United States.  
1283 <https://doi:10.18140/FLX/1669684>. 2020.

1284 Schuur, E.A. FLUXNET-CH4 US-EML Eight Mile Lake Permafrost thaw gradient, Healy Alaska. United States.  
1285 <https://doi:10.18140/FLX/1669674>. 2020.

1286 Seyfferth, A. L., Bothfeld, F., Vargas, R., Stuckey, J. W., Wang, J., Kearns, K., Michael, H. A., Guimond, J., Yu,  
1287 X., & Sparks, D. L. Spatial and temporal heterogeneity of geochemical controls on carbon cycling in a tidal  
1288 salt marsh. *Geochim. Cosmochim. Ac.*, 282, 1–18. <https://doi.org/10.1016/j.gca.2020.05.013>. 2020.

1289 Shortt, Robert, Kyle Hemes, Daphne Szutu, Joseph Verfaillie, & Dennis Baldocchi. FLUXNET-CH4 US-Sne  
1290 Sherman Island Restored Wetland. United States. <https://doi:10.18140/FLX/1669693>. 2020.

1291 Sims, D. A., Rahman, A. F., Cordova, V. D., El-Masri, B. Z., Baldocchi, D. D., Flanagan, L. B., Goldstein, A. H.,  
1292 Hollinger, D. Y., Misson, L., Monson, R. K., Oechel, W. C., Schmid, H. P., Wofsy, S. C., & Xu, L. On the use  
1293 of MODIS EVI to assess gross primary productivity of North American ecosystems. *J. Geophys. Res.-Biogeo.*  
1294 111(G4). <https://doi.org/10.1029/2006jg000162>. 2006.

1295 Sonnentag, Oliver, & Manuel Helbig. FLUXNET-CH4 CA-SCB Scotty Creek Bog. Canada.  
1296 <https://doi:10.18140/FLX/1669613>. 2020a.

1297 Sonnentag, Oliver, & Manuel Helbig. FLUXNET-CH4 CA-SCC Scotty Creek Landscape. Canada. <https://doi:10.18140/FLX/1669628>. 2020b.

1299 Spahni, R., Wania, R., Neef, L., van Weele, M., Pison, I., Bousquet, P., Frankenberg, C., Foster, P. N., Joos, F.,  
1300 Prentice, I. C., & van Velthoven, P. Constraining global methane emissions and uptake by ecosystems. In  
1301 *Biogeosciences*, 8(6), 1643–1665. <https://doi.org/10.5194/bg-8-1643-2011>. 2011.

1302 Sparks, Jed P. FLUXNET-CH4 US-MAC MacArthur Agro-Ecology. United States.  
1303 <https://doi:10.18140/FLX/1669683>. 2020.

1304 Sturtevant, C. S., Ruddell, B. L., Knox, S. H., Verfaillie, J. G., Matthes, J. H., Oikawa, P. Y., & Baldocchi, D. D.  
1305 Identifying scale-emergent, nonlinear, asynchronous processes of wetland methane exchange. *J. Geophys.*  
1306 *Res.-Biogeo.*, 121, 188–204. <https://doi.org/10.1002/2015JG003054>. 2016.

1307 Tagesson, T., Mölder, M., Mastepanov, M., Sigsgaard, C., Tamstorf, M. P., Lund, M., Falk, J. M., Lindroth, A.,  
1308 Christensen, T. R., & Ström, L. Land-atmosphere exchange of methane from soil thawing to soil freezing in a  
1309 high-Arctic wet tundra ecosystem. *Glob. Change Biol.*, 18(6), 1928–1940. <https://doi.org/10.1111/j.1365-2486.2012.02647.x>. 2012.

1310

1311 Tang, Angela Che Ing, Guan Xhuan Wong, Lulie Melling, Edward Baran Aeries, Joseph Wenceslaus Waili, Kevin  
1312 Kemudang Musin, Kim San Lo, & Frankie Kiew. FLUXNET-CH4 MY-MLM Maludam National Park.  
1313 Malaysia. <https://doi.org/10.18140/FLX/1669650>. 2020.

1314 Taoka, T., Iwata, H., Hirata, R., Takahashi, Y., Miyabara, Y., & Itoh, M. Environmental Controls on Diffusive and  
1315 Ebullitive Methane Emission at a Sub-Daily Time Scale in the Littoral Zone of a Mid-Latitude Shallow Lake.  
1316 *J. Geophys. Res.-Biogeo.*, 125(9), <https://doi.org/10.1029/2020JG005753>. 2020.

1317 Torn, Margaret, & Sigrid Dengel. FLUXNET-CH4 US-NGB NGEE Arctic Barrow. United States. <https://doi.org/10.18140/FLX/1669687>. 2020a.

1318  
1319 Torn, Margaret, & Sigrid Dengel. FLUXNET-CH4 US-NGC NGEE Arctic Council. United States.  
1320 <https://doi.org/10.18140/FLX/1669688>. 2020b.

1321 Treat, C. C., Anthony Bloom, A., & Marushchak, M. E. Nongrowing season methane emissions-a significant  
1322 component of annual emissions across northern ecosystems. *Glob. Change Biol.*, 24(8), 3331–3343.  
1323 <https://doi.org/10.1111/gcb.14137>. 2018.

1324 Turetsky, M. R., Kotowska, A., Bubier, J., Dise, N. B., Crill, P., Hornibrook, E. R. C., Minkinen, K., Moore, T. R.,  
1325 Myers-Smith, I. H., Nykänen, H., Olefeldt, D., Rinne, J., Saarnio, S., Shurpali, N., Tuittila, E.-S., Waddington,  
1326 J. M., White, J. R., Wickland, K. P., & Wilkening, M. A synthesis of methane emissions from 71 northern,  
1327 temperate, and subtropical wetlands. *Glob. Change Biol.*, 20(7), 2183–2197.  
1328 <https://doi.org/10.1111/gcb.12580>. 2014.

1329 Ueyama, Masahito, Takashi Hirano, & Yasuhiro Kominami. FLUXNET-CH4 JP-BBY Bibai bog. Japan.  
1330 <https://doi.org/10.18140/FLX/1669646>. 2020.

1331 Valach, Alex, Daphne Szutu, Elke Eichelmann, Sara Knox, Joseph Verfaillie, & Dennis Baldocchi. FLUXNET-CH4  
1332 US-Tw1 Twitchell Wetland West Pond. United States. <https://doi.org/10.18140/FLX/1669696>. 2020a.

1333 Valach, Alex, Kuno Kasak, Daphne Szutu, Joseph Verfaillie, & Dennis Baldocchi. FLUXNET-CH4 US-Tw5 East  
1334 Pond Wetland. United States. <https://doi.org/10.18140/FLX/1669699>. 2020b.

1335 Varlagin, Andrej. FLUXNET-CH4 RU-Fy2 Fyodorovskoye dry spruce. Russian Federation.  
1336 <https://doi.org/10.18140/FLX/1669657>. 2020.

1337 Vazquez-Lule, Alma, & Rodrigo Vargas. FLUXNET-CH4 US-StJ St Jones Reserve. United States.  
1338 <https://doi.org/10.18140/FLX/1669695>. 2020.

1339 Vázquez-Lule, A., & Vargas, R. Biophysical drivers of net ecosystem and methane exchange across phenological  
1340 phases in a tidal salt marsh. *Agricultural and Forest Meteorology*, 300, 108309.  
1341 <https://doi.org/10.1016/j.agrformet.2020.108309>. 2021.

1342 Verma, S. B., Ullman, F. G., Billesbach, D., Clement, R. J., Kim, J., & Verry, E. S. Eddy correlation measurements  
1343 of methane flux in a northern peatland ecosystem. *Bound. Lay. Meteorol.*, 58(3), 289–304.  
1344 <https://doi.org/10.1007/BF02033829>. 1992.

1345 Vesala, Timo, Eeva-Stiina Tuittila, Ivan Mammarella, & Pavel Alekseychik. FLUXNET-CH4 FI-Si2 Siikaneva-2  
1346 Bog. Finland. <https://doi.org/10.18140/FLX/1669639>. 2020a.

1347 Vesala, Timo, Eeva-Stiina Tuittila, Ivan Mammarella, & Janne Rinne. FLUXNET-CH4 FI-Sii Siikaneva. Finland.  
1348 <https://doi.org/10.18140/FLX/1669640>. 2020b.

1349 Villarreal, S., Guevara, M., Alcaraz-Segura, D., Brunsell, N. A., Hayes, D., Loescher, H. W., & Vargas, R.  
1350 Ecosystem functional diversity and the representativeness of environmental networks across the conterminous  
1351 United States. *Agr. Forest Meteorol.*, 262, 423–433. <https://doi.org/10.1016/j.agrformet.2018.07.016>. 2018.

1352 Villarreal, S., Guevara, M., Alcaraz-Segura, D., & Vargas, R. Optimizing an Environmental Observatory Network  
1353 Design Using Publicly Available Data. *J. Geophys. Res.-Biogeo.*, 124(7), 1812–1826.  
1354 <https://doi.org/10.1029/2018JG004714>. 2019.

1355 Vourelitis, George, Higo Dalmagro, Jose de S. Nogueira, Mark Johnson, & Paulo Arruda. FLUXNET-CH4 BR-Npw  
1356 Northern Pantanal Wetland. Brazil. <https://doi.org/10.18140/FLX/1669368>. 2020.

1357 Vuichard, N., & Papale, D. Filling the gaps in meteorological continuous data measured at FLUXNET sites with  
1358 ERA-Interim reanalysis. *Earth Syst. Sci. Data*, 7(2), 157–171. <https://doi.org/10.5194/essd-7-157-2015>. 2015.

1359 Weston, N. B., Dixon, R. E., & Joye, S. B. Ramifications of increased salinity in tidal freshwater sediments:  
1360 Geochemistry and microbial pathways of organic matter mineralization. *J. Geophys. Res.*, 111(G1).  
1361 <https://doi.org/10.1029/2005jg000071>. 2006.

1362 Weston, N. B., Vile, M. A., Neubauer, S. C., & Velinsky, D. J. Accelerated microbial organic matter mineralization  
1363 following salt-water intrusion into tidal freshwater marsh soils. *Biogeochemistry*, 102, 135–151.  
1364 <https://doi.org/10.1007/s10533-010-9427-4>. 2011.

1365 Wik, M., Crill, P. M., Varner, R. K., & Bastviken, D. Multiyear measurements of ebullitive methane flux from three  
1366 subarctic lakes. *J. Geophys. Res.-Biogeo.* 118(3), 1307–1321. <https://doi.org/10.1002/jgrg.20103>. 2013.

1367 Windham-Myers, Lisamarie, Ellen Stuart-Haëntjens, Brian Bergamaschi, Sara Knox, Frank Anderson, & Kyle  
1368 Nakatsuka. FLUXNET-CH4 US-Srr Suisun marsh - Rush Ranch. United States.  
1369 <https://doi:10.18140/FLX/1669694>. 2020.

1370 Wohlfahrt, Georg, Albin Hammerle, & Lukas Hörtnagl. FLUXNET-CH4 AT-Neu Neustift. Austria.  
1371 <https://doi:10.18140/FLX/1669365>. 2020.

1372 Wutzler, T., Lucas-Moffat, A., Migliavacca, M., Knauer, J., Sickel, K., Šigut, L., Menzer, O., & Reichstein, M.  
1373 Basic and extensible post-processing of eddy covariance flux data with REddyProc. *Biogeosciences*, 15, 5015–  
1374 5030. <https://doi.org/10.5194/bg-2018-56-sc1>. 2018.

1375 Xu, X., Riley, W. J., Koven, C. D., Billesbach, D. P., -W. Chang, R. Y., Commene, R., Euskirchen, E. S., Hartery,  
1376 S., Harazono, Y., Iwata, H., McDonald, K. C., Miller, C. E., Oechel, W. C., Poulter, B., Raz-Yaseef, N.,  
1377 Sweeney, C., Torn, M., Wofsy, S. C., Zhang, Z., & Zona, D. A multi-scale comparison of modeled and  
1378 observed seasonal methane emissions in northern wetlands. *Biogeosciences*, 13(17), 5043–5056.  
1379 <https://doi.org/10.5194/bg-13-5043-2016>. 2016.

1380 Yvon-Durocher, G., Allen, A. P., Bastviken, D., Conrad, R., Gudas, C., St-Pierre, A., Thanh-Duc, N., & del  
1381 Giorgio, P. A. Methane fluxes show consistent temperature dependence across microbial to ecosystem scales.  
1382 *Nature*, 507(7493), 488–491. <https://doi.org/10.1038/nature13164>. 2014.

1383 Zhang, Z. Fluet-Choinard, E., Jensen, K., McDonald, K., Hugelius, G., Gumbrecht, T., Carrol, M., Prigent, C.,  
1384 Bartsch, A., & Poulter, B. Development of a global dataset of Wetland Area and Dynamics for Methane  
1385 Modeling (WAD2M) [Data set]. Zenodo. <http://doi.org/10.5281/zenodo.3998454>. 2020.

1386 Zhang, Z. Fluet-Choinard, E., Jensen, K., McDonald, K., Hugelius, G., Gumbrecht, T., Carrol, M., Prigent, C.,  
1387 Bartsch, A., & Poulter, B. Development of a global dataset of Wetland Area and Dynamics for Methane  
1388 Modeling (WAD2M). *Earth Syst. Sci. Data* [In press]. 2021.

1389 Zona, D., Gioli, B., Commene, R., Lindaas, J., Wofsy, S. C., Miller, C. E., Dinardo, S. J., Dengel, S., Sweeney, C.,  
1390 Karion, A., Chang, R. Y.-W., Henderson, J. M., Murphy, P. C., Goodrich, J. P., Moreaux, V., Liljedahl, A.,  
1391 Watts, J. D., Kimball, J. S., Lipson, D. A., & Oechel, W. C. Cold season emissions dominate the Arctic tundra  
1392 methane budget. *P. Natl. A. Sci. USA.*, 113(1), 40–45. <https://doi.org/10.1073/pnas.1516017113>. 2016.

1393 Zona, Donatella, & Walter C Oechel. FLUXNET-CH4 US-Atq Atqasuk. United States.  
1394 <https://doi:10.18140/FLX/1669663>. 2020a.

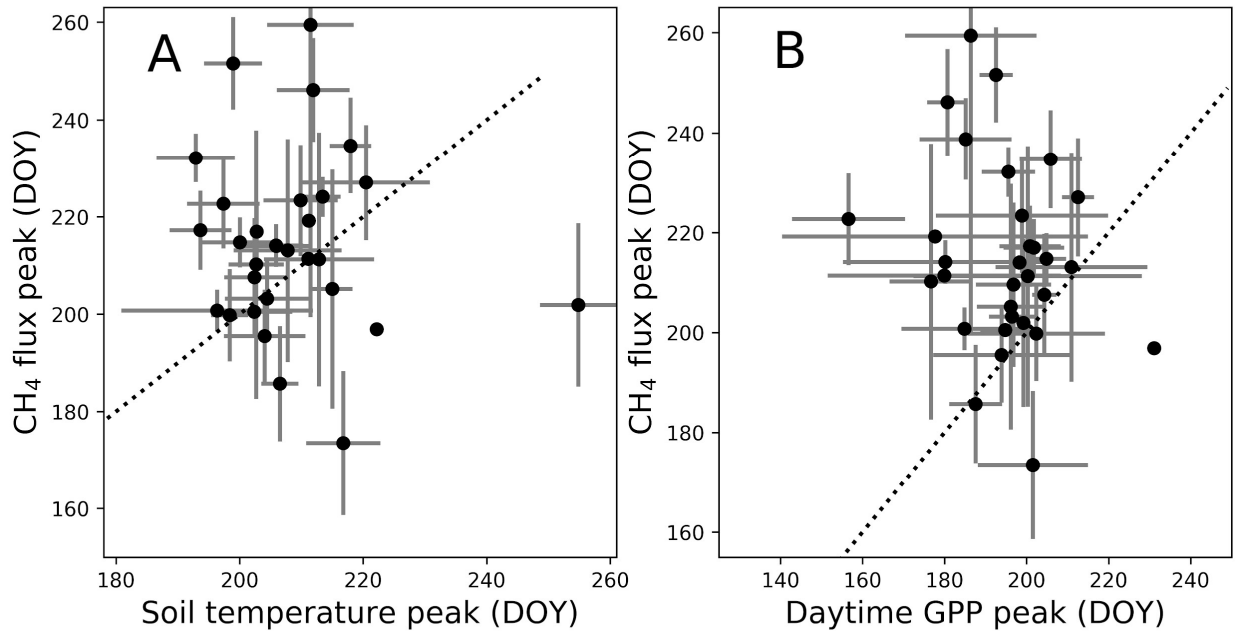
1395 Zona, Donatella, & Walter C Oechel. FLUXNET-CH4 US-Beo Barrow Environmental Observatory (BEO) tower.  
1396 United States. <https://doi:10.18140/FLX/1669664>. 2020b.

1397 Zona, Donatella, & Walter C Oechel. FLUXNET-CH4 US-Bes Barrow-Bes (Biocomplexity Experiment South  
1398 tower). United States. <https://doi:10.18140/FLX/1669665>. 2020c.

1399 Zona, Donatella, & Walter C Oechel. FLUXNET-CH4 US-Ivo Ivotuk. United States.  
1400 <https://doi:10.18140/FLX/1669679>. 2020d.

1401 APPENDIX A

1402



1403

1404

1405 Figure A1: Peak methane (CH<sub>4</sub>) flux timing versus peak gross primary productivity (GPP) timing (A) and peak soil  
1406 temperature timing by day of year (B). Points represent site average and error bars represent standard deviations. Dotted  
1407 line represents 1:1 relationship.

1408

1409 **APPENDIX B**

1410

1411 **Table B1: Data variable names, descriptions, and units**

1412 **FLUXNET-CH4 Data Variables**

1413 This webpage describes data variables and file formatting for the FLUXNET-CH4 Community Product.

1414 **1. Data Variable: Base names**

1415 Base names indicate fundamental quantities that are either measured or calculated/derived. They can also  
 1416 indicate quantified quality information.

1417 Table 1. Base names for data variables

<i>Variable</i>	<i>Description</i>	<i>Units</i>
<b>TIMEKEEPING</b>		
TIMESTAMP_START	ISO timestamp start of averaging period, used in half-hourly data	YYYYMMDDHHMM
TIMESTAMP_END	ISO timestamp end of averaging period, used in half-hourly data	YYYYMMDDHHMM
TIMESTAMP	ISO timestamp used in daily aggregation files	YYYYMMDD
<b>MET_RAD</b>		
SW_IN	Shortwave radiation, incoming	W m <sup>-2</sup>
SW_OUT	Shortwave radiation, outgoing	W m <sup>-2</sup>
LW_IN	Longwave radiation, incoming	W m <sup>-2</sup>
LW_OUT	Longwave radiation, outgoing	W m <sup>-2</sup>

PPFD_IN	Photosynthetic photon flux density, incoming	$\mu\text{molPhoton m}^{-2} \text{ s}^{-1}$
---------	--	---

PPFD_OUT	Photosynthetic photon flux density, outgoing	$\mu\text{molPhoton m}^{-2} \text{ s}^{-1}$
----------	--	---

NETRAD	Net radiation	$\text{W m}^{-2}$
--------	---------------	-------------------

### **MET\_WIND**

USTAR	Friction velocity	$\text{m s}^{-1}$
-------	-------------------	-------------------

WD	Wind direction	Decimal degrees
----	----------------	-----------------

WS	Wind speed	$\text{m s}^{-1}$
----	------------	-------------------

### **HEAT**

H	Sensible heat turbulent flux (with storage term if provided by site PI)	$\text{W m}^{-2}$
---	---	-------------------

LE	Latent heat turbulent flux (with storage term if provided by site PI)	$\text{W m}^{-2}$
----	---	-------------------

G	Soil heat flux	$\text{W m}^{-2}$
---	----------------	-------------------

### **MET\_ATM**

PA	Atmospheric pressure	kPa
----	----------------------	-----

TA	Air temperature	deg C
----	-----------------	-------

VPD	Vapor Pressure Deficit	hPa
RH	Relative humidity, range 0-100	%

### **MET\_PRECIP**

P	Precipitation	mm
---	---------------	----

### **PRODUCTS**

NEE	Net Ecosystem Exchange	$\mu\text{molCO}_2 \text{ m}^{-2} \text{ s}^{-1}$
GPP	Gross primary productivity	$\mu\text{molCO}_2 \text{ m}^{-2} \text{ s}^{-1}$
RECO	Ecosystem respiration	$\mu\text{molCO}_2 \text{ m}^{-2} \text{ s}^{-1}$

### **GASES**

FCH4	Methane (CH <sub>4</sub> ) turbulent flux (no storage correction)	$\text{nmolCH}_4 \text{ m}^{-2} \text{ s}^{-1}$
------	---	---

### **MET\_SOIL**

TS	Soil temperature	deg C
WTD	Water table depth (negative values indicate below the surface)	m

1419 **2. Data Variable: Qualifiers**

1420 Qualifiers are suffixes appended to variable base names that provide additional information about the  
1421 variable. For example, the `_DT` qualifier in the variable label `GPP_DT` indicates that gross primary  
1422 production (GPP) has been partitioned using the flux partitioning method from Lasslop et al. 2010.

1423 Multiple qualifiers can be added, and they must **follow the order in which they are presented here**.

1424 **2.1. Qualifiers: General**

1425 General qualifiers indicate additional information about a variable.

1426 · `_F` : Variable has been gap-filled by the FLUXNET-CH4 team. Gaps in meteorological variables  
1427 (including air temperature (TA), incoming shortwave (SW\_IN) and longwave (LW\_IN) radiation, vapor  
1428 pressure deficit (VPD), pressure (PA), precipitation (P), and wind speed (WS) ) were filled with ERA-  
1429 Interim (ERA-I) reanalysis data ((Vuichard and Papale 2015)). Other variables were filled using the MDS  
1430 approach in REdDyProc (see Delwiche et al. 2020 for more details).

1431 · `_DT` : Variable acquired using the flux partitioning method from (Lasslop et al. 2010), with values  
1432 estimated by fitting the light-response curve.

1433 · `_NT` : Variable acquired using the flux partitioning method from (Reichstein et al. 2005), with values  
1434 estimated from night-time data and extrapolated to day time.

1435 · `_RANDUNC`: Random uncertainty introduced from several different sources including errors  
1436 associated with the flux measurement system (gas analyzer, sonic anemometer, data acquisition system,  
1437 flux calculations), errors associated with turbulent transport, and statistical errors relating to the location  
1438 and activity of the sites of flux exchange (“footprint heterogeneity”) (Hollinger and Richardson 2005).

1439 · `_ANNOPTLM` : Gap-filled variable using an artificial neural net routine from Matlab with the  
1440 Levenberg-Marquardt algorithm as the training function, and parameters optimized across runs (more  
1441 detail in (Sara Helen Knox et al. 2016; Sara H. Knox et al. 2019)).

1442 · `_UNC` : Uncertainty introduced from ANNOPTLM gap-filling routine, as described in Knox et al.  
1443 2016 and Knox et al. 2019.

1444 · `_QC` : Reports quality checks on FCH4 gap-filled data (`_ANNOPTLM`) based on length of data gap.  
1445 1 = data gap shorter than 2 months, 3 = data gap exceeds 2 months which could lead to poor quality gap-  
1446 filled data. Nondimensional.

1447

1448 **2.2. Qualifiers: Positional (`_V`)**

1449 Positional qualifiers are used to indicate relative positions of observations at the site. For FLUXNET-CH4,  
1450 positional qualifiers are used to distinguish soil temperature probes for sites with more than one probe.  
1451 Probe depths for each positional qualifier per site are included in the metadata file included with data  
1452 download and also in Table B7 of Delwiche et al. 2020. For sites where the original database file release  
1453 in Ameriflux, AsiaFlux, or EuroFlux contains multiple probes at the same `_V` depth, we average values  
1454 and report only the average for each `_V` position. The one exception to this is site US-UAF where the  
1455 original positional qualifier from the data we downloaded from Ameriflux had different depths for the

1456 same qualifier. We still averaged the probe data, so \_V qualifiers from US-UAF represent an average of  
1457 more than one depth.

### 1458 3.0 Missing data

1459 Missing data are reported using -9999. Data for all days in a leap year are reported.

### 1460 4.0 References

- 1461 Hollinger, D. Y., and A. D. Richardson. 2005. "Uncertainty in Eddy Covariance Measurements and Its  
1462 Application to Physiological Models." *Tree Physiology* 25 (7): 873–85.
- 1463 Knox, Sara Helen, Jaclyn Hatala Matthes, Cove Sturtevant, Patricia Y. Oikawa, Joseph Verfaillie, and  
1464 Dennis Baldocchi. 2016. "Biophysical Controls on Interannual Variability in Ecosystem-Scale  
1465 CO<sub>2</sub> and CH<sub>4</sub> Exchange in a California Rice Paddy." *Journal of Geophysical Research:  
1466 Biogeosciences*. <https://doi.org/10.1002/2015jg003247>.
- 1467 Knox, Sara H., Robert B. Jackson, Benjamin Poulter, Gavin McNicol, Etienne Fluet-Chouinard, Zhen  
1468 Zhang, Gustaf Hugelius, et al. 2019. "FLUXNET-CH<sub>4</sub> Synthesis Activity: Objectives, Observations,  
1469 and Future Directions." *Bulletin of the American Meteorological Society* 100 (12): 2607–32.
- 1470 Lasslop, Gitta, Markus Reichstein, Dario Papale, Andrew D. Richardson, Almut Arneth, Alan Barr, Paul  
1471 Stoy, and Georg Wohlfahrt. 2010. "Separation of Net Ecosystem Exchange into Assimilation and  
1472 Respiration Using a Light Response Curve Approach: Critical Issues and Global Evaluation." *Global  
1473 Change Biology*. <https://doi.org/10.1111/j.1365-2486.2009.02041.x>.
- 1474 Reichstein, Markus, Eva Falge, Dennis Baldocchi, Dario Papale, Marc Aubinet, Paul Berbigier, Christian  
1475 Bernhofer, et al. 2005. "On the Separation of Net Ecosystem Exchange into Assimilation and  
1476 Ecosystem Respiration: Review and Improved Algorithm." *Global Change Biology*.  
1477 <https://doi.org/10.1111/j.1365-2486.2005.001002.x>.
- 1478 Vuichard, N., and D. Papale. 2015. "Filling the Gaps in Meteorological Continuous Data Measured at  
1479 FLUXNET Sites with ERA-Interim Reanalysis." *Earth System Science Data*.  
1480 <https://doi.org/10.5194/essd-7-157-2015>.

**Table B2 Site year annual sums and uncertainties**

	SITE_ID	Year	Ann_Flux_g_C_m-2	Ann_Flux_Uncertainty_g_C_m-2	Mean_Soil_Temp_C	Mean_Water_Table_Depth_m
1	AT-Neu	2010	0.38	0.03	8.65	NaN
2	AT-Neu	2011	0.25	0.02	8.61	NaN
3	AT-Neu	2012	NaN	NaN	9.39	NaN
4	BR-Npw	2013	NaN	NaN	NaN	NaN
5	BR-Npw	2014	NaN	NaN	25.95	NaN
6	BR-Npw	2015	20.95	1.18	26.2	-0.47
7	BR-Npw	2016	17.48	1.14	25.31	-0.41
8	BW-Gum	2018	51.73	10.59	NaN	NaN
9	BW-Nxr	2018	47.32	3.70	NaN	NaN
10	CA-SCB	2014	10.42	0.66	9.6	-0.15
11	CA-SCB	2015	NaN	NaN	5.58	-0.1
12	CA-SCB	2016	12.12	0.31	5.38	-0.15
13	CA-SCB	2017	9.48	0.27	6.32	-0.21
14	CA-SCC	2013	NaN	NaN	7.2	NaN
15	CA-SCC	2014	4.94	0.12	4.38	NaN
16	CA-SCC	2015	6.76	0.15	3.15	NaN
17	CA-SCC	2016	6.76	0.12	NaN	NaN
18	CH-Cha	2012	2.13	0.38	11.88	NaN
19	CH-Cha	2013	2.30	0.36	10.89	NaN
20	CH-Cha	2014	3.46	0.40	12.2	NaN
21	CH-Cha	2015	3.93	0.68	11.93	NaN
22	CH-Cha	2016	NaN	NaN	12.28	NaN
23	CH-Dav	2016	1.21	0.40	4.33	NaN
24	CH-Dav	2017	NaN	NaN	4.41	NaN
25	CH-Oe2	2018	0.29	0.13	12.32	NaN
26	CN-Hgu	2015	NaN	NaN	NaN	NaN
27	CN-Hgu	2016	0.81	0.16	7.26	NaN
28	CN-Hgu	2017	0.82	0.45	7.66	NaN
29	DE-Dgw	2015	NaN	NaN	NaN	NaN
30	DE-Dgw	2016	7.51	0.22	NaN	NaN
31	DE-Dgw	2017	10.42	0.16	NaN	NaN
32	DE-Dgw	2018	NaN	NaN	NaN	NaN
33	DE-Hte	2011	59.85	6.39	NaN	-0.41
34	DE-Hte	2012	36.83	3.46	NaN	-0.21
35	DE-Hte	2013	49.72	2.34	NaN	-0.25
36	DE-Hte	2014	NaN	NaN	13.26	-0.19
37	DE-Hte	2015	51.37	1.75	10.78	-0.26
38	DE-Hte	2016	50.77	2.09	9.8	-0.25
39	DE-Hte	2017	46.61	1.40	10.39	-0.4
40	DE-Hte	2018	41.62	2.52	6.12	-0.22
41	DE-SfN	2012	NaN	NaN	NaN	-0.08

42	DE-SfN	2013	3.62	0.93	10.32	-0.05
43	DE-SfN	2014	NaN	NaN	8.16	NaN
44	DE-Zrk	2013	NaN	NaN	13.03	NaN
45	DE-Zrk	2014	NaN	NaN	11.67	NaN
46	DE-Zrk	2015	30.76	1.00	10.85	NaN
47	DE-Zrk	2016	31.14	1.23	11.28	0.12
48	DE-Zrk	2017	29.10	0.87	10.84	0.31
49	DE-Zrk	2018	31.10	1.20	10.54	0.25
50	FI-Hyy	2016	NaN	NaN	5.41	NaN
51	FI-Lom	2006	13.77	0.76	4.47	0
52	FI-Lom	2007	17.22	0.25	4.33	0.04
53	FI-Lom	2008	15.52	0.22	3.79	0.06
54	FI-Lom	2009	17.63	0.27	3.98	0.02
55	FI-Lom	2010	13.78	0.29	3.71	0.03
56	FI-Si2	2012	9.27	1.17	9.4	0.06
57	FI-Si2	2013	10.22	1.17	10.47	0.13
58	FI-Si2	2014	NaN	NaN	7.7	0.1
59	FI-Si2	2015	NaN	NaN	8.18	0.09
60	FI-Si2	2016	NaN	NaN	7.67	0.09
61	FI-Sii	2013	14.58	0.32	6.45	0.04
62	FI-Sii	2014	12.93	0.78	6.42	0.03
63	FI-Sii	2015	NaN	NaN	6.92	-0.02
64	FI-Sii	2016	16.56	0.68	5.87	-0.01
65	FI-Sii	2017	8.63	0.23	8.4	0.06
66	FI-Sii	2018	9.46	1.10	6.68	0.11
67	FR-LGt	2017	NaN	NaN	10.45	-0.24
68	FR-LGt	2018	2.45	0.60	10.87	-0.22
69	HK-MPM	2016	11.62	0.61	25.06	-0.61
70	HK-MPM	2017	10.60	0.30	23.14	-0.64
71	HK-MPM	2018	11.04	0.59	NaN	-0.8
72	ID-Pag*	2016	0.09	0.07	NaN	NaN
73	ID-Pag*	2017	0.09	0.09	NaN	NaN
74	IT-BCi	2017	NaN	NaN	17.16	NaN
75	IT-BCi	2018	NaN	NaN	17.36	NaN
76	IT-Cas	2009	25.44	1.46	9.62	NaN
77	IT-Cas	2010	17.80	1.26	12.37	NaN
78	JP-BBY	2015	9.53	0.29	10.12	0
79	JP-BBY	2016	16.42	0.45	10.02	0
80	JP-BBY	2017	19.61	0.65	9.33	-0.03
81	JP-BBY	2018	NaN	NaN	9.79	-0.04
82	JP-Mse	2012	9.50	1.97	14.52	0.03
83	JP-SwL	2016	66.68	4.29	NaN	1.91
84	KR-CRK	2015	NaN	NaN	14.41	0.02
85	KR-CRK	2016	29.12	0.91	12.48	0.03

<b>86</b>	KR-CRK	2017	25.84	0.86	13.94	0.02
<b>87</b>	KR-CRK	2018	28.82	1.15	11.32	0.02
<b>88</b>	MY-MLM	2014	9.55	0.59	26.8	-0.09
<b>89</b>	MY-MLM	2015	NaN	NaN	26.9	-0.01
<b>90</b>	NL-Hor	2007	NaN	NaN	12.4	NaN
<b>91</b>	NL-Hor	2008	NaN	NaN	10.37	NaN
<b>92</b>	NL-Hor	2009	NaN	NaN	11.61	NaN
<b>93</b>	NK-Kop	2012	23.98	1.38	12.17	-0.08
<b>94</b>	NK-Kop	2013	15.33	0.43	12.68	-0.13
<b>95</b>	NK-Kop	2014	15.67	0.39	12.38	-0.11
<b>96</b>	NK-Kop	2015	14.37	2.66	12.46	-0.1
<b>97</b>	PH-RiF	2012	NaN	NaN	27.78	NaN
<b>98</b>	PH-RiF	2013	12.41	0.99	28.17	NaN
<b>99</b>	PH-RiF	2014	NaN	NaN	27.47	NaN
<b>100</b>	RU-Ch2	2014	6.99	0.14	-4.21	NaN
<b>101</b>	RU-Ch2	2015	5.86	0.14	-4.87	NaN
<b>102</b>	RU-Ch2	2016	NaN	NaN	-2.88	NaN
<b>103</b>	RU-Che	2014	3.84	0.14	-3.31	NaN
<b>104</b>	RU-Che	2015	4.19	0.22	-3.28	NaN
<b>105</b>	RU-Che	2016	4.24	0.19	-1.65	NaN
<b>106</b>	RU-Cok	2008	NaN	NaN	NaN	NaN
<b>107</b>	RU-Cok	2009	NaN	NaN	NaN	NaN
<b>108</b>	RU-Cok	2010	NaN	NaN	NaN	NaN
<b>109</b>	RU-Cok	2011	NaN	NaN	NaN	NaN
<b>110</b>	RU-Cok	2012	NaN	NaN	-0.46	NaN
<b>111</b>	RU-Cok	2013	NaN	NaN	-5.73	NaN
<b>112</b>	RU-Cok	2014	NaN	NaN	-4.82	NaN
<b>113</b>	RU-Cok	2015	4.45	0.15	-4.4	NaN
<b>114</b>	RU-Cok	2016	NaN	NaN	-11.1	NaN
<b>115</b>	RU-Fy2	2015	NaN	NaN	9.83	NaN
<b>116</b>	RU-Fy2	2016	2.69	0.59	6.88	0.68
<b>117</b>	RU-Fy2	2017	2.17	0.52	6.1	0.19
<b>118</b>	RU-Fy2	2018	5.66	1.37	6.48	0.79
<b>119</b>	SE-Deg	2014	11.24	1.98	5.02	-0.02
<b>120</b>	SE-Deg	2015	11.11	0.08	5.04	0.02
<b>121</b>	SE-Deg	2016	11.19	0.15	5.19	-0.01
<b>122</b>	SE-Deg	2017	NaN	NaN	4.19	0
<b>123</b>	SE-Deg	2018	9.42	0.09	5.49	-0.03
<b>124</b>	UK-LBT	2011	NaN	NaN	NaN	NaN
<b>125</b>	UK-LBT	2012	NaN	NaN	NaN	NaN
<b>126</b>	UK-LBT	2013	50.50	0.97	NaN	NaN
<b>127</b>	UK-LBT	2014	42.57	2.25	NaN	NaN
<b>128</b>	US-A03	2015	NaN	NaN	-6.65	NaN
<b>129</b>	US-A03	2016	NaN	NaN	-6.14	NaN

<b>130</b>	US-A03	2017	7.26	2.58	-4.48	NaN
<b>131</b>	US-A03	2018	4.35	0.62	-4.93	NaN
<b>132</b>	US-A10	2012	NaN	NaN	NaN	NaN
<b>133</b>	US-A10	2013	NaN	NaN	NaN	NaN
<b>134</b>	US-A10	2014	NaN	NaN	NaN	NaN
<b>135</b>	US-A10	2015	NaN	NaN	NaN	NaN
<b>136</b>	US-A10	2016	NaN	NaN	NaN	NaN
<b>137</b>	US-A10	2017	NaN	NaN	NaN	NaN
<b>138</b>	US-A10	2018	NaN	NaN	NaN	NaN
<b>139</b>	US-Atq	2013	NaN	NaN	-5.65	NaN
<b>140</b>	US-Atq	2014	1.80	0.19	-4.48	NaN
<b>141</b>	US-Atq	2015	1.75	0.11	-0.43	NaN
<b>142</b>	US-Atq	2016	1.75	0.00	NaN	NaN
<b>143</b>	US-Beo	2013	NaN	NaN	-2.67	NaN
<b>144</b>	US-Beo	2014	2.74	0.05	-4.95	NaN
<b>145</b>	US-Bes	2013	NaN	NaN	-6.01	NaN
<b>146</b>	US-Bes	2014	3.32	0.04	-5.69	NaN
<b>147</b>	US-Bes	2015	3.06	0.54	-6.24	NaN
<b>148</b>	US-Bi1	2016	NaN	NaN	15.62	NaN
<b>149</b>	US-Bi1	2017	NaN	NaN	17.17	NaN
<b>150</b>	US-Bi1	2018	0.69	0.29	16.82	NaN
<b>151</b>	US-Bi2	2017	0.86	0.20	20.42	NaN
<b>152</b>	US-Bi2	2018	1.69	0.29	17.12	NaN
<b>153</b>	US-BZB	2014	8.02	4.61	4.03	NaN
<b>154</b>	US-BZB	2015	7.52	0.82	3.9	NaN
<b>155</b>	US-BZB	2016	11.61	2.25	4.89	NaN
<b>156</b>	US-BZF	2014	6.61	0.63	4.32	NaN
<b>157</b>	US-BZF	2015	10.82	0.90	3.99	NaN
<b>158</b>	US-BZF	2016	NaN	NaN	5.93	NaN
<b>159</b>	US-BZS	2015	0.68	0.68	0.48	NaN
<b>160</b>	US-BZS	2016	0.89	0.27	0.67	NaN
<b>161</b>	US-CRT	2011	2.21	0.15	11.49	-0.92
<b>162</b>	US-CRT	2012	2.21	0.11	12.38	-1.45
<b>163</b>	US-DPW	2013	NaN	NaN	NaN	NaN
<b>164</b>	US-DPW	2014	58.91	0.69	NaN	NaN
<b>165</b>	US-DPW	2015	NaN	NaN	NaN	NaN
<b>166</b>	US-DPW	2016	43.60	1.29	NaN	NaN
<b>167</b>	US-DPW	2017	43.60	0.06	NaN	NaN
<b>168</b>	US-EDN	2018	-0.04	0.06	NaN	NaN
<b>169</b>	US-EML	2015	NaN	NaN	5.71	NaN
<b>170</b>	US-EML	2016	1.04	0.08	3.07	NaN
<b>171</b>	US-EML	2017	0.36	0.27	3.8	NaN
<b>172</b>	US-EML	2018	0.36	0.07	NaN	NaN
<b>173</b>	US-Ho1	2012	NaN	NaN	NaN	-0.43

<b>174</b>	US-Ho1	2013	-0.05	0.02	NaN	-0.33
<b>175</b>	US-Ho1	2014	-0.04	0.02	NaN	-0.38
<b>176</b>	US-Ho1	2015	-0.16	0.01	NaN	-0.48
<b>177</b>	US-Ho1	2016	-0.22	0.01	NaN	-0.57
<b>178</b>	US-Ho1	2017	-0.24	0.01	NaN	-0.56
<b>179</b>	US-Ho1	2018	-0.24	0.01	NaN	NaN
<b>180</b>	US-HRA	2017	-0.24	0.56	NaN	NaN
<b>181</b>	US-HRC	2017	-0.24	0.81	NaN	NaN
<b>182</b>	US-ICs	2014	NaN	NaN	-1.55	NaN
<b>183</b>	US-ICs	2015	NaN	NaN	-0.62	NaN
<b>184</b>	US-ICs	2016	NaN	NaN	-1.48	NaN
<b>185</b>	US-Ivo	2013	NaN	NaN	3.19	NaN
<b>186</b>	US-Ivo	2014	5.05	0.22	0.02	NaN
<b>187</b>	US-Ivo	2015	3.89	0.27	0.47	NaN
<b>188</b>	US-Ivo	2016	5.77	0.55	-1.01	NaN
<b>189</b>	US-LA1	2011	NaN	NaN	18.92	NaN
<b>190</b>	US-LA1	2012	12.68	0.63	24.23	NaN
<b>191</b>	US-LA2	2011	12.68	0.19	NaN	NaN
<b>192</b>	US-LA2	2012	48.42	1.57	23.09	NaN
<b>193</b>	US-LA2	2013	43.34	1.32	23.19	NaN
<b>194</b>	US-Los	2014	6.66	1.48	8.3	-0.06
<b>195</b>	US-Los	2015	5.51	0.40	5.65	-0.1
<b>196</b>	US-Los	2016	8.67	0.35	6.3	-0.07
<b>197</b>	US-Los	2017	6.00	0.33	5.5	-0.09
<b>198</b>	US-Los	2018	5.71	0.37	4.29	-0.19
<b>199</b>	US-MAC	2013	5.71	2.68	NaN	NaN
<b>200</b>	US-MAC	2014	26.37	1.69	23.18	-0.71
<b>201</b>	US-MAC	2015	15.40	0.85	23.29	-0.55
<b>202</b>	US-MRM	2012	0.30	0.19	11.16	NaN
<b>203</b>	US-MRM	2013	0.37	0.14	8.99	NaN
<b>204</b>	US-Myb	2010	NaN	NaN	NaN	0.95
<b>205</b>	US-Myb	2011	33.83	0.72	17.18	1.23
<b>206</b>	US-Myb	2012	64.20	0.58	16.25	1.12
<b>207</b>	US-Myb	2013	59.81	0.92	15.7	1.19
<b>208</b>	US-Myb	2014	58.97	0.68	11.27	1.24
<b>209</b>	US-Myb	2015	60.85	0.55	NaN	1.3
<b>210</b>	US-Myb	2016	45.72	0.48	NaN	1.22
<b>211</b>	US-Myb	2017	30.32	0.84	18.5	1.35
<b>212</b>	US-Myb	2018	29.33	0.55	17.05	1.19
<b>213</b>	US-NC4	2012	38.28	1.70	17.12	NaN
<b>214</b>	US-NC4	2013	18.60	3.88	NaN	NaN
<b>215</b>	US-NC4	2014	26.98	0.60	18.02	NaN
<b>216</b>	US-NC4	2015	23.37	2.30	16.27	NaN
<b>217</b>	US-NC4	2016	62.20	2.78	16.35	NaN

<b>218</b>	US-NGB	2012	NaN	NaN	NaN	NaN
<b>219</b>	US-NGB	2013	NaN	NaN	NaN	NaN
<b>220</b>	US-NGB	2014	NaN	NaN	NaN	NaN
<b>221</b>	US-NGB	2015	NaN	NaN	NaN	NaN
<b>222</b>	US-NGB	2016	NaN	NaN	NaN	NaN
<b>223</b>	US-NGB	2017	2.31	0.11	NaN	NaN
<b>224</b>	US-NGB	2018	2.52	0.22	NaN	NaN
<b>225</b>	US-NGC	2017	2.52	0.06	NaN	NaN
<b>226</b>	US-NGC	2018	2.52	0.05	NaN	NaN
<b>227</b>	US-ORv	2011	3.53	0.54	16.64	NaN
<b>228</b>	US-ORv	2012	9.11	0.45	14.23	NaN
<b>229</b>	US-ORv	2013	7.70	0.41	13.19	NaN
<b>230</b>	US-ORv	2014	8.46	0.26	12	NaN
<b>231</b>	US-ORv	2015	NaN	NaN	13.36	NaN
<b>232</b>	US-OWC	2015	NaN	NaN	22.11	0.9
<b>233</b>	US-OWC	2016	113.99	3.25	21.19	0.54
<b>234</b>	US-PFa	2010	NaN	NaN	NaN	NaN
<b>235</b>	US-PFa	2011	0.34	0.05	NaN	NaN
<b>236</b>	US-PFa	2012	0.30	0.04	NaN	NaN
<b>237</b>	US-PFa	2013	0.31	0.05	NaN	NaN
<b>238</b>	US-PFa	2014	NaN	NaN	NaN	NaN
<b>239</b>	US-PFa	2015	0.63	0.03	NaN	NaN
<b>240</b>	US-PFa	2016	0.85	0.02	NaN	NaN
<b>241</b>	US-PFa	2017	0.80	0.06	NaN	NaN
<b>242</b>	US-PFa	2018	NaN	NaN	NaN	NaN
<b>243</b>	US-Snd	2010	NaN	NaN	16.85	NaN
<b>244</b>	US-Snd	2011	NaN	NaN	14.96	NaN
<b>245</b>	US-Snd	2012	6.34	0.25	16.06	NaN
<b>246</b>	US-Snd	2013	6.04	0.48	16.59	-0.65
<b>247</b>	US-Snd	2014	3.23	0.36	17.52	-0.78
<b>248</b>	US-Snd	2015	3.23	0.21	NaN	NaN
<b>249</b>	US-Sne	2016	NaN	NaN	17.85	-0.2
<b>250</b>	US-Sne	2017	45.96	0.40	17.05	0.16
<b>251</b>	US-Sne	2018	39.63	0.66	16.83	0.09
<b>252</b>	US-Srr	2014	0.71	0.10	NaN	NaN
<b>253</b>	US-Srr	2015	0.88	0.11	NaN	NaN
<b>254</b>	US-Srr	2016	0.86	0.10	16.3	-0.18
<b>255</b>	US-Srr	2017	0.86	0.11	NaN	NaN
<b>256</b>	US-StJ	2016	9.55	1.04	11.66	-0.26
<b>257</b>	US-Tw1	2011	26.09	2.70	14.01	NaN
<b>258</b>	US-Tw1	2012	NaN	NaN	11.58	0.24
<b>259</b>	US-Tw1	2013	33.93	1.78	11.92	0.25
<b>260</b>	US-Tw1	2014	49.60	1.67	13.14	0.25
<b>261</b>	US-Tw1	2015	54.80	2.58	12.79	0.33

262	US-Tw1	2016	45.93	1.90	12.91	0.41
263	US-Tw1	2017	38.66	2.09	12.53	0.38
264	US-Tw1	2018	27.60	1.64	12.1	0.24
265	US-Tw3	2013	NaN	NaN	19.63	NaN
266	US-Tw3	2014	NaN	NaN	17.91	NaN
267	US-Tw4	2013	NaN	NaN	NaN	NaN
268	US-Tw4	2014	16.26	0.39	NaN	0.48
269	US-Tw4	2015	27.61	0.43	17.2	0.36
270	US-Tw4	2016	33.49	0.37	14.8	0.18
271	US-Tw4	2017	47.95	0.58	13.78	0.07
272	US-Tw4	2018	37.41	0.48	13.02	0.08
273	US-Tw5	2018	59.72	1.15	16.67	0.69
274	US-Twt	2009	NaN	NaN	17.66	-0.01
275	US-Twt	2010	9.87	1.15	15.67	-0.18
276	US-Twt	2011	12.32	4.92	14.95	-0.11
277	US-Twt	2012	8.12	0.51	16.05	-0.04
278	US-Twt	2013	12.64	0.48	15.98	-0.11
279	US-Twt	2014	17.02	0.97	17.44	-0.09
280	US-Twt	2015	14.43	0.38	17.04	-0.14
281	US-Twt	2016	11.07	0.59	16.44	-0.29
282	US-Twt	2017	11.07	0.31	NaN	NaN
283	US-Uaf	2011	0.32	0.04	-2.14	-0.17
284	US-Uaf	2012	NaN	NaN	-2.43	-0.18
285	US-Uaf	2013	NaN	NaN	-1.15	-0.18
286	US-Uaf	2014	NaN	NaN	-1.18	-0.13
287	US-Uaf	2015	NaN	NaN	-0.49	-0.12
288	US-Uaf	2016	0.68	0.05	-0.05	-0.1
289	US-Uaf	2017	0.58	0.06	1.09	-0.13
290	US-Uaf	2018	NaN	NaN	0.87	-0.13
291	US-WPT	2011	41.05	1.57	17.22	0.43
292	US-WPT	2012	54.96	1.71	14.27	0.28
293	US-WPT	2013	52.76	1.29	12.89	0.44

*\*Data from ID-Pag spans 365 days from June 2016 to June 2017. Annual methane flux for each year is the sum of these 365 days, with uncertainty being calculated separately for each year.*

### Column Descriptions

SITE_ID	Site identification code as assigned by regional flux data network
Year	Data year
Ann_Flux_g_C_m-2	Total annual methane flux (gC/m <sup>2</sup> )
Ann_Flux_Uncertainty_g_C_m-2	Gap-filling and rancom uncertainty associated with annual flux (gC/m <sup>2</sup> )
Mean_Soil_Temp_C	Annual mean soil temperature (degree C). For sites with multiple probes, we use the probe closest to the surface
Mean_Water_Table_Depth_m	Annual mean water table depth (m)



20	HK-MPM	Mai Po Mangrove	Derrick Lai, Jiangong Liu	Hong Kong	22.498	114.029	10.18140/FLX/1669642	2016	2018	8 EuroFlux
21	ID-Pag	Palangkaraya undrained forest	Takashi Hirano	Indonesia	-2.320	113.900	10.18140/FLX/1669643	2016	2017	7 EuroFlux
22	IT-BCi	Borgo Cioffi	Vincenzo Magliulo	Italy	40.524	14.957	10.18140/FLX/1669644	2017	2018	1 EuroFlux
23			Giovanni Manca, Ignacio Goded, Carsten Gruening, Ana Meijide	Italy	45.070	8.718	10.18140/FLX/1669645	2009	2010	1 EuroFlux
24	JP-BBY	Bibai bog	Masahito Ueyama	Japan	43.323	141.811	10.18140/FLX/1669646	2015	2018	9 AsiaFlux
25	JP-Mise	Mase rice paddy field	Akira Miyata	Japan	36.054	140.027	10.18140/FLX/1669647	2012	2012	9 AsiaFlux
26	JP-SwL	Suwa Lake	Hiroki Iwata	Japan	36.047	138.108	10.18140/FLX/1669648	2016	2016	9 AsiaFlux
27			Youngryel Ryu, Minseok Kang	Korea	38.201	127.251	10.18140/FLX/1669649	2015	2018	9 AsiaFlux
28			Angela C. I. Tang, Guan Xhuan Wong, Lulie Melling	Malaysia	1.454	111.149	10.18140/FLX/1669650	2014	2015	8 AsiaFlux
29	NL-MLM	Maludam National Park	Han Dolman	Netherlands	52.240	5.071	10.18140/FLX/1669651	2007	2009	1 EuroFlux
30	NZ-Kop	Kopuatai	Dave Campbell	New Zealand	-37.388	175.554	10.18140/FLX/1669652	2012	2015	13 OzFlux
31	PH-RiF	Philippines Rice Institute flooded	Ma. Carmelita Alberto	Philippines	14.141	121.265	10.18140/FLX/1669653	2012	2014	8 EuroFlux
32	RU-Ch2	Chersky reference	Matthias Goeckede	Russia	68.617	161.351	10.18140/FLX/1669654	2014	2016	11 EuroFlux
33	RU-Che	Cherski	Matthias Goeckede	Russia	68.613	161.341	10.18140/FLX/1669655	2014	2016	11 EuroFlux
34	RU-Cok	Chokurdakh	Han Dolman	Russia	70.829	147.494	10.18140/FLX/1669656	2008	2016	11 EuroFlux
35	RU-Fy2	Fyodorovskoye dry spruce	Andrej Varlagin	Russia	56.448	32.902	10.18140/FLX/1669657	2015	2018	3 EuroFlux
36	SE-Deg	Degero	Matthias Peichl, Mats Nilsson	Sweden	64.182	19.557	10.18140/FLX/1669659	2014	2018	1 EuroFlux
37	UK-LBT	London_BT	Carole Helfter	UK	51.522	-0.139	10.18140/FLX/1670207	2011	2014	0 EuroFlux
38			Ryan Sullivan, David Cook, David Billesbach	USA	70.495	-149.882	10.18140/FLX/1669661	2015	2018	-9 AmeriFlux
39	US-A03	ARM-AMF3-Oliktok	Ryan Sullivan, David Cook, David Billesbach	USA	71.324	-156.615	10.18140/FLX/1669662	2012	2018	-9 AmeriFlux
40	US-A10	ARM-NSA-Barrow	Donatella Zona	USA	70.470	-157.409	10.18140/FLX/1669663	2013	2016	-9 AmeriFlux
	US-Atq	Atqasuk								

41	US-Beo	Barrow Environmental Observatory (BEO) tower	Donatella Zona	USA	71.281	-156.612	10.18140/FLX/1669664	2013	2014	-8	AmeriFlux
42	US-Bes	Barrow-Bes (Biocomplexity Experiment South tower)	Donatella Zona	USA	71.281	-156.597	10.18140/FLX/1669665	2013	2015	-8	AmeriFlux
43	US-Bi1	Bouldin Island Alfalfa	Dennis Baldocchi	USA	38.099	-121.499	10.18140/FLX/1669666	2016	2018	-8	AmeriFlux
44	US-Bi2	Bouldin Island corn	Dennis Baldocchi	USA	38.109	-121.535	10.18140/FLX/1669667	2017	2018	-8	AmeriFlux
45	US-BZB	Bonanza Creek Thermokarst Bog	Eugenie Euskirchen	USA	64.696	-148.321	10.18140/FLX/1669668	2014	2016	-9	AmeriFlux
46	US-BZF	Bonanza Creek Rich Fen	Eugenie Euskirchen	USA	64.704	-148.313	10.18140/FLX/1669669	2014	2016	-9	AmeriFlux
47	US-BZS	Bonanza Creek Black Spruce	Eugenie Euskirchen	USA	64.696	-148.324	10.18140/FLX/1669670	2015	2016	-9	AmeriFlux
48	US-CRT	Curtice Walter-Berger cropland	Jiquen Chen, Housen Chu	USA	41.628	-83.347	10.18140/FLX/1669671	2011	2012	-5	AmeriFlux
49			Charless Ross Hinkle, Rosvel Bracho, Scott Graham, Brian Benscoter	USA	28.052	-81.436	10.18140/FLX/1669672	2013	2017	-5	AmeriFlux
50	US-DPW	Disney Wilderness Preserve Wetland	Graham, Brian Benscoter	USA	28.052	-81.436	10.18140/FLX/1669672	2013	2017	-5	AmeriFlux
51	US-EDN	Eden Landing Ecological Reserve	Patty Oikawa	USA	37.616	-122.114	10.18140/FLX/1669673	2018	2018	-8	AmeriFlux
52	US-EML	Eight Mile Lake Permafrost thaw gradient, Healy Alaska.	Ted Schuur	USA	63.878	-149.254	10.18140/FLX/1669674	2015	2018	-9	AmeriFlux
53	US-Ho1	Howland Forest (main tower)	Andrew Richardson, David Hollinger	USA	45.204	-68.740	10.18140/FLX/1669675	2012	2018	-5	AmeriFlux
54	US-HRA	Humnokke Farm Rice Field – Field A	Benjamin Runkle	USA	34.585	-91.752	10.18140/FLX/1669676	2017	2017	-6	AmeriFlux
55	US-HRC	Humnokke Farm Rice Field – Field C	Benjamin Runkle	USA	34.589	-91.752	10.18140/FLX/1669677	2017	2017	-6	AmeriFlux
56	US-ICs	Innavait Creek Watershed Wet Sedge Tundra	Eugenie Euskirchen	USA	68.606	-149.311	10.18140/FLX/1669678	2014	2016	-9	AmeriFlux
57	US-Ivo	Ivotuk	Donatella Zona	USA	68.487	-155.750	10.18140/FLX/1669679	2013	2016	-9	AmeriFlux
58	US-LA1	Pointe-aux-Chenes Brackish Marsh	Ken Krauss	USA	29.501	-90.445	10.18140/FLX/1669680	2011	2012	-6	AmeriFlux
58	US-LA2	Salvador WMA Freshwater Marsh	Ken Krauss	USA	29.859	-90.287	10.18140/FLX/1669681	2011	2013	-6	AmeriFlux
59	US-Los	Lost Creek	Ankur Desai	USA	46.083	-89.979	10.18140/FLX/1669682	2014	2018	-6	AmeriFlux

60	US-MAC	MacArthur Agro-Ecology	Jed Sparks, Sam Chamberlain	USA	27.163	-81.187	10.18140/FLX/1669683	2013	2015	-5	AmeriFlux
61	US-MRM	Marsh Resource Meadowslands Mitigation Bank	Karina Schäfer	USA	40.816	-74.044	10.18140/FLX/1669684	2012	2013	5	AmeriFlux
62	US-MYb	Mayberry Wetland	Dennis Baldocchi	USA	38.050	-121.765	10.18140/FLX/1669685	2010	2018	-8	AmeriFlux
63	US-NC4	NC_AlligatorRiver	Asko Noormets	USA	35.788	-75.904	10.18140/FLX/1669686	2012	2016	-5	AmeriFlux
64	US-NGB	NGEE Arctic Barrow	Margaret Torn	USA	71.280	-156.609	10.18140/FLX/1669687	2012	2018	-9	AmeriFlux
65	US-NGC	NGEE Arctic Council	Margaret Torn	USA	64.861	-163.701	10.18140/FLX/1669688	2017	2018	-9	AmeriFlux
66	US-ORv	Olentangy River Wetland Research Park	Gil Bohrer	USA	40.020	-83.018	10.18140/FLX/1669689	2011	2015	-5	AmeriFlux
67	US-OWC	Old Woman Creek	Gil Bohrer	USA	41.380	-82.512	10.18140/FLX/1669690	2015	2016	-5	AmeriFlux
68	US-PFa	Park Falls/WLEF	Ankur Desai	USA	45.946	-90.272	10.18140/FLX/1669691	2010	2018	-6	AmeriFlux
69	US-Snd	Sherman Island	Dennis Baldocchi	USA	38.037	-121.754	10.18140/FLX/1669692	2010	2015	-8	AmeriFlux
70	US-Sne	Sherman Island Restored Wetland	Dennis Baldocchi	USA	38.037	-121.755	10.18140/FLX/1669693	2016	2018	-8	AmeriFlux
71	US-Srr	Suisun marsh - Rush Ranch	Lisamarie Windham-Myers	USA	38.201	-122.026	10.18140/FLX/1669694	2014	2017	-8	AmeriFlux
72	US-Stj	St Jones Reserve	Rodrigo Vargas	USA	39.088	-75.437	10.18140/FLX/1669695	2016	2016	-5	AmeriFlux
73	US-Tw1	Twitchell Wetland West Pond	Dennis Baldocchi	USA	38.107	-121.647	10.18140/FLX/1669696	2011	2018	-8	AmeriFlux
74	US-Tw3	Twitchell Alfalfa	Dennis Baldocchi	USA	38.116	-121.647	10.18140/FLX/1669697	2013	2014	-8	AmeriFlux
75	US-Tw4	Twitchell East End Wetland	Dennis Baldocchi	USA	38.103	-121.641	10.18140/FLX/1669698	2013	2018	-8	AmeriFlux
76	US-Tw5	East Pond Wetland	Dennis Baldocchi	USA	38.107	-121.643	10.18140/FLX/1669699	2018	2018	-8	AmeriFlux
77	US-Twt	Twitchell Island	Dennis Baldocchi	USA	38.109	-121.653	10.18140/FLX/1669700	2009	2017	-8	AmeriFlux
78	US-Uaf	University of Alaska, Fairbanks	Masahito Ueyama	USA	64.866	-147.856	10.18140/FLX/1669701	2011	2018	-9	AmeriFlux
79	US-WPT	Winous Point North Marsh	Jiquen Chen, Housen Chu	USA	41.465	-82.996	10.18140/FLX/1669702	2011	2013	-5	AmeriFlux

### Column Descriptions

SITE\_ID

SITE\_NAME

SITE\_PERSONNEL

COUNTRY

LAT

LON

Site identification code as assigned by regional flux data network

Site name determined by site personnel

People associated with site FLUXNET-CH4 data

Site country

Latitude

Longitude

DATA\_DOI  
YEAR\_START  
YEAR\_END  
UTC\_OFFSET  
ORIGINAL\_DATA\_SOURCE

DOI link for site FLUXNET-CH4 data  
Year data begins  
Year data ends  
Site data offset from Coordinated Universal Time (in hours)  
Regional network hosting the site methane data that was incorporated into FLUXNET-CH4

**Table B3-B: Site metadata, select data, and DOI links**

SITE_ID	SITE_CLA SSIFICATI ON	UPLAND_CL ASS	IGBP	KOPPEN	MEAN_AN NUAL_TEM P_C_WORL DCLIM	MEAN_ANN UAL_PRECI P_MM_WO RLDCLIM	MOSS_B ROWN	MOSS_SPH AGNUM	AERENC HYMAT OUS	ERI_SH RUB	TREE	DOM_VEG	IN_SEASONA LITY_ANALY SIS	
1		Alpine												
	AT-Neu	Upland	meadow	GRA	Dfb	7.0	1029	0	0	1	0	0	aerenchymatous	0
2	BR-Npw	Swamp		WSA	Aw	25.2	1318	0	0	1	0	1	tree	0
3	BW-Gum	Swamp		WET	Bsh	23.1	459	0	0	1	0	1	aerenchymatous	0
4	BW-Nxr	Swamp		GRA	Bsh	23.5	433	0	0	1	0	1	aerenchymatous	0
5	CA-SCB	Bog		WET	Dfc	-2.8	414	0	1	1	1	0	moss_sphagnum	1
6	CA-SCC	Upland	Needleleaf forest	ENF	Dfc	-2.9	414	0	1	0	1	1	tree	0
7	CH-Cha	Upland	Grassland	GRA	Cfb	9.6	1194	0	0	1	0	0	aerenchymatous	0
8	CH-Dav	Upland	Needleleaf forest	ENF	ET	3.8	1053	1	0	0	1	1	tree	0
9	CH-Oe2	Upland	Crop - wheat	CRO	Cfb	9.1	1122	0	0	1	0	0	aerenchymatous	0
10	CN-Hgu	Upland	Alpine meadow	GRA	Cwc	2.8	702	0	0	1	0	0	aerenchymatous	0
11	DE-Dgw	Lake		WAT	Cfb	8.3	567	0	0	0	0	0	no vegetation	0
12	DE-Hte	Fen		WET	Dfb	8.5	584	0	0	1	0	0	aerenchymatous	1
13	DE-Sfn	Bog		WET	Cfb	8.3	1123	0	1	1	1	1	tree	1
14	DE-Zrk	Fen		WET	Dfb	8.3	580	0	0	1	0	0	aerenchymatous	1
15	FI-Hyy	Upland	Needleleaf forest	ENF	Dfc	3.1	671	1	1	0	1	1	tree	0
16	FI-Lom	Fen		WET	Dfc	-1.0	512	1	1	1	1	0	aerenchymatous	1
17	FI-Si2	Bog		WET	Dfc	3.2	664	0	1	1	1	1	moss_sphagnum	1
18	FI-Sii	Fen		WET	Dfc	3.2	666	0	1	1	0	0	moss_sphagnum	1
19	FR-LGt	Fen		WET	Cfb	11.0	707	0	1	1	1	0	aerenchymatous	0
20	HK-MPM	Mangro ve		EBF	Cfa	22.7	1991	0	0	1	0	1	aerenchymatous	0
21	ID-Pag	Swamp		EBF	Af	27.4	2386	0	0	1	0	1	tree	0
22	IT-BCi	Upland	Crop - corn	CRO	Csa	16.3	1035	0	0	1	0	0	aerenchymatous	0
23	IT-Cas	Rice		CRO	Cfa	12.3	773	0	0	1	0	0	aerenchymatous	0

24	JP-BBY	Bog		WET	Dfb	6.7	1153	0	1	1	1	1	0	aerenchymatous	1
25	JP-Mse	Rice		CRO	Cfa	14.1	1305	0	1	1	0	0	0	aerenchymatous	0
26	JP-SwL	Lake		WAT	Dfb	10.2	1141	0	1	1	0	0	0	aerenchymatous	0
27	KR-CRK	Rice		CRO	Dwa	9.9	1234	0	1	1	0	0	0	aerenchymatous	0
28	MY-MLM	Swamp		EBF	Af	26.9	3401	0	0	0	0	0	1	tree	0
29	NL-Hor	Drained	Grassland	GRA	Cfb	9.7	827	0	1	1	0	0	0	aerenchymatous	0
30	NZ-Kop	Bog		EBF	Cfb	13.9	1343	0	1	1	0	0	0	aerenchymatous	1
31	PH-RiF	Rice		CRO	Am	26.9	2010	0	1	1	0	0	0	aerenchymatous	0
32	RU-Ch2	Wet tundra		WET	Dfc	-12.3	172	0	1	1	1	0	0	aerenchymatous	1
33	RU-Che	Drained		WET	Dfc	-12.3	172	0	1	1	1	0	0	aerenchymatous	0
34	RU-Cok	Wet tundra		OSH	Dfc	-14.1	210	0	1	1	1	0	0	moss_sphagnum	0
35	RU-Fy2	Upland	Needleleaf forest	ENF	Dfb	4.3	694	0	1	0	1	1	1	tree	0
36	SE-Deg	Fen		GRA	Dfc	1.7	620	0	1	1	1	0	0	moss_sphagnum	1
37	UK-LBT	Upland	Urban	URB	Cfb	11.0	646	0	0	0	0	0	0	no vegetation	0
38	US-A03	Wet tundra		BSV	ET	-11.9	144	0	1	1	0	0	0	moss_sphagnum	0
39	US-A10	Wet tundra		BSV	ET	-12.0	107	0	1	1	0	0	0	moss_sphagnum	0
40	US-Atq	Wet tundra		WET	ET	-10.3	133	1	0	1	1	0	0	aerenchymatous	1
41	US-Beo	Wet tundra		WET	ET	-11.9	109	1	1	1	0	0	0	aerenchymatous	1
42	US-Bes	Wet tundra		WET	ET	-12.0	109	0	1	1	0	0	0	aerenchymatous	1
43	US-Bi1	Drained	Crop - alfalfa	CRO	Csa	15.5	382	0	0	1	0	0	0	aerenchymatous	0
44	US-Bi2	Drained	Crop - corn	CRO	Csa	15.5	380	0	1	1	0	0	0	aerenchymatous	0
45	US-BZB	Bog		WET	Dfd	-2.4	292	0	1	1	1	0	0	eri_shrub	1
46	US-BZF	Fen		WET	Dfd	-2.5	294	1	1	1	0	0	0	aerenchymatous	1
47	US-BZS	Upland	Needleleaf forest	ENF	Dfd	-2.4	292	1	0	0	0	0	1	tree	0
48	US-CRT	Upland	Crop - soy	CRO	Dfa	9.7	855	0	1	1	0	0	0	aerenchymatous	0
49	US-DPW	Marsh		WET	Cwa	22.1	1223	0	1	1	0	0	0	aerenchymatous	1



75	US-Tw4	Marsh	WET	Csa	15.4	370	0	1	0	0	aerenchymatous	1
76	US-Tw5	Marsh	WET	Csa	15.4	371	0	1	0	0	aerenchymatous	1
77	US-Twt	Rice	CRO	Csa	15.3	372	0	1	0	0	aerenchymatous	0
78	US-Uaf	Bog	ENF	Dwc	-2.8	298	1	1	1	1	moss_sphagnum	1
79	US-WPT	Marsh	WET	Dfa	9.9	881	0	1	0	0	aerenchymatous	1

### Column Descriptions

SITE_ID	Site identification code as assigned by regional flux data network
SITE_CLASSIFICATION	Site classification based on literature description of sites
UPLAND_CLASS	For upland sites, category of upland type
IGBP	International Geosphere–Biosphere Programme (IGBP) ecosystem surface classification
KOPPEN	Koppen climate zone abbreviation
MEAN_ANNUAL_TEMP_C_W	Mean annual precipitation from WorldClim2 Global Climate Data
ORLDCLIM	Mean annual precipitation from WorldClim2 Global Climate Data
MEAN_ANNUAL_PRECIP_M	Mean annual precipitation from WorldClim2 Global Climate Data
M_WORLDCLIM	Mean annual precipitation from WorldClim2 Global Climate Data
MOSS_BROWN	Presence/absence (1/0) brown moss. Presence/absence designated by Avni Malhotra using site-literature
MOSS_SPHAGNUM	Presence/absence (1/0) sphagnum moss. Presence/absence designated by Avni Malhotra using site-literature
AERENCHYMATOUS	Presence/absence (1/0) aerenchymatous vegetation. Presence/absence designated by Avni Malhotra using site-literature
ERI_SHRUB	Presence/absence (1/0) ericaceous shrubs. Presence/absence designated by Avni Malhotra using site-literature
TREE	Presence/absence (1/0) trees. Presence/absence designated by Avni Malhotra using site-literature
DOM_VEG	Dominant vegetation type in tower footprint. Dom_veg provided to Avni Malhotra by site personnel via sur
IN_SEASONALITY_ANALYSIS	Is site in freshwater wetland seasonality analysis? 1 = yes, 0 = no.

**Table B3-C: Site metadata, select data, and DOI links**

SITE_ID	Mean_Air_Temp_C	Mean_Air_Temp_C	Ann_Flux_g_CH4-C_m-2	Ann_Flux_tdev_g_CH4-C_m-2	JFM_flux_g_CH4-C_m-2	JFM_flux_tdev_g_CH4-C_m-2	AMJ_flux_g_CH4-C_m-2	AMJ_flux_tdev_g_CH4-C_m-2	JAS_flux_g_CH4-C_m-2	JAS_flux_tdev_g_CH4-C_m-2	OND_flux_g_CH4-C_m-2	OND_flux_tdev_g_CH4-C_m-2
1	6.60	0.51	0.32	0.09	0.03	0.03	0.05	0.04	0.16	0.07	0.09	0.01
2	25.44	0.73	19.21	2.45	9.68	1.46	8.52	1.15	0.01	0.16	0.15	
3	22.79		51.73				19.32					
4	23.06		47.32				8.88		16.90		18.09	
5	-0.75	1.92	10.67	1.34			2.96	0.70	6.58	0.77	1.16	0.11
6	-0.24	2.04	6.15	1.05			1.79	0.45	3.41	0.67		
7	9.74	0.54	2.95	0.88	0.75	0.18	0.99	0.37	0.60	0.28	0.61	0.25
8	4.37	0.09	1.21		0.28	0.05	0.37	0.21	0.13	0.24	0.24	
9	11.00		0.29						0.14	0.13	0.13	
10	3.77	1.31	0.82	0.01			0.23	0.04	0.28	0.15	0.15	
11	9.72	0.38	8.97	2.06	0.07	0.06	1.49	0.57	4.15	0.76	2.51	1.05
12	10.04	0.54	48.11	7.41	2.98	0.72	17.18	3.66	24.28	4.07	6.17	1.46
13	8.28	0.72	3.62		0.43	0.10	0.23		1.67	0.43	0.72	0.25
14	9.55	0.51	30.53	0.96	1.18	0.24	12.27	1.55	16.18	1.47	1.51	0.56
15	4.36								-0.02			
16	-0.35	0.78	15.58	1.83	0.93	0.22	3.75	0.51	9.49	1.25	1.68	0.24
17	5.14	0.84	9.74	0.67			2.71	0.59	5.83	1.15	1.19	0.08
18	4.72	0.42	12.43	3.36	0.68	0.11	3.34	0.75	6.79	2.90	1.58	0.42
19	11.07	0.37	2.45		0.02		1.09		0.85	0.29	0.29	
20	23.75	0.10	11.09	0.51	0.97		2.33	0.52	5.56	0.34	2.95	0.26
21	26.57	0.19	0.09	0.00	0.19		0.13		-0.24		0.05	
22	16.69	0.39			-5.18						-2.69	
23	12.58	0.58	21.62	5.40	0.60		5.59	3.71	15.31	2.24	0.42	0.12
24	7.11	0.44	15.19	5.15	1.60	0.39	2.61	0.97	8.27	2.60	3.67	0.03
25	13.75		9.50				1.59		7.42	0.45	0.45	
26	11.67		66.68						39.86		18.53	
27	10.96	0.46	27.92	1.81	0.92	0.15	8.81	0.92	16.69	1.77	1.25	0.11
28	27.09	0.11	9.55		3.28		2.60	0.02	1.62		2.34	
29	10.75	0.60										
30	13.68	0.28	17.34	4.46	3.99	0.84	3.03	1.63	3.63	0.52	5.87	0.30

31	PH-RIF	26.54	0.15	12.41	3.57	1.02	2.58	2.66	5.53	0.01	3.34	
32	RU-Ch2	-9.88	1.26	6.43	0.79	0.29	0.87	0.09	4.65	0.48	1.44	0.28
33	RU-Che	-9.77	1.25	4.09	0.22	0.37	0.47	0.08	2.18	0.12	1.19	0.04
34	RU-Cok	-12.38	0.92	4.45			0.74	0.09	3.42			
35	RU-Fy2	5.80	0.53	3.50	1.88	1.65	-0.27	0.04	-0.39	0.10	2.36	1.32
36	SE-Deg	2.57	0.77	10.74	0.88	0.59	3.30	0.29	5.70	0.78	1.44	0.09
37	UK-LBT	10.62	0.78	46.54	5.61	13.70	12.52		12.26	1.66	14.04	1.87
38	US-A03	-7.15	0.66	5.81	2.06		1.27	0.19	3.25	0.32		
39	US-A10								1.08			
40	US-Atq	-10.88	2.23	1.77	0.03	0.00	0.30	0.07	1.05	0.03	0.55	
41	US-Beo	-9.50	0.20	2.74	0.09	0.09	0.27		1.77		0.69	0.12
42	US-Bes	-10.46	0.21	3.19	0.18	0.09	0.58	0.26	2.20	0.18	0.71	
43	US-Bi1	13.87	1.20	0.69		0.45	-0.07	0.02	-0.13		0.17	0.05
44	US-Bi2	15.01	0.28	1.28	0.59	0.66	0.30	0.21	0.10	0.06	0.54	0.02
45	US-BZB	-0.62	0.55	9.05	2.23		2.41	0.39	6.06	1.43		
46	US-BZF	-0.31	0.55	8.72	2.98		3.21	2.77	6.35	2.24		
47	US-BZS	0.26	0.68	0.78	0.15		0.23	0.01	0.53	0.11		
48	US-CRT	11.32	0.91	2.21	0.00	0.58			0.26		0.59	
49	US-DPW	22.23	0.41	48.71	8.84	1.53	11.27	2.75	27.64	7.55	12.90	2.54
50	US-EDN	14.99		-0.04			-0.19		0.16			
51	US-EML	-1.72	3.76	0.59	0.39	-0.03	0.06	0.17	0.35	0.12	0.27	
52	US-Ho1	6.48	1.32	-0.16	0.09	-0.04	-0.03	0.02	-0.02	0.05	-0.07	0.02
53	US-HRA	19.36		-0.24			1.28		6.08			
54	US-HRC	20.23		-0.24			3.07		8.38			
55	US-ICs	-6.02	0.48						1.23	0.30		
56	US-Ivo	-8.27	0.54	4.90	0.95	0.70	0.80	0.05	2.55	0.54	1.26	0.42
57	US-LA1	24.12	0.42	12.68	0.68	0.68	2.27		7.58		1.39	1.08
58	US-LA2	20.34	4.43	34.81	19.34	4.27	14.50	2.18	21.72	2.75	6.96	0.79
59	US-Los	5.01	1.23	6.51	1.28	0.36	1.71	0.46	3.57	0.96	0.81	0.25
60	US-MAC	23.15	0.96	15.82	10.34	1.32	3.71	2.07	14.70	5.53	2.81	0.25
61	US-MRMI	13.14	0.88	0.34	0.05	0.09	0.07	0.01	0.11	0.01		
62	US-MYb	15.53	0.58	47.88	14.90	4.51	14.12	5.54	22.04	7.87	6.52	3.17
63	US-NC4	16.74	0.85	33.89	17.41	0.80	5.70	1.62	20.41	9.80	6.77	2.19
64	US-NGB	-9.45	0.92	2.41	0.15		0.26	0.15	2.00	0.26		

65	US-NGC	1.21	0.82	2.52	0.00	0.88	0.10	2.55	0.93	0.86	0.41	0.17
66	US-ORV	12.20	0.92	7.20	2.51	0.88	0.10	2.55	0.93	3.14	1.16	0.99
67	US-OWC	13.02	1.72	113.99				31.03		66.03	10.07	9.81
68	US-PFa	5.42	1.24	0.54	0.25	0.15	0.05	0.39	0.19	0.00	0.00	
69	US-Snd	14.76	1.16	4.71	1.71	2.00	1.79	1.11	0.74	1.35	0.61	1.74
70	US-Sne	15.04	0.45	42.80	4.48	2.44	0.71	14.95	5.12	12.61	10.68	4.71
71	US-Srr	15.93	0.45	0.83	0.08	0.09	0.06	0.31	0.04	0.42	0.09	0.08
72	US-StJ	13.96		9.55				1.40		5.24		2.92
73	US-Tw1	15.16	0.74	39.51	11.03	4.92	1.91	10.13	3.74	18.02	4.08	7.11
74	US-Tw3	16.04	0.87									0.29
75	US-Tw4	15.52	0.56	32.54	11.74	4.39	1.75	9.49	4.83	12.78	6.07	5.89
76	US-Tw5	15.03		59.72				21.49		29.78		8.45
77	US-Twt	14.26	1.71	12.07	2.75	3.07	1.10	1.05	0.59	5.49	3.15	1.73
78	US-Uaf	-2.87	1.03	0.53	0.19			0.07		0.33	0.12	
79	US-WPT	11.40	0.99	49.59	7.48	1.66	0.22	16.31	3.99	28.75	3.05	3.26

### Column Descriptions

SITE_ID	Site identification code as assigned by regional flux data network
Mean_Air_Temp_C	Mean annual air temperature, calculated from flux tower variable TA_F (C)
Ann_Flux_g_CH4-C_m-2	Mean annual methane flux (g CH4-C/m2/year)
JFM_flux_g_CH4-C_m-2	Mean methane flux in January, February, March (gCH4-C/m2/year)
AMJ_flux_g_CH4-C_m-2	Mean methane flux in April, May, June (gCH4-C/m2/year)
JAS_flux_g_CH4-C_m-2	Mean methane flux in July, August, September (gCH4-C/m2/year)
OND_flux_g_CH4-C_m-2	Mean methane flux in October, November, December (gCH4-C/m2/year)
Mean_Air_Temp_stdev_C	Standard deviation of annual air temperature (C)
Ann_Flux_stdev_g_CH4-C_m-2	Standard deviation of annual methane flux (gCH4-C/m2/year)
JFM_flux_stdev_g_CH4-C_m-2	Standard deviation of methane flux in January, February, March (gCH4-C/m2/year)
AMJ_flux_stdev_g_CH4-C_m-2	Standard deviation of methane flux in April, May, June (gCH4-C/m2/year)
JAS_flux_stdev_g_CH4-C_m-2	Standard deviation of methane flux in July, August, September (gCH4-C/m2/year)
OND_flux_stdev_g_CH4-C_m-2	Standard deviation of methane flux in October, November, December (gCH4-C/m2/year)

**Table B3-D: Site metadata, select data, and DOI links**

	SITE_ID	SOIL_TEMP_PROBE_DEPTHS
1	AT-Neu	TS_1 = -0.05cm; TS_2 = -0.1cm; TS_3 = -0.2cm;
2	BR-Npw	
3	BW-Gum	
4	BW-Nxr	
5	CA-SCB	TS_1 = 0cm; TS_2 = -0.02cm; TS_3 = -0.04cm; TS_4 = -0.08cm; TS_5 = -0.16cm; TS_6 = -0.32cm; TS_7 = -0.64cm ;TS_8 = -1.28cm;
6	CA-SCC	TS_1 = -0.1cm; TS_2 = -0.15cm; TS_3 = -0.2cm; TS_4 = -0.25cm; TS_5 = -0.3cm; TS_6 = -0.5cm; TS_7 = -0.6cm; TS_8 = -0.7cm;
7	CH-Cha	TS_1 = -0.01cm; TS_2 = -0.02cm; TS_3 = -0.04cm; TS_4 = -0.07cm; TS_5 = -0.1cm; TS_6 = -0.15cm; TS_7 = -0.25cm; TS_8 = -0.4cm; TS_9 = -0.95cm;
8	CH-Dav	TS_1 = -0.05cm; TS_2 = -0.15cm; TS_3 = -0.5cm;
9	CH-Oe2	TS_1 = -0.05cm; TS_2 = -0.1cm; TS_3 = -0.15cm; TS_5 = -0.3cm; TS_6 = -0.5cm;
10	CN-Hgu	
11	DE-Dgw	
12	DE-Hte	TS_1 = 0cm; TS_2 = -0.1cm; TS_3 = -0.2cm;
13	DE-Sfn	TS_1 = -0.02cm; TS_3 = -0.1cm; TS_4 = -0.2cm; TS_5 = -0.5cm;
14	DE-Zrk	TS_1 = -0.05cm; TS_2 = -0.1cm; TS_3 = -0.2cm; TS_4 = -0.3cm; TS_5 = -0.5cm;
15	FI-Hvy	TS_1 = -0.02cm; TS_2 = -0.04cm; TS_3 = -0.12cm; TS_4 = -0.25cm; TS_5 = -0.5cm;
16	FI-Lom	TS_1 = -0.07cm; TS_2 = -0.3cm; TS_3 = -0.5cm;
17	FI-SI2	TS_1 = -0.05cm; TS_2 = -0.2cm; TS_3 = -0.35cm; TS_4 = -0.5cm; TS_1 = -0.05cm; TS_2 = -0.2cm; TS_3 = -0.35cm; TS_4 = -0.5cm;
18	FI-Sii	before 2016(TS_1 = -0.05cm; TS_2 = -0.2cm; TS_3 = -0.35cm; TS_4 = -0.5cm; TS_2 = -0.2cm; TS_3 = -0.35cm; TS_4 = -0.5cm; TS_2 = -0.2cm; TS_3 = -0.35cm; TS_4 = -0.5cm) after 2017 (TS_1 = 0cm; TS_2 = -0.5cm; TS_3 = -0.1cm; TS_4 = -0.15cm; TS_5 = -0.25cm; TS_6 = -0.45cm; TS_7 = -0.95cm)
19	FR-LGt	TS_1 = -0.02cm; TS_2 = -0.05cm; TS_3 = -0.1cm; TS_4 = -0.2cm; TS_5 = -0.4cm;
20	HK-MPM	
21	ID-Pag	TS_1 = -0.05cm;
22	IT-BCi	TS_1 = -0.05cm; TS_2 = -0.1cm; TS_3 = -0.3cm; TS_4 = -0.5cm; TS_5 = -1cm;
23	IT-Cas	TS_1 = -0.05cm; TS_2 = -0.3cm; TS_3 = -0.5cm;
24	JP-BBY	TS_1 = -0.183cm; TS_2 = -0.233cm; TS_3 = -0.283cm; TS_4 = -0.383cm; TS_5 = -0.483cm;
25	JP-Mise	TS_1 = -0.01cm; TS_2 = -0.025cm; TS_3 = -0.05cm; TS_4 = -0.1cm; TS_5 = -0.2cm; TS_6 = -0.4cm;
26	JP-SwL	
27	KR-CRK	TS_1 = -0.05cm; TS_2 = -0.15cm;
28	MY-MLM	TS_1 = -0.05cm;
29	NL-Hor	TS_1 = -0.01cm; TS_2 = -0.02cm; TS_3 = -0.04cm; TS_4 = -0.05cm; TS_5 = -0.1cm; TS_6 = -0.15cm; TS_7 = -0.25cm; TS_8 = -0.4cm; TS_9 = -0.6cm;
30	NZ-Kop	TS_1 = -0.5cm; TS_2 = -0.1cm; TS_3 = -0.2cm;
31	PH-RiF	

32	RU-Ch2	TS_1 = -0.04cm; TS_2 = -0.08cm; TS_3 = -0.16cm;
33	RU-Che	TS_1 = -0.04cm; TS_2 = -0.08cm; TS_3 = -0.16cm;
34	RU-Cok	
35	RU-Fy2	
36	SE-Deg	TS_1 = -0.02cm; TS_2 = -0.05cm; TS_3 = -0.1cm; TS_4 = -0.15cm; TS_5 = -0.3cm; TS_6 = -0.5cm;
37	UK-LBT	
38	US-A03	TS_1 = -0.025cm; TS_2 = -0.1cm; TS_3 = -0.3cm;
39	US-A10	TS_1 = -0.025cm; TS_2 = -0.1cm; TS_3 = -0.3cm;
40	US-Atq	
41	US-Beo	
42	US-Bes	
43	US-Bi1	TS_1 = -0.02cm; TS_2 = -0.04cm; TS_3 = -0.08cm; TS_4 = -0.16cm; TS_5 = -0.32cm;
44	US-Bi2	TS_1 = -0.02cm; TS_2 = -0.04cm; TS_3 = -0.08cm; TS_4 = -0.16cm; TS_5 = -0.32cm;
45	US-BZB	TS_1 = -0.075cm; TS_2 = -0.05cm;
46	US-BZF	TS_1 = -0.075cm; TS_2 = -0.05cm;
47	US-BZS	
48	US-CRT	
49	US-DPW	
50	US-EDN	TS_1 = -0.25cm; TS_2 = -0.15cm; TS_3 = -0.05cm; TS_4 = 0cm; TS_5 = 0.05cm; TS_6 = 0.1cm; TS_7 = 0.2cm; TS_8 = 0.3cm;
51	US-EML	TS_1 = -0.05cm; TS_2 = -0.1cm; TS_3 = -0.2cm; TS_4 = -0.4cm;
52	US-Ho1	TS_1 = -0.05cm; TS_2 = -0.1cm;
53	US-HRA	
54	US-HRC	
55	US-ICs	TS_1 = -0.075cm; TS_2 = -0.05cm;
56	US-Ivo	TS_1 = -0.05cm; TS_2 = -0.1cm; TS_3 = -0.15cm; TS_4 = -0.3cm; TS_5 = -0.4cm;
57	US-LA1	TS = -0.1cm;
58	US-LA2	TS = -0.1cm;
59	US-Los	TS_1 = 0cm; TS_2 = -0.05cm; TS_3 = -0.1cm; TS_4 = -0.2cm; TS_5 = -0.5cm;
60	US-MAC	
61	US-MRM	
62	US-Myb	TS_1 = -0.02cm; TS_2 = -0.04cm; TS_3 = -0.08cm; TS_4 = -0.16cm; TS_5 = -0.32cm;
63	US-NC4	TS_1 = -0.05cm; TS_2 = -0.2cm;
64	US-NGB	
65	US-NGC	

66	US-ORv	TS_1 = -0.08cm;
67	US-OWC	TS_1 = -0.05cm; TS_2 = -0.3cm;
68	US-PFa	
69	US-Snd	TS_1 = -0.08cm; TS_2 = -0.16cm; TS_3 = nancm; TS_4 = nancm; TS_5 = nancm; TS_6 = nancm;
70	US-Sne	TS_1 = -0.01cm; TS_2 = -0.02cm; TS_3 = -0.08cm; TS_4 = -0.16cm; TS_5 = -0.32cm;
71	US-Srr	
72	US-StJ	TS_2 = -0.05cm; TS_3 = -0.1cm;
73	US-Tw1	TS_1 = -0.02cm; TS_2 = -0.04cm; TS_3 = -0.08cm; TS_4 = -0.16cm; TS_5 = -0.32cm;
74	US-Tw3	TS_1 = -0.02cm; TS_2 = -0.04cm; TS_3 = -0.08cm; TS_4 = -0.16cm; TS_5 = -0.32cm;
75	US-Tw4	TS_1 = -0.02cm; TS_2 = -0.04cm; TS_3 = -0.08cm; TS_4 = -0.16cm; TS_5 = -0.32cm;
76	US-Tw5	TS_1 = -0.02cm; TS_2 = -0.1cm; TS_3 = -0.02cm; TS_4 = -0.08cm; TS_5 = -0.16cm;
77	US-Twt	TS_1 = -0.02cm; TS_2 = -0.04cm; TS_3 = -0.08cm; TS_4 = -0.16cm; TS_5 = -0.32cm;
78	US-Uaf	TS_1 = -0.09cm; TS_2 = -0.183cm; TS_3 = -0.283cm; TS_4 = -0.367cm; TS_5 = -0.5cm; TS_6 = -0.6cm; TS_7 = -0.75cm; TS_8 = -0.925cm; TS_9 = -1cm;
79	US-WPT	TS_1 = -0.1cm; TS_2 = -0.3cm;

### Column Descriptions

SITE\_ID Site identification code as assigned by regional flux data network

SOIL\_TEMP\_PROBE\_

DEPTHS Depth of soil temperature probe (m), with negative values being under the surface

**Table B4: Bioclimatic predictor data used in the Principal Component Analysis (PCA)**

	SITE_ID	Enhanced_Vegetation_Index_(EVI)	Wong_Simple_Ratio_Water_Index_(SRWI)	Latent_Heat_(LE)	Mean_Annual_Temperature_(MAT)
1	BR-Npw	0.31	0.86	87.6	25.3
2	BW-Gum	0.28	0.87	60.9	23
3	BW-Nxr	0.22	0.82	52.6	23.5
4	CA-SCB	0.16	1.2	27.4	-2.7
5	DE-Hte	0.28	1.01	40.2	8.6
6	DE-SfN	0.41	1.03	48.5	8.2
7	DE-Zrk	0.33	1.05	42.5	8.2
8	FI-Lom	0.2	1.27	23.6	-1.5
9	FI-Si2	0.27	1.12	31.6	3.3
10	FI-Sii	0.27	1.12	31.6	3.3
11	FR-LGt	0.4	0.97	50	10.8
12	ID-Pag	0.5	1.1	119.7	27.2
13	JP-BBY	0.25	1.21	45.4	6.5
14	MY-MLM	0.42	1.17	116.6	26.9
15	NZ-Kop	0.53	1.06	71.2	13.9
16	RU-Ch2	-0.01	1.25	20	-12.1
17	RU-Cok	0.04	1.18	16.8	-14.2
18	SE-Deg	0.27	1.12	29	2
19	US-A03	-0.07	1.28	16.1	-11.4
20	US-Atq	-0.1	1.31	16.9	-10.2
21	US-BZB	0.17	1.09	26	-2.8
22	US-BZF	0.17	1.09	26	-2.8
23	US-DPW	0.32	0.88	71.8	22.2
24	US-ICs	-0.04	1.3	18.5	-8.8
25	US-Ivo	-0.08	1.34	18.4	-7.7
26	US-LA2	0.37	0.98	69.9	20
27	US-Los	0.29	1.1	46.6	4
28	US-Myb	0.23	0.86	51	15.5
29	US-NC4	0.34	0.96	68.4	16.5
30	US-NGC	0.1	1.24	22.3	-3.2
31	US-ORv	0.32	0.99	50.8	10.6
32	US-OWC	0.27	1.05	55.8	9.9
33	US-Sne	0.23	0.86	51	15.5
34	US-Tw1	0.26	0.91	51	15.5
35	US-Tw4	0.26	0.91	51	15.5
36	US-Tw5	0.26	0.91	51	15.5
37	US-Uaf	0.22	1.1	25.3	-2.8
38	US-WPT	0.27	0.96	55.8	9.8

**Column Descriptions**

SITE\_ID

Site identification code as assigned by regional flux

Enhanced_Vegetation_Index_(EVI)	Enhanced vegetation index (unitless) from MOD13A3 (Didan 2015), 2001-2018 monthly data
Wong_Simple_Ratio_Water_Index_(SR WI)	Simple Ratio Water Index (unitless) from MOD09A1 (Vermote 2015), ~2001-2018 monthly data
Latent_Heat_(LE)	Latent heat in W m <sup>-2</sup> from FLUXCOM (Jung et al., 2019), 2003-2013 monthly data
Mean_Annual_Temperature_(MAT)	Mean annual temperature (C) from BioClim (Fick & Hijman 2017), 2001-2018 monthly data

## References

- 1 Didan, K. MOD13A3 MODIS/Terra vegetation Indices Monthly L3 Global 1km SIN Grid V006 [Data set]. NASA EOSDIS Land Processes DAAC. 2015.
- 2 Fick, S.E. & R.J. Hijmans. WorldClim 2: new 1km spatial resolution climate surfaces for global land areas. *International Journal of Climatology*, 37(12): 4302-4315. 2017.
- 3 Jung, M., Koirala, S., Weber, U., Ichii, K., Gans, F., Camps-Valls, G., Papale, D., Schwalm, C., Tramontana, G., & Reichstein, M. The FLUXCOM ensemble of global land-atmosphere energy fluxes. *Scientific Data*, 6(74). doi:10.1038/s41597-019-0076-8. 2019.
- 4 Vermote, E. MOD09A1 MODIS Surface Reflectance 8-Day L3 Global 500m SIN Grid V006. NASA EOSDIS Land Processes DAAC. <http://doi.org/10.5067/MODIS/MOD09A1.006> (Terra). 2015.

Table B5-A Timesat output for FCH4, GPP\_DT, TA, and TS (TS from shallowest probe at each site)

SITE_ID	Year	Start_FCH4_(DOY)	End_FCH4_(DOY)	Base_value_FCH4_(nmolC H4/m2/s)	Ampl_FCH4_(nmolC H4/m2/s)	Peak_FCH4_(DOY)	Peak_value_FCH4_(nmolC H4/m2/s)
1	AT-Neu	2010	NaN	NaN	NaN	NaN	NaN
2	AT-Neu	2011	NaN	NaN	NaN	NaN	NaN
3	AT-Neu	2012	NaN	NaN	NaN	NaN	NaN
4	BR-Npw	2014	NaN	NaN	NaN	NaN	NaN
5	BR-Npw	2015	NaN	NaN	NaN	NaN	NaN
6	BR-Npw	2016	192.7	345.8	-2.0	270.0	152.8
7	BW-Gum	2018	34.1	151.1	132.9	89.0	319.1
8	BW-Gum	2019	230.4	NaN	134.2	281.9	336.3
9	BW-Nxr	2018	65.1	NaN	29.2	287.5	237.9
10	CA-SCB	2014	138.8	299.1	17.5	222.4	89.8
11	CA-SCB	2015	NaN	NaN	NaN	NaN	NaN
12	CA-SCB	2016	109.2	290.4	11.8	207.9	93.8
13	CA-SCB	2017	119.0	300.4	14.0	221.5	72.9
14	CA-SCC	2013	NaN	NaN	NaN	203.4	44.8
15	CA-SCC	2014	128.4	313.1	3.1	215.0	43.3
16	CA-SCC	2015	98.0	303.9	1.7	210.9	56.3
17	CA-SCC	2016	102.7	NaN	1.7	208.0	59.6
18	DE-Dgw	2015	NaN	NaN	NaN	NaN	NaN
19	DE-Dgw	2016	NaN	NaN	NaN	NaN	NaN
20	DE-Dgw	2017	NaN	NaN	NaN	NaN	NaN
21	DE-Hte	2011	NaN	NaN	NaN	NaN	NaN
22	DE-Hte	2012	82.6	330.1	20.3	205.5	222.1
23	DE-Hte	2013	101.9	NaN	29.9	201.1	378.7
24	DE-Hte	2014	NaN	338.5	38.3	204.8	314.1
25	DE-Hte	2015	75.1	322.4	29.2	202.0	306.9
26	DE-Hte	2016	83.9	289.7	21.5	202.0	369.3
27	DE-Hte	2017	90.0	304.5	18.3	194.0	290.9
28	DE-Hte	2018	85.6	258.1	21.0	196.0	343.0
29	DE-Sfn	2012	79.6	340.7	4.3	217.0	14.5

30	DE-Sfn	2013	NaN	NaN	2.7	3.0	301.9	5.7
31	DE-Sfn	2014	NaN	NaN	NaN	NaN	NaN	NaN
32	DE-Zrk	2013	NaN	NaN	NaN	NaN	NaN	NaN
33	DE-Zrk	2014	NaN	NaN	NaN	NaN	NaN	NaN
34	DE-Zrk	2015	87.0	273.0	9.3	242.5	208.7	251.9
35	DE-Zrk	2016	107.9	274.0	9.9	224.2	187.3	234.2
36	DE-Zrk	2017	110.0	270.1	11.2	203.6	190.0	214.8
37	DE-Zrk	2018	88.1	261.0	8.5	250.8	196.0	259.2
38	FI-Lom	2006	142.8	288.8	7.8	111.0	215.1	118.9
39	FI-Lom	2007	139.3	270.6	10.9	165.0	214.5	175.9
40	FI-Lom	2008	134.0	284.8	10.8	127.7	211.5	138.5
41	FI-Lom	2009	121.5	291.0	12.1	132.3	215.0	144.4
42	FI-Lom	2010	137.1	282.8	13.4	101.6	214.0	115.0
43	FI-Si2	2012	NaN	NaN	NaN	NaN	220.6	80.0
44	FI-Si2	2013	NaN	NaN	NaN	NaN	211.1	77.4
45	FI-Si2	2014	NaN	280.7	7.2	NaN	212.8	111.1
46	FI-Si2	2015	NaN	309.5	9.5	NaN	212.0	72.2
47	FI-Si2	2016	NaN	NaN	NaN	NaN	NaN	NaN
48	FI-Sii	2013	123.8	307.6	7.2	104.3	202.5	111.5
49	FI-Sii	2014	118.8	NaN	2.3	NaN	215.1	112.7
50	FI-Sii	2015	NaN	NaN	NaN	NaN	236.0	112.7
51	FI-Sii	2016	114.5	311.3	8.9	121.1	214.0	130.0
52	FI-Sii	2017	118.9	300.4	6.5	57.1	203.0	63.6
53	FI-Sii	2018	116.3	295.1	7.5	53.8	187.0	61.3
54	HK-MPM	2016	NaN	NaN	NaN	NaN	NaN	NaN
55	HK-MPM	2017	NaN	NaN	NaN	NaN	NaN	NaN
56	HK-MPM	2018	NaN	NaN	NaN	NaN	NaN	NaN
57	ID-Pag	2016	274.1	NaN	-2.8	5.1	NaN	2.3
58	JP-BBY	2015	166.7	NaN	18.3	NaN	237.7	71.4
59	JP-BBY	2016	NaN	324.9	18.3	105.7	244.3	124.0
60	JP-BBY	2017	138.5	323.1	15.2	130.1	236.0	145.3
61	JP-BBY	2018	NaN	332.1	17.8	74.7	221.0	92.6
62	JP-Mse	2012	NaN	NaN	NaN	NaN	NaN	NaN
63	KR-CRK	2015	NaN	NaN	NaN	NaN	NaN	NaN

64	KR-CRK	2016	NaN	NaN	NaN	NaN	NaN	NaN	NaN	NaN	NaN	NaN
65	KR-CRK	2017	NaN	NaN	NaN	NaN	NaN	NaN	NaN	NaN	NaN	NaN
66	KR-CRK	2018	NaN	NaN	NaN	NaN	NaN	NaN	NaN	NaN	NaN	NaN
67	MY-MLM	2014	229.6	562.4	15.5	19.8	64.2	35.3	NaN	NaN	NaN	NaN
68	MY-MLM	2015	NaN	NaN	NaN	NaN	NaN	NaN	NaN	NaN	NaN	NaN
69	NZ-Kop	2012	-94.5	227.6	36.9	28.3	176.2	65.2	176.2	176.2	176.2	65.2
70	NZ-Kop	2013	7.2	251.5	21.1	61.7	182.0	82.8	182.0	182.0	182.0	82.8
71	NZ-Kop	2014	10.0	228.4	22.6	42.7	161.0	65.2	161.0	161.0	161.0	65.2
72	NZ-Kop	2015	-8.5	NaN	23.0	34.7	150.0	57.8	150.0	150.0	150.0	57.8
73	PH-RiF	2012	154.2	303.9	4.0	62.9	239.1	66.9	239.1	239.1	239.1	66.9
74	PH-RiF	2013	304.1	455.0	5.3	54.0	380.3	59.3	380.3	380.3	380.3	59.3
75	PH-RiF	2014	133.9	265.7	6.1	121.8	178.3	127.9	178.3	178.3	178.3	127.9
76	PH-RiF	2015	NaN	NaN	3.8	56.3	NaN	60.1	NaN	NaN	NaN	60.1
77	RU-Ch2	2014	150.8	312.2	0.7	70.2	216.5	70.9	216.5	216.5	216.5	70.9
78	RU-Ch2	2015	153.3	NaN	8.0	NaN	209.0	56.1	209.0	209.0	209.0	56.1
79	RU-Ch2	2016	NaN	NaN	NaN	NaN	218.8	68.3	218.8	218.8	218.8	68.3
80	RU-Che	2014	NaN	NaN	NaN	NaN	NaN	NaN	NaN	NaN	NaN	NaN
81	RU-Che	2015	NaN	NaN	NaN	NaN	NaN	NaN	NaN	NaN	NaN	NaN
82	RU-Che	2016	NaN	NaN	NaN	NaN	NaN	NaN	NaN	NaN	NaN	NaN
83	SE-Deg	2014	NaN	NaN	NaN	80.8	204.2	91.7	204.2	204.2	204.2	91.7
84	SE-Deg	2015	103.3	318.7	5.1	73.7	211.3	78.8	211.3	211.3	211.3	78.8
85	SE-Deg	2016	102.5	324.1	4.3	74.3	205.3	78.7	205.3	205.3	205.3	78.7
86	SE-Deg	2017	NaN	NaN	NaN	NaN	NaN	NaN	NaN	NaN	NaN	NaN
87	SE-Deg	2018	117.2	327.6	6.9	50.9	192.0	57.8	192.0	192.0	192.0	57.8
88	US-Atq	2013	NaN	NaN	NaN	NaN	NaN	NaN	NaN	NaN	NaN	NaN
89	US-Atq	2014	145.7	328.7	0.9	13.2	215.0	14.1	215.0	215.0	215.0	14.1
90	US-Atq	2015	153.3	264.0	1.0	18.6	193.2	19.6	193.2	193.2	193.2	19.6
91	US-Beo	2013	NaN	NaN	NaN	NaN	NaN	NaN	NaN	NaN	NaN	NaN
92	US-Beo	2014	157.0	356.3	0.4	23.0	211.4	23.4	211.4	211.4	211.4	23.4
93	US-Bes	2013	NaN	NaN	NaN	NaN	NaN	NaN	NaN	NaN	NaN	NaN
94	US-Bes	2014	157.3	312.6	0.6	34.3	206.5	34.9	206.5	206.5	206.5	34.9
95	US-Bes	2015	146.8	283.8	0.6	35.0	193.1	35.7	193.1	193.1	193.1	35.7
96	US-BZB	2014	NaN	NaN	NaN	NaN	226.9	67.5	226.9	226.9	226.9	67.5
97	US-BZB	2015	NaN	NaN	NaN	NaN	219.4	68.4	219.4	219.4	219.4	68.4

<b>98</b>	US-BZB	2016	NaN	NaN	NaN	NaN	NaN	NaN	NaN	NaN	NaN	226.1	98.4
<b>99</b>	US-BZF	2014	NaN	NaN	NaN	NaN	NaN	NaN	NaN	NaN	NaN	231.6	57.7
<b>100</b>	US-BZF	2015	NaN	NaN	NaN	NaN	NaN	NaN	NaN	NaN	NaN	179.0	87.0
<b>101</b>	US-BZF	2016	NaN	NaN	NaN	NaN	NaN	NaN	NaN	NaN	NaN	220.1	119.1
<b>102</b>	US-BZS	2015	NaN	NaN	NaN	NaN	NaN	NaN	NaN	NaN	NaN	NaN	NaN
<b>103</b>	US-BZS	2016	NaN	NaN	NaN	NaN	NaN	NaN	NaN	NaN	NaN	NaN	NaN
<b>104</b>	US-DPW	2013	151.7	364.0	16.4	395.0	240.7	411.4	NaN	NaN	NaN	240.7	411.4
<b>105</b>	US-DPW	2014	98.9	332.5	34.5	338.0	228.9	372.4	NaN	NaN	NaN	228.9	372.4
<b>106</b>	US-DPW	2015	NaN	376.3	25.0	NaN	248.6	247.3	NaN	NaN	NaN	248.6	247.3
<b>107</b>	US-DPW	2016	84.2	389.2	23.5	184.3	237.0	207.8	NaN	NaN	NaN	237.0	207.8
<b>108</b>	US-HRA	2017	NaN	NaN	NaN	NaN	NaN	NaN	NaN	NaN	NaN	NaN	NaN
<b>109</b>	US-HRC	2018	NaN	NaN	NaN	NaN	NaN	NaN	NaN	NaN	NaN	NaN	NaN
<b>110</b>	US-ICs	2014	NaN	NaN	NaN	NaN	NaN	NaN	NaN	NaN	NaN	NaN	NaN
<b>111</b>	US-ICs	2015	NaN	NaN	NaN	NaN	NaN	NaN	NaN	NaN	NaN	NaN	NaN
<b>112</b>	US-ICs	2016	138.2	302.1	0.2	18.0	200.5	18.2	NaN	NaN	NaN	200.5	18.2
<b>113</b>	US-ivo	2013	NaN	400.0	1.9	29.9	238.9	31.9	NaN	NaN	NaN	238.9	31.9
<b>114</b>	US-ivo	2014	158.5	301.8	6.7	30.0	226.8	36.7	NaN	NaN	NaN	226.8	36.7
<b>115</b>	US-ivo	2015	156.8	278.0	6.9	19.4	231.1	26.3	NaN	NaN	NaN	231.1	26.3
<b>116</b>	US-ivo	2016	164.7	352.4	6.1	32.5	232.0	38.7	NaN	NaN	NaN	232.0	38.7
<b>117</b>	US-LA1	2012	NaN	NaN	NaN	NaN	NaN	NaN	NaN	NaN	NaN	NaN	NaN
<b>118</b>	US-LA2	2012	62.8	NaN	38.8	225.7	229.2	264.5	NaN	NaN	NaN	229.2	264.5
<b>119</b>	US-LA2	2013	NaN	NaN	25.1	193.2	216.2	218.3	NaN	NaN	NaN	216.2	218.3
<b>120</b>	US-Los	2014	127.1	309.8	4.0	35.1	219.3	39.1	NaN	NaN	NaN	219.3	39.1
<b>121</b>	US-Los	2015	143.4	324.4	3.2	34.6	220.7	37.8	NaN	NaN	NaN	220.7	37.8
<b>122</b>	US-Los	2016	143.8	310.1	3.3	75.8	193.6	79.1	NaN	NaN	NaN	193.6	79.1
<b>123</b>	US-Los	2017	134.1	255.2	3.6	58.3	185.0	61.9	NaN	NaN	NaN	185.0	61.9
<b>124</b>	US-Los	2018	143.0	288.8	3.0	52.4	191.0	55.4	NaN	NaN	NaN	191.0	55.4
<b>125</b>	US-MAC	2013	NaN	NaN	NaN	NaN	NaN	NaN	NaN	NaN	NaN	NaN	NaN
<b>126</b>	US-MAC	2014	NaN	NaN	NaN	NaN	NaN	NaN	NaN	NaN	NaN	NaN	NaN
<b>127</b>	US-MAC	2015	NaN	NaN	NaN	NaN	NaN	NaN	NaN	NaN	NaN	NaN	NaN
<b>128</b>	US-Myb	2010	NaN	NaN	NaN	NaN	NaN	NaN	NaN	NaN	NaN	NaN	NaN
<b>129</b>	US-Myb	2011	72.4	369.3	18.3	174.2	253.5	192.5	NaN	NaN	NaN	253.5	192.5
<b>130</b>	US-Myb	2012	97.2	345.3	18.9	366.6	214.7	385.5	NaN	NaN	NaN	214.7	385.5
<b>131</b>	US-Myb	2013	46.8	336.3	39.0	265.4	220.2	304.3	NaN	NaN	NaN	220.2	304.3

<b>132</b>	US-Myb	2014	57.4	334.7	37.1	276.9	206.0	314.0
<b>133</b>	US-Myb	2015	23.7	330.0	21.6	285.7	201.0	307.3
<b>134</b>	US-Myb	2016	36.9	306.0	21.9	216.0	191.0	237.9
<b>135</b>	US-Myb	2017	175.8	332.2	30.5	191.7	235.0	222.2
<b>136</b>	US-Myb	2018	33.1	322.6	28.8	99.3	169.0	128.1
<b>137</b>	US-NC4	2012	132.9	307.9	9.5	323.8	232.2	333.3
<b>138</b>	US-NC4	2013	97.2	365.1	4.3	113.3	240.7	117.5
<b>139</b>	US-NC4	2014	110.6	332.3	-0.1	181.8	253.9	181.6
<b>140</b>	US-NC4	2015	68.4	414.1	-0.8	122.5	245.0	121.7
<b>141</b>	US-NC4	2016	128.4	350.6	2.7	373.6	259.0	376.2
<b>142</b>	US-ORv	2011	NaN	297.3	7.3	15.2	178.5	22.4
<b>143</b>	US-ORv	2012	120.1	269.1	8.3	65.2	189.7	73.4
<b>144</b>	US-ORv	2013	72.4	308.4	9.0	27.4	189.4	36.4
<b>145</b>	US-ORv	2014	87.6	292.2	9.1	32.4	201.0	41.5
<b>146</b>	US-ORv	2015	86.0	NaN	8.9	38.5	170.0	47.4
<b>147</b>	US-OWC	2015	NaN	NaN	NaN	NaN	NaN	NaN
<b>148</b>	US-OWC	2016	NaN	NaN	NaN	NaN	219.2	882.8
<b>149</b>	US-Sne	2016	NaN	NaN	NaN	NaN	NaN	NaN
<b>150</b>	US-Sne	2017	76.2	337.1	14.9	244.2	187.8	259.0
<b>151</b>	US-Sne	2018	60.6	341.6	21.4	168.3	222.6	189.8
<b>152</b>	US-Srr	2014	NaN	NaN	NaN	NaN	NaN	NaN
<b>153</b>	US-Srr	2015	NaN	NaN	NaN	NaN	NaN	NaN
<b>154</b>	US-Srr	2016	NaN	NaN	NaN	NaN	NaN	NaN
<b>155</b>	US-Srr	2017	NaN	NaN	NaN	NaN	NaN	NaN
<b>156</b>	US-StJ	2016	NaN	NaN	NaN	NaN	NaN	NaN
<b>157</b>	US-Tw1	2011	140.5	352.4	36.3	104.5	233.8	140.8
<b>158</b>	US-Tw1	2012	NaN	309.6	28.1	243.5	242.9	271.6
<b>159</b>	US-Tw1	2013	33.4	307.1	42.2	114.3	218.0	156.5
<b>160</b>	US-Tw1	2014	174.6	331.5	65.3	253.2	240.0	318.5
<b>161</b>	US-Tw1	2015	62.3	330.3	63.8	204.1	207.0	267.9
<b>162</b>	US-Tw1	2016	32.3	323.8	48.5	160.0	221.0	208.5
<b>163</b>	US-Tw1	2017	27.8	305.0	43.1	138.1	226.0	181.1
<b>164</b>	US-Tw1	2018	155.0	314.9	38.7	127.5	228.0	166.3
<b>165</b>	US-Tw4	2014	93.8	461.3	27.4	36.5	226.8	63.8

<b>166</b>	US-Tw4	2015	114.5	334.1	39.8	86.5	228.2	126.3
<b>167</b>	US-Tw4	2016	42.8	357.1	43.2	101.8	215.6	144.9
<b>168</b>	US-Tw4	2017	110.7	318.8	55.1	201.2	222.0	256.3
<b>169</b>	US-Tw4	2018	63.0	237.3	53.0	165.1	173.0	218.1
<b>170</b>	US-Tw5	2018	NaN	331.9	26.5	339.3	196.9	365.8
<b>171</b>	US-Twt	2009	NaN	NaN	NaN	NaN	NaN	NaN
<b>172</b>	US-Twt	2010	NaN	NaN	NaN	NaN	NaN	NaN
<b>173</b>	US-Twt	2011	NaN	NaN	NaN	NaN	NaN	NaN
<b>174</b>	US-Twt	2012	NaN	NaN	NaN	NaN	NaN	NaN
<b>175</b>	US-Twt	2013	NaN	NaN	NaN	NaN	NaN	NaN
<b>176</b>	US-Twt	2014	NaN	NaN	NaN	NaN	NaN	NaN
<b>177</b>	US-Twt	2015	NaN	NaN	NaN	NaN	NaN	NaN
<b>178</b>	US-Twt	2016	NaN	NaN	NaN	NaN	NaN	NaN
<b>179</b>	US-Uaf	2011	157.6	NaN	0.8	2.1	242.0	2.8
<b>180</b>	US-Uaf	2012	151.8	NaN	0.7	1.6	265.9	2.3
<b>181</b>	US-Uaf	2013	167.0	NaN	0.8	1.4	267.0	2.2
<b>182</b>	US-Uaf	2014	182.2	NaN	0.9	3.2	247.0	4.1
<b>183</b>	US-Uaf	2015	176.0	NaN	0.8	3.5	245.0	4.3
<b>184</b>	US-Uaf	2016	184.7	NaN	0.9	7.3	248.0	8.2
<b>185</b>	US-Uaf	2017	182.0	NaN	0.9	6.0	248.0	6.8
<b>186</b>	US-Uaf	2018	158.5	NaN	0.9	4.9	250.0	5.8
<b>187</b>	US-WPT	2011	103.5	294.1	5.6	355.3	207.1	360.9
<b>188</b>	US-WPT	2012	90.0	296.5	9.0	380.5	195.6	389.5
<b>189</b>	US-WPT	2013	72.5	297.0	7.5	343.3	220.0	350.8

### Column Descriptions

SITE_ID	Site identification code as assigned by regional flux data network
Year	Data year
Start_FCH4_(DOY)	Season start for elevated methane fluxes (DOY), point "f" in Figure 1
End_FCH4_(DOY)	Season end for elevated methane fluxes (DOY), point "h" in Figure 1
Base_value_FCH4_(nmolCH4/m2/s)	Baseline methane flux during non-elevated season (nmol CH4 /m2/ s), average of points "a" and "b" in Figure 1

Ampl\_FCH4\_(nmolCH4/m2/s)

Amplitude of methane flux during elevated flux season (nmol CH4/m2/s), difference between point "e" in Figure 1 and Base\_value\_FCH4

Peak\_FCH4\_(DOY)

Day of maximum elevated methane flux (DOY), point "g" in Figure 1

Peak\_value\_FCH4\_(nmolCH4/m2/s)

Maximum value of methane flux (nmol CH4/m2/s), point "e" in Figure 1

Table B5-B Timesat output for FCH4, GPP\_DT, TA, and TS (TS from shallowest probe at each site)

	SITE_ID	Year	Start_GPP_D T_(DOY)	End_GPP_ DT_(DOY)	Base_value_G PP_DT_( $\mu$ mol CO2/m2/s)	Ampl_GPP_D T_( $\mu$ molCO2/ m2/s)	Peak_GPP_D T_(DOY)	Peak_value_G PP_DT_( $\mu$ mol CO2/m2/s)
1	AT-Neu	2010	61.39	332.24	-0.22	9.75	175.90	9.53
2	AT-Neu	2011	76.71	303.74	0.18	11.36	167.90	11.54
3	AT-Neu	2012	84.67	305.48	0.29	9.75	179.00	10.04
4	BR-Npw	2014	59.47	367.83	2.03	5.10	242.90	7.13
5	BR-Npw	2015	61.54	385.15	2.05	5.15	228.00	7.20
6	BR-Npw	2016	83.78	375.61	2.44	4.74	203.00	7.19
7	BW-Gum	2018	NaN	NaN	NaN	NaN	NaN	NaN
8	BW-Gum	2019	NaN	NaN	NaN	NaN	NaN	NaN
9	BW-Nxr	2018	NaN	NaN	NaN	NaN	NaN	NaN
10	CA-SCB	2014	127.53	266.07	0.10	2.69	210.00	2.79
11	CA-SCB	2015	60.15	275.15	0.10	3.35	199.40	3.45
12	CA-SCB	2016	123.04	277.07	0.05	3.66	191.90	3.71
13	CA-SCB	2017	113.78	274.63	0.04	2.99	202.00	3.02
14	CA-SCC	2013	126.43	273.72	0.20	3.21	198.80	3.41
15	CA-SCC	2014	130.06	269.31	0.30	3.22	194.30	3.52
16	CA-SCC	2015	104.41	269.97	0.28	4.54	196.90	4.82
17	CA-SCC	2016	106.89	284.75	0.09	3.67	191.00	3.76
18	DE-Dgw	2015	13.43	348.62	0.04	0.40	227.30	0.44
19	DE-Dgw	2016	31.35	294.27	0.04	0.49	167.60	0.52
20	DE-Dgw	2017	80.56	293.50	0.04	0.46	191.00	0.50
21	DE-Hte	2011	111.70	280.46	0.05	6.87	170.10	6.92
22	DE-Hte	2012	122.64	296.52	0.31	7.11	200.10	7.42
23	DE-Hte	2013	133.51	293.97	0.29	6.10	206.40	6.39
24	DE-Hte	2014	37.51	277.70	0.27	5.50	160.00	5.77
25	DE-Hte	2015	127.82	303.30	0.27	5.35	191.00	5.61
26	DE-Hte	2016	117.96	328.49	0.16	5.39	184.00	5.55
27	DE-Hte	2017	123.83	301.59	0.11	5.71	177.00	5.82
28	DE-Hte	2018	121.03	334.06	0.06	6.99	190.00	7.05
29	DE-Sfn	2012	-13.79	320.94	0.37	4.34	168.10	4.71

30	DE-Sfn	2013	64.35	316.65	0.31	3.96	198.00	4.27
31	DE-Sfn	2014	43.97	335.84	0.41	4.10	193.00	4.51
32	DE-Zrk	2013	110.23	283.50	0.09	4.30	186.30	4.39
33	DE-Zrk	2014	86.61	309.76	0.06	3.56	180.40	3.62
34	DE-Zrk	2015	99.44	264.19	0.10	3.54	186.60	3.64
35	DE-Zrk	2016	90.31	301.90	0.13	4.38	218.00	4.51
36	DE-Zrk	2017	92.93	303.86	0.11	4.07	180.00	4.18
37	DE-Zrk	2018	105.21	314.58	0.06	6.90	212.00	6.96
38	FI-Lom	2006	147.75	261.40	0.06	5.89	197.40	5.95
39	FI-Lom	2007	145.82	257.55	0.06	6.36	197.90	6.43
40	FI-Lom	2008	151.61	258.87	0.06	7.24	200.00	7.30
41	FI-Lom	2009	147.57	262.55	0.02	6.55	197.00	6.57
42	FI-Lom	2010	153.94	262.64	0.03	6.39	199.00	6.41
43	FI-Si2	2012	33.66	276.85	0.07	1.52	209.00	1.59
44	FI-Si2	2013	106.78	338.07	0.13	1.63	182.90	1.76
45	FI-Si2	2014	40.93	290.00	0.13	2.19	146.00	2.32
46	FI-Si2	2015	113.24	267.77	0.13	1.93	197.00	2.06
47	FI-Si2	2016	43.90	284.85	0.13	1.85	166.00	1.98
48	FI-Sii	2013	118.98	282.46	-0.03	3.70	185.70	3.67
49	FI-Sii	2014	100.30	294.41	0.00	2.43	199.70	2.44
50	FI-Sii	2015	84.64	321.89	0.06	2.63	204.30	2.69
51	FI-Sii	2016	118.70	284.09	0.09	3.43	200.00	3.52
52	FI-Sii	2017	117.46	290.52	0.05	3.04	206.00	3.09
53	FI-Sii	2018	113.63	295.59	0.04	2.32	185.00	2.36
54	HK-MPM	2016	NaN	NaN	NaN	NaN	NaN	NaN
55	HK-MPM	2017	NaN	NaN	NaN	NaN	NaN	NaN
56	HK-MPM	2018	NaN	NaN	NaN	NaN	NaN	NaN
57	ID-Pag	2016	NaN	NaN	NaN	NaN	NaN	NaN
58	JP-BBY	2015	123.64	304.32	0.23	5.32	203.40	5.56
59	JP-BBY	2016	114.13	302.43	0.03	7.94	203.20	7.98
60	JP-BBY	2017	119.90	300.38	0.03	7.58	199.80	7.61
61	JP-BBY	2018	96.26	311.58	0.01	5.44	217.00	5.45
62	JP-Mse	2012	144.63	266.88	0.63	9.81	209.70	10.44
63	KR-CRK	2015	134.99	267.83	0.10	10.68	202.10	10.78

64	KR-CRK	2016	137.21	262.37	0.06	12.44	198.80	12.50
65	KR-CRK	2017	143.28	266.25	0.13	12.20	193.50	12.33
66	KR-CRK	2018	138.97	263.80	0.17	10.96	198.00	11.13
67	MY-MLM	2014	179.97	437.86	8.48	2.67	272.60	11.16
68	MY-MLM	2015	194.24	NaN	8.76	8.31	271.10	17.07
69	NZ-Kop	2012	38.67	334.88	1.33	2.50	194.80	3.83
70	NZ-Kop	2013	58.12	351.65	1.50	2.61	190.00	4.10
71	NZ-Kop	2014	42.25	355.00	1.41	2.78	209.00	4.18
72	NZ-Kop	2015	44.32	366.21	1.19	3.28	193.00	4.47
73	PH-RiF	2012	NaN	NaN	NaN	NaN	NaN	NaN
74	PH-RiF	2013	NaN	NaN	NaN	NaN	NaN	NaN
75	PH-RiF	2014	NaN	NaN	NaN	NaN	NaN	NaN
76	PH-RiF	2015	NaN	NaN	NaN	NaN	NaN	NaN
77	RU-Ch2	2014	142.91	252.79	0.02	5.10	210.30	5.11
78	RU-Ch2	2015	157.47	247.95	-0.02	5.00	202.60	4.97
79	RU-Ch2	2016	145.27	257.90	-0.04	4.15	201.50	4.11
80	RU-Che	2014	161.74	258.77	0.14	5.51	206.90	5.65
81	RU-Che	2015	157.04	250.25	0.01	5.39	203.30	5.40
82	RU-Che	2016	140.55	258.30	-0.10	6.94	188.60	6.84
83	SE-Deg	2014	115.38	285.94	0.02	2.78	196.30	2.79
84	SE-Deg	2015	113.50	278.71	0.02	2.69	203.40	2.70
85	SE-Deg	2016	118.80	290.27	0.02	2.32	195.50	2.35
86	SE-Deg	2017	121.86	276.14	0.02	2.45	199.00	2.47
87	SE-Deg	2018	118.54	276.63	0.00	1.72	188.00	1.72
88	US-Atq	2013	33.24	256.46	0.03	3.05	161.70	3.09
89	US-Atq	2014	139.11	244.88	0.09	1.77	194.30	1.86
90	US-Atq	2015	132.75	243.97	0.08	3.41	191.00	3.48
91	US-Beo	2013	39.33	285.28	0.01	0.88	159.80	0.88
92	US-Beo	2014	88.23	261.54	0.02	1.99	200.00	2.02
93	US-Bes	2013	49.45	269.44	0.04	0.84	187.90	0.87
94	US-Bes	2014	174.64	262.25	0.04	1.60	220.70	1.64
95	US-Bes	2015	160.53	248.82	0.04	2.53	198.40	2.57
96	US-BZB	2014	NaN	NaN	NaN	NaN	NaN	NaN
97	US-BZB	2015	NaN	NaN	NaN	NaN	NaN	NaN

<b>98</b>	US-BZB	2016	NaN	NaN	NaN	NaN	NaN	NaN	NaN	NaN
<b>99</b>	US-BZF	2014	132.71	NaN	NaN	201.27	0.18	5.84	NaN	6.01
<b>100</b>	US-BZF	2015	129.12	NaN	NaN	258.65	0.16	6.93	NaN	7.10
<b>101</b>	US-BZF	2016	128.63	NaN	NaN	227.99	0.18	9.14	NaN	9.32
<b>102</b>	US-BZS	2015	NaN	NaN	NaN	NaN	NaN	NaN	NaN	NaN
<b>103</b>	US-BZS	2016	NaN	NaN	NaN	NaN	NaN	NaN	NaN	NaN
<b>104</b>	US-DPW	2013	NaN	NaN	NaN	NaN	NaN	NaN	NaN	NaN
<b>105</b>	US-DPW	2014	55.72	NaN	NaN	332.08	0.65	4.60	NaN	5.24
<b>106</b>	US-DPW	2015	53.69	NaN	NaN	372.93	0.73	4.77	NaN	5.50
<b>107</b>	US-DPW	2016	71.21	NaN	NaN	343.87	0.85	4.83	NaN	5.68
<b>108</b>	US-HRA	2017	131.27	NaN	NaN	244.82	0.39	20.14	NaN	20.53
<b>109</b>	US-HRC	2018	135.69	NaN	NaN	237.65	1.34	18.79	NaN	20.13
<b>110</b>	US-ICs	2014	150.35	NaN	NaN	253.40	0.21	3.46	NaN	3.66
<b>111</b>	US-ICs	2015	142.83	NaN	NaN	263.16	0.15	4.42	NaN	4.57
<b>112</b>	US-ICs	2016	154.39	NaN	NaN	245.71	0.12	3.22	NaN	3.34
<b>113</b>	US-ivo	2013	149.10	NaN	NaN	257.98	0.06	3.85	NaN	3.91
<b>114</b>	US-ivo	2014	151.63	NaN	NaN	257.85	0.11	3.63	NaN	3.73
<b>115</b>	US-ivo	2015	121.66	NaN	NaN	248.35	0.07	3.97	NaN	4.03
<b>116</b>	US-ivo	2016	154.70	NaN	NaN	254.51	0.09	5.30	NaN	5.39
<b>117</b>	US-LA1	2012	-7.96	NaN	NaN	216.91	0.49	2.29	NaN	2.78
<b>118</b>	US-LA2	2012	46.97	NaN	NaN	334.04	0.34	5.64	NaN	5.98
<b>119</b>	US-LA2	2013	93.73	NaN	NaN	335.84	0.31	6.94	NaN	7.25
<b>120</b>	US-Los	2014	131.45	NaN	NaN	288.06	-0.01	6.65	NaN	6.64
<b>121</b>	US-Los	2015	130.36	NaN	NaN	288.12	0.11	6.26	NaN	6.37
<b>122</b>	US-Los	2016	130.87	NaN	NaN	291.48	0.17	7.17	NaN	7.33
<b>123</b>	US-Los	2017	136.00	NaN	NaN	292.41	0.13	7.38	NaN	7.51
<b>124</b>	US-Los	2018	134.97	NaN	NaN	285.61	0.13	7.17	NaN	7.29
<b>125</b>	US-MAC	2013	NaN	NaN	NaN	378.12	2.50	5.43	NaN	9.45
<b>126</b>	US-MAC	2014	47.02	NaN	NaN	334.19	2.51	9.17	NaN	11.68
<b>127</b>	US-MAC	2015	46.53	NaN	NaN	356.65	2.92	5.92	NaN	8.84
<b>128</b>	US-Myb	2010	28.65	NaN	NaN	305.24	0.56	1.41	NaN	1.97
<b>129</b>	US-Myb	2011	200.41	NaN	NaN	367.27	0.28	3.62	NaN	3.89
<b>130</b>	US-Myb	2012	88.45	NaN	NaN	331.93	-0.06	13.68	NaN	13.62
<b>131</b>	US-Myb	2013	47.39	NaN	NaN	341.89	-0.12	7.95	NaN	7.83

<b>132</b>	US-Myb	2014	86.80	310.73	0.16	8.20	168.00	8.36
<b>133</b>	US-Myb	2015	76.10	323.19	0.17	7.31	202.00	7.47
<b>134</b>	US-Myb	2016	24.11	328.43	0.00	4.03	176.00	4.03
<b>135</b>	US-Myb	2017	67.46	395.16	-0.24	5.79	202.00	5.55
<b>136</b>	US-Myb	2018	83.66	331.31	-0.25	10.50	201.00	10.25
<b>137</b>	US-NC4	2012	NaN	NaN	NaN	NaN	NaN	NaN
<b>138</b>	US-NC4	2013	94.35	304.81	0.78	6.97	181.00	7.75
<b>139</b>	US-NC4	2014	97.51	354.46	0.64	6.09	173.70	6.73
<b>140</b>	US-NC4	2015	92.03	315.08	0.74	9.73	185.00	10.47
<b>141</b>	US-NC4	2016	99.57	326.98	0.92	8.22	183.00	9.14
<b>142</b>	US-ORv	2011	88.77	316.45	-0.06	7.39	180.40	7.33
<b>143</b>	US-ORv	2012	93.50	303.39	0.27	9.29	181.00	9.55
<b>144</b>	US-ORv	2013	107.62	305.23	0.36	10.11	192.40	10.46
<b>145</b>	US-ORv	2014	109.31	299.17	0.24	10.14	190.00	10.38
<b>146</b>	US-ORv	2015	105.01	301.56	0.27	9.64	194.00	9.91
<b>147</b>	US-OWC	2015	NaN	301.35	0.26	6.72	151.30	6.98
<b>148</b>	US-OWC	2016	116.05	309.20	0.30	6.44	204.00	6.73
<b>149</b>	US-Sne	2016	-21.79	306.16	0.34	7.99	190.30	8.34
<b>150</b>	US-Sne	2017	NaN	NaN	NaN	NaN	NaN	NaN
<b>151</b>	US-Sne	2018	84.63	370.31	0.32	2.43	202.00	2.75
<b>152</b>	US-Srr	2014	47.02	307.53	0.78	6.04	175.60	6.83
<b>153</b>	US-Srr	2015	35.50	320.88	0.33	7.96	158.60	8.29
<b>154</b>	US-Srr	2016	44.76	318.87	0.38	8.86	170.80	9.24
<b>155</b>	US-Srr	2017	56.75	309.79	0.30	10.46	185.00	10.76
<b>156</b>	US-StJ	2016	120.72	280.75	1.30	12.01	193.80	13.31
<b>157</b>	US-Tw1	2011	NaN	NaN	NaN	NaN	NaN	NaN
<b>158</b>	US-Tw1	2012	102.12	325.54	0.00	12.83	216.10	12.83
<b>159</b>	US-Tw1	2013	98.35	338.02	-0.18	13.11	208.40	12.93
<b>160</b>	US-Tw1	2014	95.66	326.27	0.12	10.46	208.00	10.58
<b>161</b>	US-Tw1	2015	105.53	344.13	0.26	9.88	215.00	10.13
<b>162</b>	US-Tw1	2016	91.82	313.13	-0.01	10.10	209.00	10.09
<b>163</b>	US-Tw1	2017	93.36	329.76	-0.04	11.26	214.00	11.22
<b>164</b>	US-Tw1	2018	119.04	363.78	-0.02	12.73	217.00	12.70
<b>165</b>	US-Tw4	2014	160.04	363.23	0.00	4.70	236.60	4.70

<b>166</b>	US-Tw4	2015	57.22	335.89	0.01	8.11	213.00	8.13
<b>167</b>	US-Tw4	2016	76.15	311.33	0.17	8.22	185.00	8.39
<b>168</b>	US-Tw4	2017	100.19	332.90	0.14	8.76	214.00	8.90
<b>169</b>	US-Tw4	2018	98.39	337.78	0.04	11.84	206.00	11.88
<b>170</b>	US-Tw5	2018	115.94	321.33	1.77	6.68	231.10	8.45
<b>171</b>	US-Twt	2009	149.98	293.01	0.20	12.46	212.00	12.66
<b>172</b>	US-Twt	2010	141.10	311.91	0.10	13.71	224.40	13.81
<b>173</b>	US-Twt	2011	158.51	288.69	0.12	14.22	215.90	14.34
<b>174</b>	US-Twt	2012	166.84	308.78	0.21	12.31	233.00	12.52
<b>175</b>	US-Twt	2013	138.24	272.38	0.27	16.71	202.00	16.98
<b>176</b>	US-Twt	2014	148.14	281.40	0.16	15.01	205.00	15.17
<b>177</b>	US-Twt	2015	137.11	277.23	0.17	11.52	218.00	11.68
<b>178</b>	US-Twt	2016	169.14	289.90	0.29	13.80	224.00	14.08
<b>179</b>	US-Uaf	2011	114.56	283.49	0.12	6.04	196.90	6.17
<b>180</b>	US-Uaf	2012	88.03	271.24	0.18	6.58	187.30	6.76
<b>181</b>	US-Uaf	2013	124.13	271.61	0.22	5.79	192.10	6.01
<b>182</b>	US-Uaf	2014	84.63	269.30	0.14	5.32	188.00	5.46
<b>183</b>	US-Uaf	2015	90.52	264.29	0.09	5.17	196.00	5.25
<b>184</b>	US-Uaf	2016	103.06	270.75	0.14	4.66	192.00	4.80
<b>185</b>	US-Uaf	2017	102.29	275.58	0.14	6.10	198.00	6.25
<b>186</b>	US-Uaf	2018	111.65	291.46	0.04	5.60	190.00	5.64
<b>187</b>	US-WPT	2011	134.98	285.59	0.24	7.43	206.10	7.67
<b>188</b>	US-WPT	2012	129.04	293.67	0.06	6.97	205.90	7.03
<b>189</b>	US-WPT	2013	134.87	278.12	0.05	6.20	200.90	6.24

### Column Descriptions

SITE_ID	Site identification code as assigned by regional flux data network
Year	Data year
Start_GPP_DT_(DOY)	Season start for elevated GPP_DT (DOY), point "f" in Figure 1
End_GPP_DT_(DOY)	Season end for elevated GPP_DT fluxes (DOY), point "h" in Figure 1
Base_value_GPP_DT_( $\mu\text{molCO}_2/\text{m}^2/\text{s}$ )	Baseline GPP_DT flux during non-elevated season ( $\mu\text{molCO}_2/\text{m}^2/\text{s}$ ), average of points "a" and "b" in Figure 1

Ampl\_GPP\_DT\_( $\mu\text{molCO}_2/\text{m}^2/\text{s}$ )

Peak\_GPP\_DT\_(DOY)

Peak\_value\_GPP\_DT\_( $\mu\text{molCO}_2/\text{m}^2/\text{s}$ )

Amplitude of GPP\_DT flux during elevated flux season ( $\mu\text{mol CO}_2/\text{m}^2/\text{s}$ ), difference between point "e" in Figure 1 and Base\_value\_GPP\_DT

Day of maximum elevated GPP\_DT flux (DOY), point "g" in Figure 1

Maximum value of GPP\_DT flux ( $\mu\text{mol CO}_2/\text{m}^2/\text{s}$ ), point "e" in Figure 1

Table B5-C Timesat output for FCH4, GPP\_DT, TA, and TS (TS from shallowest probe at each site)

	SITE_ID	Year	Start_TA_(DOY)	End_TA_(DOY)	Base_value_TA_(C)	Ampl_TA_(C)	Peak_TA_(DOY)	Peak_value_TA_(C)
1	AT-Neu	2010	43.17	351.66	-4.84	20.94	195.90	16.10
2	AT-Neu	2011	18.47	359.91	-5.08	20.55	198.50	15.47
3	AT-Neu	2012	38.03	366.62	-5.57	22.35	197.20	16.78
4	BR-Npw	2014	NaN	NaN	NaN	NaN	NaN	NaN
5	BR-Npw	2015	NaN	NaN	NaN	NaN	NaN	NaN
6	BR-Npw	2016	7.49	348.67	19.56	7.53	211.00	27.10
7	BW-Gum	2018	NaN	NaN	NaN	NaN	NaN	NaN
8	BW-Gum	2019	NaN	NaN	NaN	NaN	NaN	NaN
9	BW-Nxr	2018	NaN	NaN	NaN	NaN	NaN	NaN
10	CA-SCB	2014	60.23	335.31	-23.33	41.29	197.40	17.96
11	CA-SCB	2015	45.11	360.83	-21.75	39.11	186.40	17.37
12	CA-SCB	2016	49.77	335.79	-18.88	37.28	193.90	18.40
13	CA-SCB	2017	64.68	327.30	-18.45	35.95	201.00	17.50
14	CA-SCC	2013	67.57	338.23	-21.08	39.13	203.80	18.05
15	CA-SCC	2014	54.14	337.83	-22.27	40.98	196.70	18.72
16	CA-SCC	2015	46.41	359.38	-20.09	37.86	187.10	17.77
17	CA-SCC	2016	47.31	350.23	-18.76	37.65	194.00	18.89
18	DE-Dgw	2015	72.47	347.56	2.18	16.25	203.80	18.42
19	DE-Dgw	2016	64.46	324.69	1.34	17.37	205.40	18.71
20	DE-Dgw	2017	43.79	375.32	-0.17	18.47	202.20	18.30
21	DE-Hte	2011	NaN	NaN	NaN	NaN	NaN	NaN
22	DE-Hte	2012	50.34	352.49	0.77	17.03	207.60	17.80
23	DE-Hte	2013	83.53	365.30	1.64	17.09	202.50	18.73
24	DE-Hte	2014	48.71	352.47	2.86	15.82	213.00	18.68
25	DE-Hte	2015	57.62	366.35	2.59	15.33	211.00	17.92
26	DE-Hte	2016	67.53	323.10	2.75	16.01	211.00	18.76
27	DE-Hte	2017	58.94	370.07	1.81	16.22	212.00	18.02
28	DE-Hte	2018	74.55	368.02	0.91	19.14	203.00	20.05
29	DE-Sfn	2012	54.86	355.18	-2.09	20.25	196.30	18.16
30	DE-Sfn	2013	64.64	344.04	-0.35	18.57	202.80	18.22
31	DE-Sfn	2014	NaN	NaN	NaN	NaN	NaN	NaN



66	KR-CRK	2018	NaN	NaN	NaN	NaN	NaN	NaN	NaN	NaN	NaN	NaN
67	MY-MLM	2014	17.51	365.80	25.97	1.95	179.40	NaN	NaN	27.91	NaN	NaN
68	MY-MLM	2015	NaN	NaN	NaN	NaN	NaN	NaN	NaN	NaN	NaN	NaN
69	NZ-Kop	2012	50.84	347.05	9.12	9.72	219.90	NaN	NaN	18.84	NaN	NaN
70	NZ-Kop	2013	39.31	352.93	9.31	8.28	209.60	NaN	NaN	17.60	NaN	NaN
71	NZ-Kop	2014	53.45	352.71	9.08	9.68	215.00	NaN	NaN	18.76	NaN	NaN
72	NZ-Kop	2015	51.01	357.77	8.55	10.41	212.00	NaN	NaN	18.96	NaN	NaN
73	PH-RiF	2012	NaN	NaN	NaN	NaN	NaN	NaN	NaN	NaN	NaN	NaN
74	PH-RiF	2013	NaN	NaN	NaN	NaN	NaN	NaN	NaN	NaN	NaN	NaN
75	PH-RiF	2014	NaN	NaN	NaN	NaN	NaN	NaN	NaN	NaN	NaN	NaN
76	PH-RiF	2015	NaN	NaN	NaN	NaN	NaN	NaN	NaN	NaN	NaN	NaN
77	RU-Ch2	2014	62.07	339.91	-31.58	46.02	208.40	NaN	NaN	14.44	NaN	NaN
78	RU-Ch2	2015	54.09	340.02	-34.37	47.59	204.40	NaN	NaN	13.23	NaN	NaN
79	RU-Ch2	2016	56.44	373.19	-34.38	48.39	201.90	NaN	NaN	14.00	NaN	NaN
80	RU-Che	2014	61.35	339.96	-31.54	45.92	208.00	NaN	NaN	14.37	NaN	NaN
81	RU-Che	2015	53.19	340.10	-34.28	47.55	204.30	NaN	NaN	13.26	NaN	NaN
82	RU-Che	2016	55.88	372.30	-34.29	48.37	201.70	NaN	NaN	14.08	NaN	NaN
83	SE-Deg	2014	69.57	327.67	-5.24	21.42	201.00	NaN	NaN	16.18	NaN	NaN
84	SE-Deg	2015	29.69	352.18	-7.38	19.31	213.90	NaN	NaN	11.93	NaN	NaN
85	SE-Deg	2016	54.69	331.26	-7.34	20.99	197.10	NaN	NaN	13.65	NaN	NaN
86	SE-Deg	2017	61.87	353.17	-8.35	21.32	210.00	NaN	NaN	12.98	NaN	NaN
87	SE-Deg	2018	74.36	373.70	-11.34	26.53	193.00	NaN	NaN	15.18	NaN	NaN
88	US-Atq	2013	NaN	NaN	NaN	NaN	NaN	NaN	NaN	NaN	NaN	NaN
89	US-Atq	2014	70.05	360.75	-25.81	32.20	203.40	NaN	NaN	6.38	NaN	NaN
90	US-Atq	2015	84.07	347.24	-26.07	34.70	196.70	NaN	NaN	8.63	NaN	NaN
91	US-Beo	2013	NaN	NaN	NaN	NaN	NaN	NaN	NaN	NaN	NaN	NaN
92	US-Beo	2014	63.26	351.27	-22.70	25.61	203.20	NaN	NaN	2.91	NaN	NaN
93	US-Bes	2013	NaN	NaN	NaN	NaN	NaN	NaN	NaN	NaN	NaN	NaN
94	US-Bes	2014	76.62	357.34	-24.74	26.57	208.30	NaN	NaN	1.83	NaN	NaN
95	US-Bes	2015	82.66	344.05	-25.16	29.49	203.30	NaN	NaN	4.32	NaN	NaN
96	US-BZB	2014	65.05	339.25	-17.12	32.08	189.60	NaN	NaN	14.95	NaN	NaN
97	US-BZB	2015	52.17	340.04	-17.27	33.86	181.60	NaN	NaN	16.58	NaN	NaN
98	US-BZB	2016	35.70	321.04	-16.88	33.52	192.50	NaN	NaN	16.64	NaN	NaN
99	US-BZF	2014	64.65	341.50	-16.78	31.98	190.50	NaN	NaN	15.20	NaN	NaN

<b>100</b>	US-BZF	2015	52.19	340.98	-16.93	33.41	181.50	16.48
<b>101</b>	US-BZF	2016	34.60	321.31	-16.57	33.21	194.00	16.63
<b>102</b>	US-BZS	2015	46.24	343.61	-17.41	34.59	180.20	17.18
<b>103</b>	US-BZS	2016	32.55	320.26	-15.91	33.02	193.80	17.11
<b>104</b>	US-DPW	2013	59.45	361.72	16.30	10.86	220.80	27.16
<b>105</b>	US-DPW	2014	38.66	326.75	15.99	11.79	210.30	27.78
<b>106</b>	US-DPW	2015	33.62	381.23	15.93	9.98	211.80	25.91
<b>107</b>	US-DPW	2016	45.53	367.09	15.72	12.81	203.00	28.53
<b>108</b>	US-HRA	2017	NaN	NaN	NaN	NaN	NaN	NaN
<b>109</b>	US-HRC	2018	NaN	NaN	NaN	NaN	NaN	NaN
<b>110</b>	US-ICs	2014	NaN	NaN	NaN	NaN	NaN	NaN
<b>111</b>	US-ICs	2015	NaN	NaN	NaN	NaN	NaN	NaN
<b>112</b>	US-ICs	2016	68.13	328.76	-16.90	26.34	196.80	9.44
<b>113</b>	US-IVO	2013	93.13	360.42	-23.36	36.20	193.60	12.84
<b>114</b>	US-IVO	2014	69.00	341.89	-21.44	30.70	193.50	9.26
<b>115</b>	US-IVO	2015	90.83	326.77	-21.52	31.94	188.60	10.42
<b>116</b>	US-IVO	2016	90.00	339.98	-21.61	31.33	197.00	9.72
<b>117</b>	US-LA1	2012	31.05	302.54	19.07	8.85	177.60	27.92
<b>118</b>	US-LA2	2012	35.18	316.87	16.70	11.55	197.40	28.25
<b>119</b>	US-LA2	2013	71.41	321.17	15.91	13.32	210.60	29.23
<b>120</b>	US-Los	2014	58.01	365.46	-14.20	33.10	195.40	18.89
<b>121</b>	US-Los	2015	50.36	367.57	-10.76	29.37	203.50	18.60
<b>122</b>	US-Los	2016	39.16	356.37	-9.11	29.07	209.40	19.96
<b>123</b>	US-Los	2017	30.73	345.36	-9.80	28.09	212.00	18.29
<b>124</b>	US-Los	2018	69.61	336.03	-9.75	29.76	197.00	20.02
<b>125</b>	US-MAC	2013	NaN	NaN	NaN	NaN	NaN	NaN
<b>126</b>	US-MAC	2014	42.39	323.96	17.10	9.77	211.20	26.87
<b>127</b>	US-MAC	2015	39.48	328.01	16.94	9.62	200.60	26.56
<b>128</b>	US-Myb	2010	NaN	NaN	NaN	NaN	NaN	NaN
<b>129</b>	US-Myb	2011	31.10	331.80	8.15	12.63	223.60	20.78
<b>130</b>	US-Myb	2012	16.54	358.52	7.18	13.47	214.90	20.66
<b>131</b>	US-Myb	2013	24.44	342.29	7.26	13.44	197.00	20.70
<b>132</b>	US-Myb	2014	11.52	353.52	8.78	12.76	211.00	21.54
<b>133</b>	US-Myb	2015	-0.97	325.62	8.88	13.12	228.00	21.99

<b>134</b>	US-Myb	2016	-3.34	351.73	7.96	12.97	208.00	20.93
<b>135</b>	US-Myb	2017	27.35	345.82	8.30	13.88	214.00	22.19
<b>136</b>	US-Myb	2018	44.40	332.57	9.03	11.46	218.00	20.49
<b>137</b>	US-NC4	2012	57.32	339.28	9.01	17.49	208.70	26.50
<b>138</b>	US-NC4	2013	69.27	352.37	6.79	19.01	204.60	25.79
<b>139</b>	US-NC4	2014	49.17	367.68	5.41	18.30	206.30	23.71
<b>140</b>	US-NC4	2015	64.43	392.18	6.92	19.42	202.00	26.33
<b>141</b>	US-NC4	2016	53.97	350.61	8.14	19.07	215.00	27.21
<b>142</b>	US-ORV	2011	63.96	358.28	0.50	25.07	195.20	25.57
<b>143</b>	US-ORV	2012	32.88	351.31	0.84	24.92	195.90	25.76
<b>144</b>	US-ORV	2013	51.21	355.78	-2.44	25.94	203.60	23.50
<b>145</b>	US-ORV	2014	51.30	370.00	-4.35	27.96	196.00	23.61
<b>146</b>	US-ORV	2015	62.52	393.56	-4.58	27.87	199.00	23.29
<b>147</b>	US-OWC	2015	NaN	NaN	NaN	NaN	NaN	NaN
<b>148</b>	US-OWC	2016	56.19	365.00	2.20	22.65	211.80	24.85
<b>149</b>	US-Sne	2016	NaN	NaN	NaN	NaN	NaN	NaN
<b>150</b>	US-Sne	2017	9.23	344.35	7.29	14.52	217.90	21.80
<b>151</b>	US-Sne	2018	49.63	357.43	7.14	13.97	220.90	21.11
<b>152</b>	US-Srr	2014	50.56	337.45	10.74	10.06	217.30	20.80
<b>153</b>	US-Srr	2015	4.98	323.35	9.49	12.20	235.30	21.69
<b>154</b>	US-Srr	2016	-6.23	346.21	8.26	11.70	211.90	19.96
<b>155</b>	US-Srr	2017	17.23	346.39	7.94	13.42	216.00	21.36
<b>156</b>	US-StJ	2016	67.33	347.07	3.01	23.37	214.00	26.37
<b>157</b>	US-Tw1	2011	59.53	328.03	7.82	13.46	222.10	21.28
<b>158</b>	US-Tw1	2012	18.52	356.80	6.67	14.88	216.30	21.56
<b>159</b>	US-Tw1	2013	29.27	344.79	7.09	14.34	196.80	21.43
<b>160</b>	US-Tw1	2014	14.74	349.77	8.52	13.61	204.00	22.13
<b>161</b>	US-Tw1	2015	7.05	324.07	8.19	13.45	222.00	21.63
<b>162</b>	US-Tw1	2016	4.40	350.56	7.22	13.89	203.00	21.11
<b>163</b>	US-Tw1	2017	25.14	343.29	7.24	15.12	206.00	22.36
<b>164</b>	US-Tw1	2018	50.84	337.80	7.43	13.37	211.00	20.80
<b>165</b>	US-Tw4	2014	15.67	348.81	8.65	13.44	206.80	22.09
<b>166</b>	US-Tw4	2015	5.29	324.60	8.49	13.42	224.80	21.90
<b>167</b>	US-Tw4	2016	2.66	347.62	7.58	14.06	201.00	21.64

168	US-Tw4	2017	30.79	337.78	7.88	15.11	208.00	22.99
169	US-Tw4	2018	44.48	331.60	8.26	13.08	213.00	21.33
170	US-Tw5	2018	76.28	338.55	9.15	12.61	208.50	21.76
171	US-Twt	2009	NaN	NaN	NaN	NaN	NaN	NaN
172	US-Twt	2010	NaN	NaN	NaN	NaN	NaN	NaN
173	US-Twt	2011	NaN	NaN	NaN	NaN	NaN	NaN
174	US-Twt	2012	NaN	NaN	NaN	NaN	NaN	NaN
175	US-Twt	2013	NaN	NaN	NaN	NaN	NaN	NaN
176	US-Twt	2014	NaN	NaN	NaN	NaN	NaN	NaN
177	US-Twt	2015	NaN	NaN	NaN	NaN	NaN	NaN
178	US-Twt	2016	NaN	NaN	NaN	NaN	NaN	NaN
179	US-Uaf	2011	59.01	330.80	-23.42	38.45	191.90	15.02
180	US-Uaf	2012	43.13	317.75	-23.94	38.57	192.30	14.63
181	US-Uaf	2013	64.43	344.15	-22.12	39.63	195.90	17.51
182	US-Uaf	2014	49.85	342.99	-20.55	34.19	190.00	13.65
183	US-Uaf	2015	51.31	346.65	-19.52	34.90	182.00	15.38
184	US-Uaf	2016	27.33	325.47	-20.83	36.13	193.00	15.31
185	US-Uaf	2017	59.18	357.64	-22.10	38.30	191.00	16.20
186	US-Uaf	2018	35.38	354.57	-21.58	36.74	196.00	15.16
187	US-WPT	2011	62.29	362.57	-1.13	26.31	199.10	25.18
188	US-WPT	2012	34.86	355.23	-0.44	25.53	198.40	25.09
189	US-WPT	2013	64.19	341.07	-1.92	24.49	205.00	22.57

### Column Description

SITE_ID	Site identification code as assigned by regional flux data network
Year	Data year
Start_TA_(DOY)	Season start for elevated TA (DOY), point "f" in Figure 1
End_TA_(DOY)	Season end for elevated TA (DOY), point "h" in Figure 1
Base_value_TA_(C)	Baseline TA during non-elevated season (C), average of points "a" and "b" in Figure 1
Ampl_TA_(C)	Amplitude of TAduring elevated temperature season (C), difference between point "e" in Figure 1 and Base_value_TA
Peak_TA_(DOY)	Day of maximum elevated TA (DOY), point "g" in Figure 1
Peak_value_TA_(C)	Maximum value of TA (C) point "e" in Figure 1







<b>100</b>	US-BZF	2015	TS_1	-0.08	108.39	331.07	-1.20	14.88	197.50	13.68
<b>101</b>	US-BZF	2016	TS_1	-0.08	95.50	315.89	-1.03	17.18	205.10	16.15
<b>102</b>	US-BZS	2015	TS_1	NaN	116.48	275.22	-0.07	4.87	202.90	4.79
<b>103</b>	US-BZS	2016	TS_1	NaN	119.07	278.90	-0.05	5.58	208.40	5.54
<b>104</b>	US-DPW	2013	NaN	NaN	NaN	NaN	NaN	NaN	NaN	NaN
<b>105</b>	US-DPW	2014	NaN	NaN	NaN	NaN	NaN	NaN	NaN	NaN
<b>106</b>	US-DPW	2015	NaN	NaN	NaN	NaN	NaN	NaN	NaN	NaN
<b>107</b>	US-DPW	2016	NaN	NaN	NaN	NaN	NaN	NaN	NaN	NaN
<b>108</b>	US-HRA	2017	NaN	NaN	NaN	NaN	NaN	NaN	NaN	NaN
<b>109</b>	US-HRC	2018	NaN	NaN	NaN	NaN	NaN	NaN	NaN	NaN
<b>110</b>	US-ICs	2014	TS_1	-0.08	147.27	263.08	-0.08	5.47	205.60	5.39
<b>111</b>	US-ICs	2015	TS_1	-0.08	141.61	255.70	-0.02	6.12	195.20	6.10
<b>112</b>	US-ICs	2016	TS_1	-0.08	146.75	265.86	-0.05	5.67	206.20	5.62
<b>113</b>	US-ivo	2013	NaN	NaN	NaN	NaN	NaN	NaN	NaN	NaN
<b>114</b>	US-ivo	2014	TS_1	-0.05	136.92	264.34	-0.20	10.84	195.70	10.64
<b>115</b>	US-ivo	2015	TS_1	-0.05	139.42	257.06	-0.14	14.86	185.60	14.72
<b>116</b>	US-ivo	2016	TS_1	-0.05	133.60	262.43	-0.10	8.90	197.30	8.80
<b>117</b>	US-LA1	2012	TS_1	-0.10	29.15	331.44	15.59	13.50	197.20	29.08
<b>118</b>	US-LA2	2012	TS_1	-0.10	36.65	336.05	15.04	14.35	193.20	29.39
<b>119</b>	US-LA2	2013	TS_1	-0.10	65.79	377.93	14.70	16.06	201.50	30.76
<b>120</b>	US-Los	2014	TS_1	0.00	136.18	417.40	1.95	8.26	244.30	10.22
<b>121</b>	US-Los	2015	TS_1	0.00	148.23	422.27	2.43	7.76	258.70	10.19
<b>122</b>	US-Los	2016	TS_1	0.00	135.20	415.75	2.47	8.08	255.10	10.56
<b>123</b>	US-Los	2017	TS_1	0.00	141.15	414.62	1.89	7.45	256.00	9.34
<b>124</b>	US-Los	2018	TS_1	0.00	169.83	421.79	1.46	7.42	260.00	8.88
<b>125</b>	US-MAC	2013	NaN	NaN	NaN	NaN	NaN	NaN	NaN	NaN
<b>126</b>	US-MAC	2014	NaN	NaN	NaN	NaN	NaN	NaN	NaN	NaN
<b>127</b>	US-MAC	2015	NaN	NaN	NaN	NaN	NaN	NaN	NaN	NaN
<b>128</b>	US-Myb	2010	NaN	NaN	NaN	NaN	NaN	NaN	NaN	NaN
<b>129</b>	US-Myb	2011	TS_3	-0.08	NaN	329.50	12.12	8.86	231.70	20.98
<b>130</b>	US-Myb	2012	TS_3	-0.08	35.60	372.21	9.39	10.96	216.10	20.36
<b>131</b>	US-Myb	2013	TS_3	-0.08	34.38	354.74	9.25	11.28	210.90	20.52
<b>132</b>	US-Myb	2014	TS_3	-0.08	26.04	365.88	9.64	12.28	210.00	21.93
<b>133</b>	US-Myb	2015	TS_3	-0.08	17.34	340.72	9.77	11.85	212.00	21.62

<b>134</b>	US-Myb	2016	TS_3	-0.08	5.05	357.82	9.61	11.19	201.00	20.80
<b>135</b>	US-Myb	2017	TS_3	-0.08	27.31	352.90	9.86	13.10	214.00	22.96
<b>136</b>	US-Myb	2018	TS_3	-0.08	36.27	326.10	10.20	10.72	207.00	20.92
<b>137</b>	US-NC4	2012	TS_1	-0.05	42.43	336.03	7.87	15.75	215.40	23.62
<b>138</b>	US-NC4	2013	TS_1	-0.05	59.96	368.85	6.92	16.83	210.50	23.74
<b>139</b>	US-NC4	2014	TS_1	-0.05	54.42	362.34	6.73	16.81	208.50	23.54
<b>140</b>	US-NC4	2015	TS_1	-0.05	68.13	387.31	8.27	16.06	205.00	24.33
<b>141</b>	US-NC4	2016	TS_1	-0.05	52.97	351.38	9.41	15.04	220.00	24.45
<b>142</b>	US-ORv	2011	NaN	NaN	NaN	NaN	NaN	NaN	NaN	NaN
<b>143</b>	US-ORv	2012	TS	NaN	57.42	352.55	4.36	20.61	203.90	24.97
<b>144</b>	US-ORv	2013	TS	NaN	63.67	356.74	2.93	19.98	210.80	22.90
<b>145</b>	US-ORv	2014	TS	NaN	68.11	364.96	2.11	20.17	205.30	22.28
<b>146</b>	US-ORv	2015	TS	NaN	68.77	387.78	1.77	21.26	206.00	23.04
<b>147</b>	US-OWC	2015	NaN	NaN	NaN	NaN	NaN	NaN	NaN	NaN
<b>148</b>	US-OWC	2016	TS_1	-0.05	0.00	0.00	0.00	0.00	211.20	23.91
<b>149</b>	US-Sne	2016	NaN	NaN	NaN	NaN	NaN	NaN	NaN	NaN
<b>150</b>	US-Sne	2017	TS_1	-0.01	46.07	337.92	10.33	13.14	212.70	23.47
<b>151</b>	US-Sne	2018	TS_1	-0.01	48.41	325.09	10.28	12.15	217.30	22.43
<b>152</b>	US-Srr	2014	NaN	NaN	NaN	NaN	NaN	NaN	NaN	NaN
<b>153</b>	US-Srr	2015	NaN	NaN	NaN	NaN	NaN	NaN	NaN	NaN
<b>154</b>	US-Srr	2016	TS_1	NaN	NaN	326.29	10.03	10.71	200.50	20.74
<b>155</b>	US-Srr	2017	TS_1	NaN	11.34	346.85	7.22	13.71	199.50	20.93
<b>156</b>	US-StJ	2016	TS_2	-0.05	68.37	347.38	4.05	16.22	213.70	20.27
<b>157</b>	US-Tw1	2011	NaN	NaN	NaN	NaN	NaN	NaN	NaN	NaN
<b>158</b>	US-Tw1	2012	TS_1	-0.02	50.54	359.96	5.99	11.52	225.20	17.51
<b>159</b>	US-Tw1	2013	TS_1	-0.02	35.80	337.57	4.39	14.59	206.60	18.97
<b>160</b>	US-Tw1	2014	TS_1	-0.02	41.23	395.41	6.67	10.89	208.30	17.56
<b>161</b>	US-Tw1	2015	TS_1	-0.02	50.66	342.55	9.02	7.83	235.00	16.85
<b>162</b>	US-Tw1	2016	TS_1	-0.02	34.57	361.06	8.78	7.94	218.00	16.72
<b>163</b>	US-Tw1	2017	TS_1	-0.02	41.17	343.75	7.55	10.22	228.00	17.77
<b>164</b>	US-Tw1	2018	TS_1	-0.02	60.47	327.43	6.70	10.42	222.00	17.12
<b>165</b>	US-Tw4	2014	NaN	NaN	NaN	NaN	NaN	NaN	NaN	NaN
<b>166</b>	US-Tw4	2015	TS_1	-0.02	15.93	327.22	10.04	11.56	199.40	21.60
<b>167</b>	US-Tw4	2016	TS_1	-0.02	9.56	358.75	8.16	11.29	201.70	19.45

168	US-Tw4	2017	TS_1	-0.02	38.35	347.31	8.07	11.52	211.90	19.59
169	US-Tw4	2018	TS_1	-0.02	58.11	344.87	8.00	10.93	218.00	18.93
170	US-Tw5	2018	TS_1	-0.02	NaN	414.83	0.00	8.89	222.20	18.37
171	US-Twt	2009	NaN	NaN	NaN	NaN	NaN	NaN	NaN	NaN
172	US-Twt	2010	NaN	NaN	NaN	NaN	NaN	NaN	NaN	NaN
173	US-Twt	2011	NaN	NaN	NaN	NaN	NaN	NaN	NaN	NaN
174	US-Twt	2012	NaN	NaN	NaN	NaN	NaN	NaN	NaN	NaN
175	US-Twt	2013	NaN	NaN	NaN	NaN	NaN	NaN	NaN	NaN
176	US-Twt	2014	NaN	NaN	NaN	NaN	NaN	NaN	NaN	NaN
177	US-Twt	2015	NaN	NaN	NaN	NaN	NaN	NaN	NaN	NaN
178	US-Twt	2016	NaN	NaN	NaN	NaN	NaN	NaN	NaN	NaN
179	US-Uaf	2011	TS_1	-0.09	86.20	372.46	-12.29	21.95	199.60	9.67
180	US-Uaf	2012	TS_1	-0.09	73.77	338.53	-11.83	20.86	202.40	9.03
181	US-Uaf	2013	TS_1	-0.09	109.63	395.51	-10.08	20.52	200.40	10.44
182	US-Uaf	2014	TS_1	-0.09	76.07	365.40	-10.94	19.94	206.00	9.00
183	US-Uaf	2015	TS_1	-0.09	80.99	423.19	-9.77	19.76	190.00	10.00
184	US-Uaf	2016	TS_1	-0.09	77.38	315.75	-7.74	19.13	198.00	11.39
185	US-Uaf	2017	TS_1	-0.09	84.88	380.17	-7.39	19.08	196.00	11.69
186	US-Uaf	2018	TS_1	-0.09	96.04	333.33	-5.60	17.72	199.00	12.11
187	US-WPT	2011	TS_1	-0.10	80.95	342.17	5.27	19.27	202.60	24.54
188	US-WPT	2012	TS_1	-0.10	40.29	345.57	3.70	21.60	197.40	25.30
189	US-WPT	2013	TS_1	-0.10	74.61	340.47	3.73	18.23	207.20	21.96

### Column Descriptions

SITE\_ID Site identification code as assigned by regional flux data network

Year Data year

Probe\_name Temperature probe name as given in data files

Soil\_temp\_depth\_m Depth of soil temperature probe (m), with negative values being under the surface

Start\_TS\_(DOY) Season start for elevated TS (DOY), point "f" in Figure 1

End\_TS\_(DOY) Season end for elevated TS (DOY), point "h" in Figure 1

Base\_value\_TS\_(C) Baseline TS during non-elevated season (C), average of points "a" and "b" in Figure 1

Ampl\_TS\_(C) Amplitude of TS during elevated temperature season (C), difference between point "e" in Figure 1 and Base\_value\_TS

Peak\_TS\_(DOY)  
Peak\_value\_TS\_(C)

Day of maximum elevated TS (DOY), point "g" in Figure 1  
Maximum value of TS (C) point "e" in Figure 1

**Table B6: Timesat output for all soil temperature probes**

	SITE_ID	Year	Probe_name	Soil_temp_depth_m	Start_TS_(DOY)	End_TS_(DOY)	Base_value_TS_(C)	Ampl_T_S_(C)	Peak_TS_(DOY)	Peak_value_TS_(C)
1	AT-Neu	2010	TS_1	-0.05	61.32	339.44	0.15	17.54	200.9	17.7
2	AT-Neu	2011	TS_1	-0.05	51.04	328.84	0.40	16.37	201	16.77
3	AT-Neu	2012	TS_1	-0.05	61.12	341.88	0.73	17.57	202.9	18.3
4	BR-Npw	2016	TS_1	NaN	18.41	343.22	22.41	5.982	188	28.4
5	CA-SCB	2014	TS_1	0	105.94	292.18	-0.63	20.62	196.6	19.99
6	CA-SCB	2014	TS_2	-0.02	105.15	294.06	-0.74	20.42	197.5	19.68
7	CA-SCB	2014	TS_3	-0.04	112.00	294.38	0.05	19.07	199.6	19.11
8	CA-SCB	2014	TS_5	-0.16	123.21	317.72	-1.38	18.6	205.3	17.23
9	CA-SCB	2015	TS_1	0	106.92	287.14	-0.39	17.23	186.8	16.84
10	CA-SCB	2015	TS_2	-0.02	107.06	287.40	-0.42	17.08	187.4	16.66
11	CA-SCB	2015	TS_3	-0.04	107.45	289.83	-0.51	16.81	188.9	16.3
12	CA-SCB	2015	TS_5	-0.16	114.95	305.55	-0.39	15.84	195.7	15.45
13	CA-SCB	2016	TS_1	0	101.64	284.09	-0.31	19.07	193.2	18.77
14	CA-SCB	2016	TS_2	-0.02	101.81	284.11	-0.30	18.96	193.5	18.66
15	CA-SCB	2016	TS_3	-0.04	102.22	285.19	-0.30	18.6	194.3	18.3
16	CA-SCB	2016	TS_5	-0.16	101.16	298.99	-0.24	16.99	201.1	16.74
17	CA-SCB	2017	TS_1	0	107.44	289.72	-0.25	17.67	198	17.42
18	CA-SCB	2017	TS_2	-0.02	107.22	288.88	-0.25	17.59	198	17.33
19	CA-SCB	2017	TS_3	-0.04	108.58	289.29	-0.26	17.28	199	17.02
20	CA-SCB	2017	TS_5	-0.16	116.34	300.28	-0.24	14.95	214	14.71
21	CA-SCC	2014	TS_1	-0.1	123.36	287.06	-0.55	15.64	203	15.09
22	CA-SCC	2014	TS_2	-0.15	114.89	287.71	-0.83	14.49	200.8	13.66
23	CA-SCC	2014	TS_3	-0.2	111.36	288.63	-0.69	11.52	194.9	10.84
24	CA-SCC	2014	TS_4	-0.25	129.50	287.24	-0.22	8.612	207.4	8.391
25	CA-SCC	2014	TS_5	-0.3	142.36	287.99	-0.10	6.329	212.1	6.225
26	CA-SCC	2015	TS_1	-0.1	113.88	285.22	-0.28	16.26	189.2	15.98
27	CA-SCC	2015	TS_2	-0.15	113.05	284.18	-0.24	14.56	192.8	14.32
28	CA-SCC	2015	TS_3	-0.2	111.76	285.45	-0.22	12.71	199.1	12.48
29	CA-SCC	2015	TS_4	-0.25	120.81	287.09	-0.16	10.08	204.8	9.922
30	CA-SCC	2015	TS_5	-0.3	131.92	285.42	-0.09	7.705	209.2	7.616
31	CA-SCC	2016	TS_1	-0.1	108.09	260.12	-0.33	18.37	190.9	18.04
32	CA-SCC	2016	TS_2	-0.15	108.96	260.19	-0.30	17.31	192.1	17.01
33	CA-SCC	2016	TS_3	-0.2	110.49	260.44	-0.26	15.4	194.1	15.14
34	CA-SCC	2016	TS_4	-0.25	119.21	260.34	-0.20	13.38	200.2	13.18
35	CA-SCC	2016	TS_5	-0.3	130.75	261.73	-0.12	10.03	202.2	9.906
36	DE-Hte	2012	TS_3	-0.2	76.96	344.01	4.98	12.26	215.5	17.23
37	DE-Hte	2013	TS_3	-0.2	60.92	377.99	3.96	11.99	207.9	15.95
38	DE-Hte	2014	TS_1	0	NaN	327.83	8.52	8.342	205.6	16.87
39	DE-Hte	2015	TS_1	0	62.92	360.55	5.17	11.67	187.4	16.84
40	DE-Hte	2016	TS_1	0	71.87	NaN	4.94	12.36	175.6	17.3
41	DE-Hte	2017	TS_1	0	61.55	343.32	4.50	11.76	186	16.26
42	DE-SfN	2012	TS_1	-0.02	NaN	372.59	0.00	23.55	206.5	15.29
43	DE-SfN	2012	TS_3	-0.1	NaN	366.65	1.64	12.91	219.7	14.55

44	DE-SfN	2012 TS_4	-0.2	NaN	367.40	4.86	7.276	242.7	12.14
45	DE-SfN	2012 TS_5	-0.5	NaN	367.40	4.86	7.276	242.7	12.14
46	DE-SfN	2013 TS_1	-0.02	55.84	381.50	0.92	13.62	216.4	14.54
47	DE-SfN	2013 TS_3	-0.1	60.45	384.77	1.56	12.5	221.1	14.06
48	DE-SfN	2013 TS_4	-0.2	83.55	394.53	3.62	8.417	243.4	12.04
49	DE-SfN	2013 TS_5	-0.5	83.55	394.53	3.62	8.417	243.4	12.04
50	DE-Zrk	2014 TS_1	-0.05	54.79	361.65	4.36	13.93	202.3	18.29
51	DE-Zrk	2014 TS_2	-0.1	59.27	366.51	4.87	12.65	207.3	17.52
52	DE-Zrk	2014 TS_3	-0.2	62.95	371.30	5.53	11.5	211.7	17.03
53	DE-Zrk	2014 TS_4	-0.3	67.45	375.14	6.05	10.4	216.5	16.45
54	DE-Zrk	2014 TS_5	-0.5	72.50	378.95	6.57	9.359	221	15.93
55	DE-Zrk	2015 TS_1	-0.05	58.29	359.29	4.28	13.24	215.5	17.52
56	DE-Zrk	2015 TS_2	-0.1	62.61	364.99	4.79	12	219.8	16.8
57	DE-Zrk	2015 TS_3	-0.2	66.01	369.78	5.42	10.87	223.7	16.29
58	DE-Zrk	2015 TS_4	-0.3	70.47	374.40	5.93	9.771	228	15.7
59	DE-Zrk	2015 TS_5	-0.5	74.71	378.76	6.43	8.751	232.2	15.19
60	DE-Zrk	2016 TS_1	-0.05	72.81	332.00	4.28	14.93	200.4	19.2
61	DE-Zrk	2016 TS_2	-0.1	76.31	337.37	4.79	13.6	204.4	18.39
62	DE-Zrk	2016 TS_3	-0.2	79.73	343.16	5.43	12.33	208.1	17.77
63	DE-Zrk	2016 TS_4	-0.3	83.58	347.57	5.94	11.14	212	17.09
64	DE-Zrk	2016 TS_5	-0.5	87.15	354.22	6.40	10.07	216	16.47
65	DE-Zrk	2017 TS_1	-0.05	69.10	351.44	4.40	14.72	199	19.12
66	DE-Zrk	2017 TS_2	-0.1	73.29	356.52	4.91	13.33	204	18.23
67	DE-Zrk	2017 TS_3	-0.2	77.19	362.40	5.56	12.02	208	17.58
68	DE-Zrk	2017 TS_4	-0.3	82.20	367.20	6.04	10.8	212	16.84
69	DE-Zrk	2017 TS_5	-0.5	86.22	372.96	6.48	9.675	217	16.15
70	DE-Zrk	2018 TS_1	-0.05	84.47	336.14	4.83	12.32	203	17.14
71	DE-Zrk	2018 TS_2	-0.1	86.60	342.59	5.30	11.27	208	16.57
72	DE-Zrk	2018 TS_3	-0.2	87.68	348.07	5.89	10.25	212	16.14
73	DE-Zrk	2018 TS_4	-0.3	89.82	354.77	6.31	9.308	217	15.61
74	DE-Zrk	2018 TS_5	-0.5	92.01	360.46	6.69	8.412	222	15.11
75	FI-Lom	2006 TS_1	-0.07	114.15	290.83	-0.11	13.42	204.8	13.31
76	FI-Lom	2006 TS_2	-0.3	117.21	307.88	0.27	12.01	214.1	12.28
77	FI-Lom	2006 TS_3	-0.5	128.82	329.03	1.06	9.071	225.8	10.13
78	FI-Lom	2007 TS_1	-0.07	126.84	302.05	0.11	13.05	200	13.16
79	FI-Lom	2007 TS_2	-0.3	134.00	321.03	0.42	11.5	207.5	11.92
80	FI-Lom	2007 TS_3	-0.5	138.37	348.03	1.06	8.873	221.1	9.936
81	FI-Lom	2008 TS_1	-0.07	135.62	296.74	0.16	12.73	202.9	12.88
82	FI-Lom	2008 TS_2	-0.3	141.46	318.74	0.58	10.62	209.6	11.2
83	FI-Lom	2008 TS_3	-0.5	146.70	349.21	1.17	8.214	221.2	9.382
84	FI-Lom	2009 TS_1	-0.07	117.16	291.86	0.14	11.73	214	11.87
85	FI-Lom	2009 TS_2	-0.3	123.51	314.51	0.67	9.692	221	10.36
86	FI-Lom	2009 TS_3	-0.5	133.69	336.65	1.30	7.896	233	9.193
87	FI-Lom	2010 TS_1	-0.07	129.91	318.54	0.05	12.13	208	12.18
88	FI-Lom	2010 TS_2	-0.3	138.09	338.24	0.52	9.962	218	10.48
89	FI-Lom	2010 TS_3	-0.5	147.34	359.95	1.19	7.344	231	8.532
90	FI-Si2	2012 TS_1	-0.05	NaN	323.46	0.00	19.85	204.6	16.02

91	FI-Si2	2012 TS_2	-0.2	103.64	333.52	-0.04	15.75	217.5	15.71
92	FI-Si2	2012 TS_3	-0.35	105.57	NaN	0.00	19.38	230.6	15.09
93	FI-Si2	2012 TS_4	-0.5	110.87	NaN	0.00	17.26	237.5	14.66
94	FI-Si2	2013 TS_1	-0.05	106.90	341.05	-0.05	16.04	199.4	15.98
95	FI-Si2	2013 TS_2	-0.2	102.57	356.13	0.23	14.91	207.3	15.14
96	FI-Si2	2013 TS_3	-0.35	NaN	376.47	0.00	18.26	209.6	14.23
97	FI-Si2	2013 TS_4	-0.5	NaN	392.35	0.00	16.71	216.4	13.48
98	FI-Si2	2014 TS_1	-0.05	104.63	331.10	-0.04	17.07	208.5	17.03
99	FI-Si2	2014 TS_2	-0.2	107.82	359.78	0.59	15.33	215.3	15.92
100	FI-Si2	2014 TS_3	-0.35	112.02	385.94	0.99	13.61	222.2	14.61
101	FI-Si2	2014 TS_4	-0.5	118.24	400.15	1.59	12.01	229.1	13.59
102	FI-Si2	2015 TS_1	-0.05	76.49	352.34	-0.87	16.31	211	15.44
103	FI-Si2	2015 TS_2	-0.2	80.08	364.72	-0.41	14.83	218	14.42
104	FI-Si2	2015 TS_3	-0.35	82.01	374.79	0.12	13.27	225	13.39
105	FI-Si2	2015 TS_4	-0.5	88.25	382.37	0.84	11.7	233	12.53
106	FI-Si2	2016 TS_1	-0.05	102.64	329.42	-0.88	16.48	206	15.6
107	FI-Si2	2016 TS_2	-0.2	102.16	361.04	-0.77	16.02	212	15.25
108	FI-Si2	2016 TS_3	-0.35	103.15	383.82	-0.63	14.7	219	14.07
109	FI-Si2	2016 TS_4	-0.5	104.76	399.01	-0.20	13.36	227	13.16
110	HK-MPM	2016 TS_2	NaN	NaN	566.87	0.00	7.789	219.8	28.92
111	HK-MPM	2016 TS_3	NaN	NaN	373.06	20.56	7.386	227.3	27.95
112	HK-MPM	2017 TS_2	NaN	NaN	NaN	0.00	8.726	218.5	29.13
113	HK-MPM	2017 TS_3	NaN	69.55	364.53	19.53	8.572	233.6	28.1
114	HK-MPM	2018 TS_2	NaN	NaN	NaN	0.00	7.231	204.9	28.66
115	HK-MPM	2018 TS_3	NaN	64.82	383.39	19.17	8.406	221.4	27.58
116	JP-BBY	2015 TS_1	-0.183	87.83	340.83	0.94	21.59	218.1	22.53
117	JP-BBY	2015 TS_2	-0.233	90.59	340.99	1.34	20.9	219.9	22.25
118	JP-BBY	2015 TS_3	-0.283	90.34	341.60	1.58	20.42	221.4	22
119	JP-BBY	2015 TS_4	-0.383	96.01	341.35	2.39	19.09	225.1	21.48
120	JP-BBY	2015 TS_5	-0.483	95.83	341.49	2.91	18.09	228.9	21
121	JP-BBY	2016 TS_1	-0.183	80.75	330.60	0.36	22.19	217.8	22.55
122	JP-BBY	2016 TS_2	-0.233	82.30	335.40	0.67	21.64	220.8	22.3
123	JP-BBY	2016 TS_3	-0.283	84.28	332.64	0.99	21.1	222	22.09
124	JP-BBY	2016 TS_4	-0.383	89.00	332.43	1.76	19.92	225.6	21.68
125	JP-BBY	2016 TS_5	-0.483	94.29	331.91	2.44	18.83	228.9	21.27
126	JP-BBY	2017 TS_1	-0.183	80.38	347.77	0.20	21.75	213.8	21.95
127	JP-BBY	2017 TS_2	-0.233	84.54	347.79	0.82	21.02	214.6	21.83
128	JP-BBY	2017 TS_3	-0.283	86.19	347.10	1.06	20.56	216.3	21.62
129	JP-BBY	2017 TS_4	-0.383	92.20	346.01	1.97	19.34	218.5	21.31
130	JP-BBY	2017 TS_5	-0.483	98.15	345.18	2.70	18.34	221	21.03
131	JP-BBY	2018 TS_1	-0.183	78.28	355.38	0.50	20.38	222	20.88
132	JP-BBY	2018 TS_2	-0.233	83.55	357.60	1.48	19.23	224	20.7
133	JP-BBY	2018 TS_3	-0.283	85.93	355.90	1.69	18.78	225	20.47
134	JP-BBY	2018 TS_4	-0.383	95.89	351.34	2.81	17.25	229	20.07
135	JP-BBY	2018 TS_5	-0.483	103.83	349.39	3.63	16.1	232	19.73
136	JP-Mse	2012 TS_1	-0.01	60.38	348.86	2.15	23.76	211.8	25.91
137	MY-MLM	2014 TS	NaN	NaN	358.37	25.06	3.968	194.5	29.03

138	MY-MLM	2015 TS	NaN	27.32	NaN	25.57	1.973	172.7	27.55
139	NZ-Kop	2012 TS_1	-0.5	62.54	360.29	8.30	8.394	219.8	16.7
140	NZ-Kop	2012 TS_2	-0.1	65.53	362.35	8.45	8.093	222.1	16.54
141	NZ-Kop	2012 TS_3	-0.2	68.77	365.64	8.73	7.243	228.2	15.98
142	NZ-Kop	2013 TS_1	-0.5	45.63	367.00	8.41	7.635	210.5	16.04
143	NZ-Kop	2013 TS_2	-0.1	47.60	370.98	8.54	7.486	212.3	16.03
144	NZ-Kop	2013 TS_3	-0.2	52.74	377.20	8.82	6.87	217.8	15.69
145	NZ-Kop	2014 TS_1	-0.5	56.88	365.68	8.16	8.79	219	16.95
146	NZ-Kop	2014 TS_2	-0.1	59.45	367.47	8.29	8.512	221	16.8
147	NZ-Kop	2014 TS_3	-0.2	62.93	372.48	8.55	7.792	226	16.34
148	NZ-Kop	2015 TS_1	-0.5	56.49	371.82	7.73	9.355	214	17.09
149	NZ-Kop	2015 TS_2	-0.1	58.32	374.74	7.87	9.063	217	16.93
150	NZ-Kop	2015 TS_3	-0.2	62.67	378.44	8.19	8.217	222	16.4
151	RU-Ch2	2014 TS_1	-0.04	138.76	263.76	-0.13	14.42	206.6	14.29
152	RU-Ch2	2014 TS_2	-0.08	146.08	262.11	-0.14	13.03	206.5	12.9
153	RU-Ch2	2014 TS_3	-0.16	155.95	264.51	-0.05	4.581	210.5	4.535
154	RU-Ch2	2015 TS_1	-0.04	143.88	269.56	-0.14	13.97	193.3	13.83
155	RU-Ch2	2015 TS_2	-0.08	147.34	265.69	-0.10	12.3	195.7	12.2
156	RU-Ch2	2015 TS_3	-0.16	159.93	266.60	-0.04	3.995	205.2	3.96
157	RU-Ch2	2016 TS_1	-0.04	126.98	273.54	-0.16	11.64	200.2	11.48
158	RU-Ch2	2016 TS_2	-0.08	133.92	272.58	-0.10	10.06	203.2	9.964
159	RU-Ch2	2016 TS_3	-0.16	147.99	275.45	-0.04	4.042	217.7	4.001
160	RU-Che	2014 TS_1	-0.04	138.05	267.57	-0.12	15.04	208	14.92
161	RU-Che	2014 TS_2	-0.08	149.72	263.67	-0.09	8.959	206.6	8.873
162	RU-Che	2014 TS_3	-0.16	154.97	265.49	-0.07	7.006	210.3	6.938
163	RU-Che	2015 TS_1	-0.04	143.85	274.68	-0.17	14.81	193.7	14.64
164	RU-Che	2015 TS_2	-0.08	149.49	267.08	-0.06	8.336	197.9	8.273
165	RU-Che	2015 TS_3	-0.16	154.48	271.03	-0.04	5.942	202.4	5.9
166	RU-Che	2016 TS_1	-0.04	126.72	274.03	-0.19	12.95	200.4	12.76
167	RU-Che	2016 TS_2	-0.08	137.01	273.70	-0.07	7.076	205.4	7.01
168	RU-Che	2016 TS_3	-0.16	142.51	275.62	-0.05	5.498	211.8	5.451
169	SE-Deg	2014 TS_1	-0.02	111.85	303.55	-0.53	17.22	201.6	16.69
170	SE-Deg	2014 TS_2	-0.05	119.11	308.12	-0.31	13.23	207.4	12.93
171	SE-Deg	2014 TS_3	-0.1	125.46	315.55	-0.10	12.54	212	12.44
172	SE-Deg	2014 TS_4	-0.15	134.61	321.20	0.29	11.63	215.6	11.93
173	SE-Deg	2014 TS_5	-0.3	126.75	330.85	0.52	11.61	220	12.13
174	SE-Deg	2014 TS_6	-0.5	130.62	341.66	0.89	11.33	223.1	12.21
175	SE-Deg	2015 TS_1	-0.02	104.25	310.59	-0.28	15.2	207.2	14.91
176	SE-Deg	2015 TS_2	-0.05	110.64	312.57	0.09	13.86	209.5	13.95
177	SE-Deg	2015 TS_3	-0.1	112.94	321.41	0.41	12.94	212.9	13.36
178	SE-Deg	2015 TS_4	-0.15	115.72	329.21	0.60	11.94	216.6	12.54
179	SE-Deg	2015 TS_5	-0.3	118.31	339.17	0.90	11.08	220.5	11.98
180	SE-Deg	2015 TS_6	-0.5	121.80	347.97	1.30	10.19	224.6	11.48
181	SE-Deg	2016 TS_1	-0.02	108.14	306.39	-0.19	14.88	200.3	14.68
182	SE-Deg	2017 TS_1	-0.02	133.38	326.87	-0.20	12.35	215	12.15
183	SE-Deg	2018 TS_1	-0.02	111.67	310.21	-0.17	14.7	198	14.52
184	US-Atq	2014 TS_1	NaN	10.75	139.53	-0.20	8.068	61	7.864

185	US-Atq	2014 TS_2	NaN	18.00	137.32	-0.08	4.191	74.3	4.109
186	US-Atq	2014 TS_3	NaN	28.49	138.48	-0.03	2.366	83.5	2.334
187	US-Beo	2014 TS_1	NaN	155.09	270.13	-0.04	4.874	211.1	4.829
188	US-Beo	2014 TS_2	NaN	168.62	270.60	-0.02	2.94	219.6	2.922
189	US-Beo	2014 TS_3	NaN	170.53	269.49	-0.02	3.128	219.9	3.104
190	US-Bes	2013 TS_1	NaN	143.22	261.99	-0.05	5.649	201.3	5.602
191	US-Bes	2013 TS_2	NaN	150.57	267.49	-0.04	6.744	205.7	6.706
192	US-Bes	2013 TS_3	NaN	146.03	267.28	-0.06	8.248	202.3	8.187
193	US-Bes	2014 TS_1	NaN	151.79	282.29	-0.10	3.924	198.5	3.822
194	US-Bes	2015 TS_1	NaN	140.45	270.98	-0.11	4.763	195.3	4.65
195	US-Bes	2015 TS_2	NaN	148.76	269.64	-0.11	5.512	202.8	5.401
196	US-Bes	2015 TS_3	NaN	146.77	271.72	-0.16	7.182	197.8	7.027
197	US-BZB	2014 TS_1	-0.075	123.11	298.35	-0.44	15.35	215.8	14.91
198	US-BZB	2014 TS_2	-0.05	115.15	292.07	-0.59	15.49	209.9	14.9
199	US-BZB	2015 TS_1	-0.075	107.82	295.60	-0.38	14.04	210.2	13.67
200	US-BZB	2015 TS_2	-0.05	98.63	293.17	-0.67	14.56	203.5	13.9
201	US-BZB	2016 TS_1	-0.075	125.09	292.39	-0.33	16.39	214.3	16.06
202	US-BZB	2016 TS_2	-0.05	109.89	290.95	-0.74	16.89	211.7	16.15
203	US-BZF	2014 TS_1	-0.075	96.05	322.79	-1.56	16.12	205.4	14.56
204	US-BZF	2014 TS_2	-0.05	112.68	322.83	-1.22	15.9	208.3	14.68
205	US-BZF	2015 TS_1	-0.075	108.39	331.07	-1.20	14.88	197.5	13.68
206	US-BZF	2015 TS_2	-0.05	111.46	336.09	-1.12	14.83	200.2	13.72
207	US-BZF	2016 TS_1	-0.075	95.50	315.89	-1.03	17.18	205.1	16.15
208	US-BZF	2016 TS_2	-0.05	100.12	317.57	-0.90	17.72	206	16.81
209	US-BZS	2015 TS_1	NaN	116.48	275.22	-0.07	4.866	202.9	4.792
210	US-BZS	2015 TS_2	NaN	97.29	283.75	-0.27	8.135	187.7	7.862
211	US-BZS	2015 TS_3	NaN	105.93	272.47	-0.13	10.61	193.1	10.47
212	US-BZS	2016 TS_1	NaN	119.07	278.90	-0.05	5.584	208.4	5.535
213	US-BZS	2016 TS_2	NaN	87.59	278.96	-0.25	12.09	203.1	11.84
214	US-BZS	2016 TS_3	NaN	98.29	277.92	-0.16	11.67	198.8	11.51
215	US-ICs	2014 TS_1	-0.075	147.27	263.08	-0.08	5.467	205.6	5.39
216	US-ICs	2014 TS_2	-0.05	147.13	262.66	-0.01	6.41	205.1	6.402
217	US-ICs	2015 TS_1	-0.075	141.61	255.70	-0.02	6.12	195.2	6.098
218	US-ICs	2015 TS_2	-0.05	140.38	256.88	-0.02	7.07	193.1	7.047
219	US-ICs	2016 TS_1	-0.075	146.75	265.86	-0.05	5.67	206.2	5.623
220	US-ICs	2016 TS_2	-0.05	146.79	265.67	-0.05	6.654	206.1	6.599
221	US-Ivo	2014 TS_1	-0.05	136.92	264.34	-0.20	10.84	195.7	10.64
222	US-Ivo	2014 TS_1	-0.4	136.92	264.34	-0.20	10.84	195.7	10.64
223	US-Ivo	2014 TS_2	-0.1	142.52	266.53	-0.16	9.908	195.5	9.744
224	US-Ivo	2014 TS_3	-0.15	144.98	262.74	-0.19	6.761	204.8	6.574
225	US-Ivo	2014 TS_4	-0.3	166.58	262.05	-0.03	4.068	214.3	4.034
226	US-Ivo	2015 TS_1	-0.05	139.42	257.06	-0.14	14.86	185.6	14.72
227	US-Ivo	2015 TS_1	-0.4	139.42	257.06	-0.14	14.86	185.6	14.72
228	US-Ivo	2015 TS_2	-0.1	141.20	256.70	-0.09	11.99	189.1	11.9
229	US-Ivo	2015 TS_3	-0.15	145.76	260.99	-0.07	6.85	199.1	6.785
230	US-Ivo	2015 TS_4	-0.3	158.88	259.63	-0.03	4.032	208.2	3.997
231	US-Ivo	2016 TS_1	-0.05	133.60	262.43	-0.10	8.895	197.3	8.796

232	US-Ivo	2016 TS_1	-0.4	133.60	262.43	-0.10	8.895	197.3	8.796
233	US-Ivo	2016 TS_2	-0.1	139.70	264.19	-0.04	6.76	202.2	6.719
234	US-Ivo	2016 TS_3	-0.15	153.78	269.47	-0.05	4.305	211.5	4.253
235	US-Ivo	2016 TS_4	-0.3	171.24	271.03	-0.01	2.644	221.2	2.631
236	US-LA1	2012 TS_1	-0.1	29.15	331.44	15.59	13.5	197.2	29.08
237	US-LA2	2012 TS_1	-0.1	36.65	336.05	15.04	14.35	193.2	29.39
238	US-LA2	2013 TS_1	-0.1	65.79	377.93	14.70	16.06	201.5	30.76
239	US-Los	2014 TS_1	0	136.18	417.40	1.95	8.263	244.3	10.22
240	US-Los	2015 TS_1	0	148.23	422.27	2.43	7.761	258.7	10.19
241	US-Los	2016 TS_1	0	135.20	415.75	2.47	8.083	255.1	10.56
242	US-Los	2017 TS_1	0	141.15	414.62	1.89	7.451	256	9.343
243	US-Los	2018 TS_1	0	169.83	421.79	1.46	7.419	260	8.883
244	US-Myb	2011 TS_3	-0.08	NaN	329.50	12.12	8.859	231.7	20.98
245	US-Myb	2011 TS_4	-0.16	NaN	333.87	12.36	8.288	235.8	20.65
246	US-Myb	2011 TS_5	-0.32	NaN	338.98	12.72	7.56	241.4	20.28
247	US-Myb	2011 TS_1	-0.02	NaN	326.62	11.96	9.156	229.3	21.12
248	US-Myb	2012 TS_3	-0.08	35.60	372.21	9.39	10.96	216.1	20.36
249	US-Myb	2012 TS_4	-0.16	40.39	375.48	9.90	10.23	220.7	20.13
250	US-Myb	2012 TS_5	-0.32	47.39	379.29	10.56	9.212	227.2	19.78
251	US-Myb	2012 TS_1	-0.02	29.91	372.10	8.98	11.77	214.4	20.74
252	US-Myb	2013 TS_3	-0.08	34.38	354.74	9.25	11.28	210.9	20.52
253	US-Myb	2013 TS_4	-0.16	40.07	359.02	9.87	10.41	215	20.28
254	US-Myb	2013 TS_5	-0.32	45.10	363.81	10.53	9.441	221.9	19.97
255	US-Myb	2013 TS_1	-0.02	NaN	355.11	8.47	12.24	208.2	20.7
256	US-Myb	2014 TS_3	-0.08	26.04	365.88	9.64	12.28	210	21.93
257	US-Myb	2014 TS_4	-0.16	38.09	364.15	10.74	11.23	211	21.97
258	US-Myb	2014 TS_5	-0.32	44.34	366.12	11.25	10.25	218	21.5
259	US-Myb	2015 TS_3	-0.08	17.34	340.72	9.77	11.85	212	21.62
260	US-Myb	2015 TS_4	-0.16	12.76	339.04	10.79	10.84	221	21.63
261	US-Myb	2015 TS_5	-0.32	18.83	343.94	11.35	9.93	226	21.28
262	US-Myb	2016 TS_3	-0.08	5.05	357.82	9.61	11.19	201	20.8
263	US-Myb	2016 TS_4	-0.16	3.39	356.20	9.84	10.87	208	20.72
264	US-Myb	2016 TS_5	-0.32	12.02	360.46	10.73	9.627	214	20.36
265	US-Myb	2017 TS_3	-0.08	27.31	352.90	9.86	13.1	214	22.96
266	US-Myb	2017 TS_4	-0.16	28.29	357.41	9.92	12.74	215	22.66
267	US-Myb	2017 TS_5	-0.32	36.79	360.41	10.85	11.23	223	22.08
268	US-Myb	2017 TS_1	-0.02	62.79	325.72	12.70	10.71	216.8	23.41
269	US-Myb	2018 TS_3	-0.08	36.27	326.10	10.20	10.72	207	20.92
270	US-Myb	2018 TS_4	-0.16	41.30	332.83	10.47	10.35	209	20.82
271	US-Myb	2018 TS_5	-0.32	48.43	336.09	11.18	9.293	215	20.47
272	US-Myb	2018 TS_1	-0.02	38.38	344.86	10.05	11.93	200.3	21.98
273	US-NC4	2012 TS_1	-0.05	42.43	336.03	7.87	15.75	215.4	23.62
274	US-NC4	2013 TS_1	-0.05	59.96	368.85	6.92	16.83	210.5	23.74
275	US-NC4	2014 TS_1	-0.05	54.42	362.34	6.73	16.81	208.5	23.54
276	US-NC4	2015 TS_1	-0.05	68.13	387.31	8.27	16.06	205	24.33
277	US-NC4	2016 TS_1	-0.05	52.97	351.38	9.41	15.04	220	24.45
278	US-ORv	2012 TS	NaN	57.42	352.55	4.36	20.61	203.9	24.97

279	US-ORv	2013 TS	NaN	63.67	356.74	2.93	19.98	210.8	22.9
280	US-ORv	2014 TS	NaN	68.11	364.96	2.11	20.17	205.3	22.28
281	US-ORv	2015 TS	NaN	68.77	387.78	1.77	21.26	206	23.04
282	US-OWC	2016 TS_1	-0.05	0.00	0.00	0.00	0	211.2	23.91
283	US-Sne	2017 TS_1	-0.01	46.07	337.92	10.33	13.14	212.7	23.47
284	US-Sne	2017 TS_2	-0.02	41.06	341.82	10.76	12.66	205.7	23.41
285	US-Sne	2017 TS_3	-0.08	42.89	343.85	11.04	12.17	208.5	23.22
286	US-Sne	2017 TS_4	-0.16	46.36	346.18	11.39	11.79	211	23.18
287	US-Sne	2017 TS_5	-0.32	50.59	350.46	11.98	10.7	216	22.67
288	US-Sne	2018 TS_1	-0.01	48.41	325.09	10.28	12.15	217.3	22.43
289	US-Sne	2018 TS_2	-0.02	33.91	331.01	10.55	11.34	210.2	21.89
290	US-Sne	2018 TS_3	-0.08	36.76	331.50	10.87	10.63	212.1	21.5
291	US-Sne	2018 TS_4	-0.16	35.64	335.45	11.23	10.09	220.1	21.32
292	US-Sne	2018 TS_5	-0.32	49.09	335.94	11.88	9.045	218	20.92
293	US-Srr	2016 TS_1	NaN	NaN	326.29	10.03	10.71	200.5	20.74
294	US-Srr	2017 TS_1	NaN	11.34	346.85	7.22	13.71	199.5	20.93
295	US-StJ	2016 TS_2	-0.05	68.37	347.38	4.05	16.22	213.7	20.27
296	US-StJ	2016 TS_3	-0.1	68.38	347.38	5.84	14.1	213.7	19.94
297	US-Tw1	2012 TS_1	-0.02	50.54	359.96	5.99	11.52	225.2	17.51
298	US-Tw1	2012 TS_2	-0.04	48.02	358.76	6.14	11.32	227	17.46
299	US-Tw1	2012 TS_3	-0.08	50.07	367.92	5.18	12.31	222.1	17.49
300	US-Tw1	2012 TS_4	-0.16	49.05	367.52	5.31	12.19	224.5	17.5
301	US-Tw1	2012 TS_5	-0.32	-79.10	347.23	7.89	9.513	225.3	17.4
302	US-Tw1	2013 TS_1	-0.02	35.80	337.57	4.39	14.59	206.6	18.97
303	US-Tw1	2013 TS_2	-0.04	36.08	337.66	4.39	14.57	206.8	18.96
304	US-Tw1	2013 TS_3	-0.08	36.81	338.09	4.40	14.54	207.5	18.94
305	US-Tw1	2013 TS_4	-0.16	37.57	338.82	4.41	14.59	208.4	19.01
306	US-Tw1	2013 TS_5	-0.32	38.64	340.06	4.46	14.62	209.6	19.07
307	US-Tw1	2014 TS_1	-0.02	41.23	395.41	6.67	10.89	208.3	17.56
308	US-Tw1	2014 TS_2	-0.04	41.86	397.14	6.70	10.85	208.6	17.55
309	US-Tw1	2014 TS_3	-0.08	43.55	400.01	6.78	10.72	209.8	17.49
310	US-Tw1	2014 TS_4	-0.16	45.61	404.82	6.88	10.56	211.3	17.44
311	US-Tw1	2014 TS_5	-0.32	49.62	416.29	7.09	10.24	213.9	17.33
312	US-Tw1	2015 TS_1	-0.02	50.66	342.55	9.02	7.831	235	16.85
313	US-Tw1	2015 TS_2	-0.04	52.00	342.38	9.09	7.706	235	16.8
314	US-Tw1	2015 TS_3	-0.08	55.61	341.98	9.26	7.385	238	16.64
315	US-Tw1	2015 TS_4	-0.16	59.57	342.95	9.51	6.972	240	16.48
316	US-Tw1	2015 TS_5	-0.32	69.39	345.18	10.00	6.208	246	16.21
317	US-Tw1	2016 TS_1	-0.02	34.57	361.06	8.78	7.943	218	16.72
318	US-Tw1	2016 TS_2	-0.04	35.49	362.19	8.86	7.837	219	16.69
319	US-Tw1	2016 TS_3	-0.08	38.58	363.10	9.04	7.546	221	16.59
320	US-Tw1	2016 TS_4	-0.16	44.73	365.88	9.33	7.14	223	16.47
321	US-Tw1	2016 TS_5	-0.32	56.22	370.54	9.86	6.35	229	16.21
322	US-Tw1	2017 TS_1	-0.02	41.17	343.75	7.55	10.22	228	17.77
323	US-Tw1	2017 TS_2	-0.04	41.75	344.56	7.61	10.11	229	17.72
324	US-Tw1	2017 TS_3	-0.08	42.61	345.02	7.75	9.803	231	17.55
325	US-Tw1	2017 TS_4	-0.16	45.05	347.17	7.97	9.368	234	17.34

326	US-Tw1	2017 TS_5	-0.32	48.82	349.23	8.38	8.5	240	16.88
327	US-Tw1	2018 TS_1	-0.02	60.47	327.43	6.70	10.42	222	17.12
328	US-Tw1	2018 TS_2	-0.04	61.54	327.44	6.75	10.36	223	17.1
329	US-Tw1	2018 TS_3	-0.08	64.60	328.44	6.85	10.18	225	17.03
330	US-Tw1	2018 TS_4	-0.16	67.67	329.40	7.01	9.925	227	16.93
331	US-Tw1	2018 TS_5	-0.32	75.09	331.40	7.31	9.459	230	16.77
332	US-Tw4	2015 TS_1	-0.02	15.93	327.22	10.04	11.56	199.4	21.6
333	US-Tw4	2015 TS_3	-0.08	20.21	329.78	10.48	10.96	202.3	21.44
334	US-Tw4	2015 TS_4	-0.16	23.88	332.52	10.86	10.42	205.7	21.28
335	US-Tw4	2015 TS_5	-0.32	29.16	338.59	11.49	9.449	212.4	20.94
336	US-Tw4	2016 TS_1	-0.02	9.56	358.75	8.16	11.29	201.7	19.45
337	US-Tw4	2016 TS_3	-0.08	13.17	360.06	8.67	10.58	205.7	19.25
338	US-Tw4	2016 TS_4	-0.16	15.94	362.56	9.11	9.991	209.2	19.11
339	US-Tw4	2016 TS_5	-0.32	21.05	367.55	9.91	8.876	216.2	18.78
340	US-Tw4	2017 TS_1	-0.02	38.35	347.31	8.07	11.52	211.9	19.59
341	US-Tw4	2017 TS_3	-0.08	42.12	351.81	8.45	10.91	215.3	19.36
342	US-Tw4	2017 TS_4	-0.16	46.03	354.70	8.83	10.35	218.6	19.18
343	US-Tw4	2017 TS_5	-0.32	53.54	361.37	9.52	9.275	224.9	18.79
344	US-Tw4	2018 TS_1	-0.02	58.11	344.87	8.00	10.93	218	18.93
345	US-Tw4	2018 TS_3	-0.08	63.91	349.15	8.38	10.41	222	18.79
346	US-Tw4	2018 TS_4	-0.16	67.95	352.10	8.71	9.862	225	18.57
347	US-Tw4	2018 TS_5	-0.32	75.31	357.88	9.33	8.8	231	18.13
348	US-Tw5	2018 TS_1	-0.02	NaN	414.83	0.00	8.894	222.2	18.37
349	US-Tw5	2018 TS_2	-0.1	NaN	401.00	0.00	12.32	204.4	22.24
350	US-Tw5	2018 TS_3	-0.02	NaN	414.83	0.00	8.894	222.2	18.37
351	US-Tw5	2018 TS_4	-0.08	NaN	423.43	0.00	7.898	227.3	18.14
352	US-Tw5	2018 TS_5	-0.16	NaN	430.15	0.00	7.531	230	17.94
353	US-Uaf	2011 TS_1	-0.09	86.20	372.46	-12.29	21.95	199.6	9.667
354	US-Uaf	2012 TS_1	-0.09	73.77	338.53	-11.83	20.86	202.4	9.028
355	US-Uaf	2013 TS_1	-0.09	109.63	395.51	-10.08	20.52	200.4	10.44
356	US-Uaf	2014 TS_1	-0.09	76.07	365.40	-10.94	19.94	206	8.999
357	US-Uaf	2015 TS_1	-0.09	80.99	423.19	-9.77	19.76	190	9.998
358	US-Uaf	2016 TS_1	-0.09	77.38	315.75	-7.74	19.13	198	11.39
359	US-Uaf	2017 TS_1	-0.09	84.88	380.17	-7.39	19.08	196	11.69
360	US-Uaf	2018 TS_1	-0.09	96.04	333.33	-5.60	17.72	199	12.11
361	US-WPT	2011 TS_1	-0.1	80.95	342.17	5.27	19.27	202.6	24.54
362	US-WPT	2011 TS_2	-0.3	NaN	347.04	6.38	16.62	209.7	23.01
363	US-WPT	2012 TS_1	-0.1	40.29	345.57	3.70	21.6	197.4	25.3
364	US-WPT	2012 TS_2	-0.3	44.91	354.96	4.52	19.21	203.8	23.72
365	US-WPT	2013 TS_1	-0.1	74.61	340.47	3.73	18.23	207.2	21.96
366	US-WPT	2013 TS_2	-0.3	77.62	352.35	4.32	16.69	211.7	21.01

### Column Descriptions

SITE\_ID                    Site identification code as assigned by regional flux data  
Year                        Data year  
Probe\_name                Temperature probe name as given in data files

Soil_temp_depth_m	Depth of soil temperature probe (m), with negative values
Start_TS_(DOY)	Season start for elevated TS (DOY), point "f" in Figure 1
End_TS_(DOY)	Season end for elevated TS (DOY), point "h" in Figure 1
Base_value_TS_(C)	Baseline TS during non-elevated season (C), average of points
Ampl_TS_(C)	Amplitude of TS during elevated temperature season (C), difference between point "e" in Figure 1 and Base_value_TS
Peak_TS_(DOY)	Day of maximum elevated TS (DOY), point "g" in Figure 1
Peak_value_TS_(C)	Maximum value of TS (C) point "e" in Figure 1

**Table B7 - Soil temperature probe depths (m)**

	SITE_ID	Year	Probe name	Soil_temp_depth_m	Additional_notes
1	AT-Neu		TS_1	-0.05	
2	AT-Neu		TS_2	-0.1	
3	AT-Neu		TS_3	-0.2	
4	BR-Npw		TS_1		
5	BR-Npw		TS_2		
6	BW-Gum		no data		
7	BW-Nxr		no data		
8	CA-SCB		TS_1	0	
9	CA-SCB		TS_2	-0.02	
10	CA-SCB		TS_3	-0.04	
11	CA-SCB		TS_4	-0.08	
12	CA-SCB		TS_5	-0.16	
13	CA-SCB		TS_6	-0.32	
14	CA-SCB		TS_7	-0.64	
15	CA-SCB		TS_8	-1.28	
16	CA-SCC		TS_1	-0.1	
17	CA-SCC		TS_2	-0.15	
18	CA-SCC		TS_3	-0.2	
19	CA-SCC		TS_4	-0.25	
20	CA-SCC		TS_5	-0.3	
21	CA-SCC		TS_6	-0.5	
22	CA-SCC		TS_7	-0.6	
23	CA-SCC		TS_8	-0.7	
24	CH-Cha		TS_1	-0.01	
25	CH-Cha		TS_2	-0.02	
26	CH-Cha		TS_3	-0.04	
27	CH-Cha		TS_4	-0.07	
28	CH-Cha		TS_5	-0.1	
29	CH-Cha		TS_6	-0.15	
30	CH-Cha		TS_7	-0.25	
31	CH-Cha		TS_8	-0.4	
32	CH-Cha		TS_9	-0.95	
33	CH-Dav		TS_1	-0.05	
34	CH-Dav		TS_2	-0.15	
35	CH-Dav		TS_3	-0.5	
36	CH-Dav		TS_4	-	
37	CH-Dav		TS_5	-	
38	CH-Dav		TS_6	-	
39	CH-Oe2		TS_1	-0.05	
40	CH-Oe2		TS_2	-0.1	
41	CH-Oe2		TS_3	-0.15	
42	CH-Oe2		TS_4	-	
43	CH-Oe2		TS_5	-0.3	
44	CH-Oe2		TS_6	-0.5	

45	CH-Oe2		TS_7	-
46	CN-Hgu		TS	
47	DE-Dgw		no data	
48	DE-Hte		TS_1	0
49	DE-Hte		TS_2	-0.1
50	DE-Hte		TS_3	-0.2
51	DE-SfN		TS_1	-0.02
52	DE-SfN		TS_3	-0.1
53	DE-SfN		TS_4	-0.2
54	DE-SfN		TS_5	-0.5
55	DE-Zrk		TS_1	-0.05
56	DE-Zrk		TS_2	-0.1
57	DE-Zrk		TS_3	-0.2
58	DE-Zrk		TS_4	-0.3
59	DE-Zrk		TS_5	-0.5
60	FI-Hyy		TS_1	-0.02
61	FI-Hyy		TS_2	-0.04
62	FI-Hyy		TS_3	-0.12
63	FI-Hyy		TS_4	-0.25
64	FI-Hyy		TS_5	-0.5
65	FI-Lom		TS_1	-0.07
66	FI-Lom		TS_2	-0.3
67	FI-Lom		TS_3	-0.5
68	FI-Si2		TS_1	-0.05
69	FI-Si2		TS_2	-0.2
70	FI-Si2		TS_3	-0.35
71	FI-Si2		TS_4	-0.5
72	FI-Sii	pre 2016	TS_1	-0.05
73	FI-Sii	pre 2016	TS_2	-0.2
74	FI-Sii	pre 2016	TS_3	-0.35
75	FI-Sii	pre 2016	TS_4	-0.5
76	FI-Sii	after 2017	TS_1	0
77	FI-Sii	after 2017	TS_2	-0.5
78	FI-Sii	after 2017	TS_3	-0.1
79	FI-Sii	after 2017	TS_4	-0.15
80	FI-Sii	after 2017	TS_5	-0.25
81	FI-Sii	after 2017	TS_6	-0.45
82	FI-Sii	after 2017	TS_7	-0.95
83	FR-LGt		TS_1	-0.02
84	FR-LGt		TS_2	-0.05
85	FR-LGt		TS_3	-0.1
86	FR-LGt		TS_4	-0.2
87	FR-LGt		TS_5	-0.4
88	HK-MPM		TS_1	
89	HK-MPM		TS_2	
90	HK-MPM		TS_3	
91	ID-Pag		TS_1	-0.05

<b>92</b>	IT-BCi	TS_1	-0.05
<b>93</b>	IT-BCi	TS_2	-0.1
<b>94</b>	IT-BCi	TS_3	-0.3
<b>95</b>	IT-BCi	TS_4	-0.5
<b>96</b>	IT-BCi	TS_5	-1
<b>97</b>	IT-Cas	TS_1	-0.035
<b>98</b>	IT-Cas	TS_2	-0.075
<b>99</b>	IT-Cas	TS_3	-0.15
<b>100</b>	JP-BBY	TS_1	-0.183
<b>101</b>	JP-BBY	TS_2	-0.233
<b>102</b>	JP-BBY	TS_3	-0.283
<b>103</b>	JP-BBY	TS_4	-0.383
<b>104</b>	JP-BBY	TS_5	-0.483
<b>105</b>	JP-Mse	TS_1	-0.01
<b>106</b>	JP-Mse	TS_2	-0.025
<b>107</b>	JP-Mse	TS_3	-0.05
<b>108</b>	JP-Mse	TS_4	-0.1
<b>109</b>	JP-Mse	TS_5	-0.2
<b>110</b>	JP-Mse	TS_6	-0.4
<b>111</b>	JP-SwL	no data	
<b>112</b>	KR-CRK	TS_1	-0.05
<b>113</b>	KR-CRK	TS_2	-0.15
<b>114</b>	MY-MLM	TS_1	-0.05
<b>115</b>	NL-Hor	TS_1	-0.01
<b>116</b>	NL-Hor	TS_2	-0.02
<b>117</b>	NL-Hor	TS_3	-0.04
<b>118</b>	NL-Hor	TS_4	-0.05
<b>119</b>	NL-Hor	TS_5	-0.1
<b>120</b>	NL-Hor	TS_6	-0.15
<b>121</b>	NL-Hor	TS_7	-0.25
<b>122</b>	NL-Hor	TS_8	-0.4
<b>123</b>	NL-Hor	TS_9	-0.6
<b>124</b>	NZ-Kop	TS_1	-0.5
<b>125</b>	NZ-Kop	TS_2	-0.1
<b>126</b>	NZ-Kop	TS_3	-0.2
<b>127</b>	PH-RiF	TS_1	
<b>128</b>	RU-Ch2	TS_1	-0.04
<b>129</b>	RU-Ch2	TS_2	-0.08
<b>130</b>	RU-Ch2	TS_3	-0.16
<b>131</b>	RU-Che	TS_1	-0.04
<b>132</b>	RU-Che	TS_2	-0.08
<b>133</b>	RU-Che	TS_3	-0.16
<b>134</b>	RU-Cok	no data	
<b>135</b>	RU-Fy2	TS_1	
<b>136</b>	RU-Fy2	TS_2	
<b>137</b>	RU-Fy2	TS_3	
<b>138</b>	RU-Fy2	TS_4	

<b>139</b>	RU-Fy2	TS_5	
<b>140</b>	SE-Deg	TS_1	-0.02
<b>141</b>	SE-Deg	TS_2	-0.05
<b>142</b>	SE-Deg	TS_3	-0.1
<b>143</b>	SE-Deg	TS_4	-0.15
<b>144</b>	SE-Deg	TS_5	-0.3
<b>145</b>	SE-Deg	TS_6	-0.5
<b>146</b>	UK-LBT	no data	
<b>147</b>	US-A03	TS_1	-0.025
<b>148</b>	US-A03	TS_2	-0.1
<b>149</b>	US-A03	TS_3	-0.3
<b>150</b>	US-A10	TS_1	-0.025
<b>151</b>	US-A10	TS_2	-0.1
<b>152</b>	US-A10	TS_3	-0.3
<b>153</b>	US-Atq	TS_1	
<b>154</b>	US-Atq	TS_2	
<b>155</b>	US-Atq	TS_3	
<b>156</b>	US-Beo	TS_1	
<b>157</b>	US-Beo	TS_2	
<b>158</b>	US-Beo	TS_3	
<b>159</b>	US-Bes	TS_1	
<b>160</b>	US-Bes	TS_2	
<b>161</b>	US-Bes	TS_3	
<b>162</b>	US-Bi1	TS_1	-0.02
<b>163</b>	US-Bi1	TS_2	-0.04
<b>164</b>	US-Bi1	TS_3	-0.08
<b>165</b>	US-Bi1	TS_4	-0.16
<b>166</b>	US-Bi1	TS_5	-0.32
<b>167</b>	US-Bi2	TS_1	-0.02
<b>168</b>	US-Bi2	TS_2	-0.04
<b>169</b>	US-Bi2	TS_3	-0.08
<b>170</b>	US-Bi2	TS_4	-0.16
<b>171</b>	US-Bi2	TS_5	-0.32
<b>172</b>	US-BZB	TS_1	-0.075
<b>173</b>	US-BZB	TS_2	-0.05
<b>174</b>	US-BZF	TS_1	-0.075
<b>175</b>	US-BZF	TS_2	-0.05
<b>176</b>	US-BZS	TS_1	
<b>177</b>	US-BZS	TS_2	
<b>178</b>	US-BZS	TS_3	
<b>179</b>	US-CRT	TS_1	
<b>180</b>	US-DPW	no data	
<b>181</b>	US-EDN	TS_1	-0.25
<b>182</b>	US-EDN	TS_2	-0.15
<b>183</b>	US-EDN	TS_3	-0.05
<b>184</b>	US-EDN	TS_4	0
<b>185</b>	US-EDN	TS_5	0.05

<b>186</b>	US-EDN	TS_6	0.1
<b>187</b>	US-EDN	TS_7	0.2
<b>188</b>	US-EDN	TS_8	0.3
<b>189</b>	US-EML	TS_1	-0.05
<b>190</b>	US-EML	TS_2	-0.1
<b>191</b>	US-EML	TS_3	-0.2
<b>192</b>	US-EML	TS_4	-0.4
<b>193</b>	US-Ho1	TS_1	-0.05
<b>194</b>	US-Ho1	TS_2	-0.1
<b>195</b>	US-HRA	no data	-0.02
<b>196</b>	US-HRC	no data	-0.02
<b>197</b>	US-ICs	TS_1	-0.075
<b>198</b>	US-ICs	TS_2	-0.05
<b>199</b>	US-Ivo	TS_1	-0.05
<b>200</b>	US-Ivo	TS_2	-0.1
<b>201</b>	US-Ivo	TS_3	-0.15
<b>202</b>	US-Ivo	TS_4	-0.3
<b>203</b>	US-Ivo	TS_5	-0.4
<b>204</b>	US-LA1	TS	-0.1
<b>205</b>	US-LA2	TS	-0.1
<b>206</b>	US-Los	TS_1	0
<b>207</b>	US-Los	TS_2	-0.05
<b>208</b>	US-Los	TS_3	-0.1
<b>209</b>	US-Los	TS_4	-0.2
<b>210</b>	US-Los	TS_5	-0.5
<b>211</b>	US-MRM	TS_1	
<b>212</b>	US-MRM	TS_2	
<b>213</b>	US-Myb	TS_1	-0.02
<b>214</b>	US-Myb	TS_2	-0.04
<b>215</b>	US-Myb	TS_3	-0.08
<b>216</b>	US-Myb	TS_4	-0.16
<b>217</b>	US-Myb	TS_5	-0.32
<b>218</b>	US-NC4	TS_1	-0.05
<b>219</b>	US-NC4	TS_2	-0.2
<b>220</b>	US-NGB	no data	
<b>221</b>	US-NGC	no data	
<b>222</b>	US-ORv	TS_1	-0.08
<b>223</b>	US-OWC	TS_1	-0.05
<b>224</b>	US-OWC	TS_2	-0.3
<b>225</b>	US-PFa		
<b>226</b>	US-Snd	TS_1	-0.08
<b>227</b>	US-Snd	TS_2	-0.16
<b>228</b>	US-Snd	TS_3	
<b>229</b>	US-Snd	TS_4	
<b>230</b>	US-Snd	TS_5	
<b>231</b>	US-Snd	TS_6	
<b>232</b>	US-Sne	TS_1	-0.01

<b>233</b>	US-Sne	TS_2	-0.02
<b>234</b>	US-Sne	TS_3	-0.08
<b>235</b>	US-Sne	TS_4	-0.16
<b>236</b>	US-Sne	TS_5	-0.32
<b>237</b>	US-Srr	TS_1	
<b>238</b>	US-Srr	TS_2	
<b>239</b>	US-Srr	TS_3	
<b>240</b>	US-Srr	TS_4	
<b>241</b>	US-Srr	TS_5	
<b>242</b>	US-StJ	TS_2	-0.05
<b>243</b>	US-StJ	TS_3	-0.1
<b>244</b>	US-Tw1	TS_1	-0.02
<b>245</b>	US-Tw1	TS_2	-0.04
<b>246</b>	US-Tw1	TS_3	-0.08
<b>247</b>	US-Tw1	TS_4	-0.16
<b>248</b>	US-Tw1	TS_5	-0.32
<b>249</b>	US-Tw3	TS_1	-0.02
<b>250</b>	US-Tw3	TS_2	-0.04
<b>251</b>	US-Tw3	TS_3	-0.08
<b>252</b>	US-Tw3	TS_4	-0.16
<b>253</b>	US-Tw3	TS_5	-0.32
<b>254</b>	US-Tw4	TS_1	-0.02
<b>255</b>	US-Tw4	TS_2	-0.04
<b>256</b>	US-Tw4	TS_3	-0.08
<b>257</b>	US-Tw4	TS_4	-0.16
<b>258</b>	US-Tw4	TS_5	-0.32
<b>259</b>	US-Tw5	TS_1	-0.02
<b>260</b>	US-Tw5	TS_2	-0.1
<b>261</b>	US-Tw5	TS_3	-0.02
<b>262</b>	US-Tw5	TS_4	-0.08
<b>263</b>	US-Tw5	TS_5	-0.16
<b>264</b>	US-Twt	TS_1	-0.02
<b>265</b>	US-Twt	TS_2	-0.04
<b>266</b>	US-Twt	TS_3	-0.08
<b>267</b>	US-Twt	TS_4	-0.16
<b>268</b>	US-Twt	TS_5	-0.32
<b>269</b>	US-Uaf	TS_1	-0.09 average of 3 depths: -0.15, -0.02, -0.1
<b>270</b>	US-Uaf	TS_2	-0.183333 average of 3 depths: -0.3, -0.05, -0.2
<b>271</b>	US-Uaf	TS_3	-0.283333 average of 3 depths: -0.45, -0.1, -0.3
<b>272</b>	US-Uaf	TS_4	-0.366667 average of 3 depths: -0.5, -0.2, -0.4
<b>273</b>	US-Uaf	TS_5	-0.5 average of 2 depths: -0.7, -0.3
<b>274</b>	US-Uaf	TS_6	-0.6 average of 2 depths: -0.8, -0.4
<b>275</b>	US-Uaf	TS_7	-0.75 average of 2 depths: -1, -0.5
<b>276</b>	US-Uaf	TS_8	-0.925 average of 2 depths: -1.25, 0.6,
<b>277</b>	US-Uaf	TS_9	-1
<b>278</b>	US-WPT	TS_1	-0.1
<b>279</b>	US-WPT	TS_2	-0.3

**Column Descriptions**

SITE_ID	Site identification code as assigned by regional flux data network
Year	When relevant, information about time-span of probe location. If
Probe_name	Temperature probe name as given in data files
Soil_temp_depth_m	Depth of soil temperature probe (m), with negative values being under
Additional_notes	When relevant, additional information about site